AD-A037 500   MISSOURI UNIV-ROLLA DEPT OF MECHANICAL AND AEROSPACE--ETC F/G 4/2
A SYSTEMS STUDY OF MARINE FOG SITUATIONS.(U)
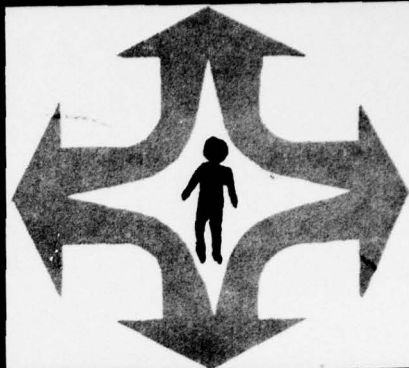FEB 77 S C LEE   N00014-69-A-0140-0006
UNCLASSIFIED   72-76-0180   NI

| OF |
AD
A037500

END
DATE
FILMED
4-77

UMR DEPARTMENT OF MECHANICAL & AEROSPACE ENGINEERING

A SYSTEMS STUDY
OF MARINE FOG SITUATIONS

BY
SHEN C. LEE

REPORT NO. 72-76-0180
FEBRUARY 1977

UNIVERSITY OF MISSOURI - ROLLA

REPORT DOCUMENTATION PAGE		READ INSTRUCTIONS BEFORE COMPLETING FORM
1. REPORT NUMBER 72-76-0180	2. GOVT ACCESSION NO.	3. RECIPIENT'S CATALOG NUMBER
4. TITLE (and Subtitle) A Systems Study of Marine Fog Situations		5. TYPE OF REPORT & PERIOD COVERED Final Report Oct. 1, 1972-Dec. 31, 1976
		6. PERFORMING ORG. REPORT NUMBER
7. AUTHOR(s) Shen C. Lee		8. CONTRACT OR GRANT NUMBER(s) N00014-69-A-0140-0006 N00014-75-C-0180
9. PERFORMING ORGANIZATION NAME AND ADDRESS University of Missouri-Rolla Rolla, Mo. 65401		10. PROGRAM ELEMENT, PROJECT, TASK AREA & WORK UNIT NUMBERS
11. CONTROLLING OFFICE NAME AND ADDRESS Atmospheric Sciences Program Code 465, Office of Naval Research Arlington, Va. 22217		12. REPORT DATE February 1977
		13. NUMBER OF PAGES 88
14. MONITORING AGENCY NAME & ADDRESS(if different from Controlling Office) Final rept. 1 Oct 72 - 31 Dec 76		15. SECURITY CLASS. (of this report) Unclassified
		15a. DECLASSIFICATION/DOWNGRADING SCHEDULE

16. DISTRIBUTION STATEMENT (of this Report)

Unlimited

79 p.

DISTRIBUTION STATEMENT A
Approved for public release;
Distribution Unlimited

17. DISTRIBUTION STATEMENT (of the abstract entered in Block 20, if different from Report)

18. SUPPLEMENTARY NOTES

19. KEY WORDS (Continue on reverse side if necessary and identify by block number)

Marine Fog Situations	Collision Coalescence
Systems Study	Thermal Radiation
Turbulence Advection	Spray Evaporation
Fog Formation	Fog Dissipation

20. ABSTRACT (Continue on reverse side if necessary and identify by block number)

Fog situations are a hazard to navigation whether they involve highways, harbors, airports, or sea lanes. Prediction and modification are therefore necessary for the safety of travel and for operational economy. Field studies conducted for this purpose indicate that many different fog situations result from a variety of natural processes, which must be systematically investigated so that the basic causes for their development can be understood and possibly controlled.

The systems study of marine fog situations that has been conducted has taken into

DD FORM 1 JAN 73 1473 EDITION OF 1 NOV 65 IS OBSOLETE
S/N 0102-014-6601

This systems study of marine fog considers

20. consideration the dynamical interaction between the synoptical variations of meteorology and the microphysical phenomena in cloud physics. The resulting numerical program simulates the transport of heat, mass, and momentum in the atmospheric boundary layer where condensation/evaporation, thermal radiation, collision coalescence, and turbulent advection take place.

Although this program is fairly complete, experimental data of the moisture supply process affected by turbulent winds at the air-sea interface are needed to establish a realistic model for systems analysis. Because of this deficiency in the current model, the radiation estimate, which is closely related to the water vapor and liquid water concentrations at various heights in the atmospheric boundary layer, can only be considered as "qualitative". When available field data are compared to predicted fog situations, it is found that the boundary layer model can qualitatively simulate fog situations over an open ocean, but the accurate prediction of a fog event at a specific time and place requires a working knowledge of the moisture supply process occasioned by air-wave interactions. Until this knowledge is acquired, the "qualitative" models currently being used in systems analysis will continue to be a source of inaccuracy.

Fog situations are known to occur on the lee side of some topographical obstructions. The wind patterns associated with this type of fog generally have different directions with respect to the prevailing wind. A hypothesis is being formulated to explain such situations on the basis of recirculating flows. Some "strange" fog conditions have been logically explained by this hypothesis. However, a realistic understanding of all marine fog situations requires the continuous effort of dynamic modeling to integrate laboratory experiments and field measurements.
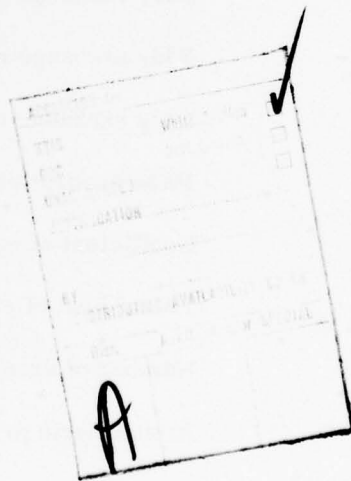
PREFACE

NOMENCLATURE

A	Total area where condensation occurs
$\dot{C}_s$	Condensation rate
C^m	Concentration of species m
C^I	Concentration of air
C^{II}	Concentration of water vapor
C^{III}	Concentration of liquid water
c'	Concentration fluctuation
c_p	Specific heat at constant pressure
D	Molecular diffusivity
D^{II}	Binary diffusivity between air and water vapor
E	Total evaporation at a given time, τ
g	Gravitational acceleration
K_c	Eddy exchange coefficient of concentration
K_h	Eddy exchange coefficient of heat
K_m	Eddy exchange coefficient of momentum
K_q	Eddy exchange coefficient of turbulence energy
k_λ	Mass absorption coefficient
k_τ	Coefficient of contact time between turbulent eddies and water surface
L_h	Latent heat of evaporation
N	Number of droplets per unit volume of fog
p	Atmospheric pressure
p'	Pressure fluctuation

p_s	Vapor partial pressure
p_g	Saturated vapor partial pressure
Ω	Turbulence kinetic energy
$R_\uparrow^{II}$	Thermal radiation of water vapor in the upward direction
$R_\downarrow^{II}$	Thermal radiation of water vapor in the downward direction
R^{III}	Thermal radiation of liquid water
R_a	Gas constant of air
Re_x	Reynolds number based on x
T	Air temperature
t'	Temperature fluctuation
U_i	Wind velocity in the i direction
u_i'	Velocity fluctuation in the i direction
V	Volume of air mass
V_d	Falling velocity of a water droplet
w^{III}	Liquid water content in a falling droplet
w'	Velocity fluctuation in the vertical direction
X_i	Space coordinate in the i direction
Z	Vertical direction of the space (i=3)
Z_r	Radiation layer at altitude Z
Z_t	Top of fog layer at altitude Z
β	Surface coefficient of non-block body radiation
ϵ	Emissivity function between fog layers
k	Thermal conductivity

μ	Dynamic viscosity
ρ	Density of air
σ	Stefan-Boltzmann constant
σ_c	Turbulent Schmidt number
σ_h	Turbulent Prandtl number
σ_q	Equivalent Prandtl number
τ	Time, an independent variable
Φ	Heat dissipation due to friction

- 4 -

CONTENTS

ILLUSTRATIONS

Figure

TABLES

ABSTRACT

Fog situations are a hazard to navigation whether they involve highways, harbors, airports, or sea lanes. Prediction and modification are therefore necessary for the safety of travel and for operational economy. Field studies conducted for this purpose indicate that many different fog situations result from a variety of natural processes, which must be systematically investigated so that the basic causes for their development can be understood and possibly controlled.

The systems study of marine fog situations that has been conducted has taken into consideration the dynamical interaction between the synoptical variations of meteorology and the microphysical phenomena in cloud physics. The resulting numerical program simulates the transport of heat, mass, and momentum in the atmospheric boundary layer where condensation/evaporation, thermal radiation, collision coalescence, and turbulent advection take place.

Although this program is fairly complete, experimental data of the moisture supply process affected by turbulent winds at the air-sea interface are needed to establish a relaistic model for systems analysis. Because of this deficiency in the current model, the radiation estimate, which is closely related to the water vapor and liquid water concentrations at various heights in the atmospheric boundary layer, can only be considered as "qualitative". When available field data are compared to predicted fog situations, it is found that the boundary layer model can qualitatively simulate fog situations over an open ocean, but the accurate prediction of a fog event at a specific time and place requires a working knowledge of the moisture supply process occasioned by air-wave interactions. Until this knowledge is acquired,

the "qualitative" models currently being used in systems analysis will continue to be a source of inaccuracy.

Fog situations are known to occur on the lee side of some topographical obstructions. The wind patterns associated with this type of fog generally have different directions with respect to the prevailing wind. A hypothesis is being formulated to explain such situations on the basis of recirculating flows. Some "strange" fog conditions have been logically explained by this hypothesis. However, a realistic understanding of all marine fog situations requires the continuous effort of dynamic modeling to integrate laboratory experiments and field measurements.

1. INTRODUCTION

Fog situations are a serious hazard to everyday life because extensive navigation in the air, on land, and at sea is an integral part of travel, commerce, and defense. Thousands of lives and millions of dollars are lost each year because of man's inability to predict and to modify undesirable fog situations.

Experimental modification of fog situations has been attempted at harbors and airports by Walker and Fox (1942-1946), Silverman and Kunkel (1970), Magono (1972), and Weinstein (1973), but their limited success makes it difficult to justify the enormous cost for practical operation. It is evident that an understanding of the formation mechanism of various fog situations is necessary if a realistic method is to be developed for successful prediction and effective modification.

2. FOGS AND CLOUDS

The similarity of fogs and clouds prompted the author to concentrate his early efforts on the study of basic cloud physics problems, such as condensation nuclei, supersaturation, and collision coalescence. Field data by Leipper (1968), Mack et al. (1972, 1975), and Larson (1976) indicate that the marine environment has numerous condensation nuclei that do not allow supersaturation to take place at the air-sea interface. In other words, fog will form as soon as excessive moisture is available at the surface layer of the marine environment. Most likely, the sea salt concentration in marine aerosols may cause fog to form even in subsaturated conditions, because sea salt nuclei are known to grow in size by absorbing moisture in a subsaturated environment (Mason, 1971).

The phenomenon of collision coalescence of cloud drops in a rain forming pro-

cess appears to be responsible for fog dissipation by hygroscopic particle seeding as discussed by Tag (1971). A hydrodynamic analysis was developed by Lin and Lee (1973, 1975, 1976a, 1976b) in their study of the collision efficiency of free falling drops in the atmosphere. In this analysis, it became evident that wake capture is a very important mechanism, which increases the collision efficiency of a collecting drop and a collector drop when their radius ratios are greater than 90 percent. However, collision efficiency becomes significantly less effective than geometric efficiency when the radius ratios are less than 30 percent. Considerable discussion was generated by this analysis, because earlier published statements claimed that wake capture was not relavent to an increase in collision efficiency. Appendix A contains the four papers in which the phenomenon is analyzed. The authors' findings indicate that it is possible to produce rainfall through the process of collision coalescence among growing drops when the condensation growth of the seeded particles in a supersaturated cloud reaches the critical size of approximately 20 μm radii. However, the application of cloud seeding is not effective in marine fog dissipation, because there are enough nuclei already present in the air-sea interface.

The necessary ingredients are condensation nuclei and saturation conditions for both fog and cloud formation; however, the mechanisms for supplying these ingredients are quite different. Clouds can generally be formed by the cooling of the available moisture at high altitudes, a condition which can be simulated in a cloud chamber. Fogs, on the other hand, can be formed by the additional mechanism of providing moisture from a nearby water source. This condition cannot be simulated in a conventional cloud chamber. Consequently, it is necessary to use a systems

study to understand the dynamic interaction that takes place between synoptical meteorology and microphysics. Moreover, the formation of clouds in severe storms--one of the few remaining catastrophic agents against which mankind has no practical defense--can only be apprehended through a systematically developed study of the dynamical and microphysical interactions in the atmosphere.

3. A SYSTEMS STUDY OF MARINE FOG SITUATIONS

During an examination of the field data of Taylor (1917), Stone (1936), George (1940), Emmons (1947), and Magono (1972), it became clear that most fog situations are caused by the interaction between the dynamical process of heat, mass and momentum transfer, and the microphysical process of condensation/evaporation, turbulent advection, and thermal radiation. The derived systems study of the marine fog situation is illustrated diagramatically by the flow chart in Figure 1. The input information consists of the boundary condition of the potential fog region and the initial condition of the meteorological data, which can be obtained from nearby weather stations and/or available weather satellites. The dynamic equations, which are given in Figure 2, are used to analyze the synoptical meteorological conditions that govern the temperature, humidity, and wind velocity of the potential fog region. The microphysical phenomena, which are outlined in Figure 3, are concerned with the interdependent processes of condensation/vaporation, turbulent advection, collision coalescence, and thermal radiation. Laboratory experiments, which are often conducted in a well controlled environment, can only provide the empirical relation of a microphysical process as a function of other meteorological parameters in a non-interacting environment. To consider any dynamic interaction between the synoptical

- 11 -

meteorological conditions and some related microphysical phenomena, it is necessary to include all microphysical processes as the appropriate driving functions of the dynamic equations. The output gives the primary results of wind velocity, air temperature, dew point, and heat budget as well as the liquid water and water vapor contents. The drived information, such as visibility and refraction index, can be calculated from the primary results at a given condition of concentration and composition of the marine aerosols. Field data can then be used to verify each analytical procedure to ensure the validity and reliability of the developed program for marine fog simulations. When the program is in a ready state for practical application, weather station data can then be used for forecasting fog situations in a given region. If the predicted fog is expected to be hazardous to navigation, possible modification schemes can be simulated to determine their effectiveness both scientifically and economically. The success of such a systems study for marine fog simulation is based on two factors:

1. The Reliability and Adequacy of Field Data

Field data have to be accurately recorded at stratigic locations during the critical period. For example, at each fog event, it is necessary to collect all fog data both inside and outside the fog bank in line with the direction of the wind. The formation process can be studied by using the data taken from the leading edge (or upwind region) of the fog bank. The dissipation process can be studied by using the trailing edge (or downwind region) data. Field data taken in the middle of a mature fog bank are valuable for studying its chemical composition but cannot provide the required information for an understanding of the dynamic interactions that occur during formation or dissipa-

- 12 -

tion. On the other hand, field data taken across fog boundaries in a direction normal to the wind consist of too many uncertainties and cannot provide the primary information that is needed for an understanding of the formation and dissipation processes.

2. The Ability of Obtaining Realistic Mathematical Solutions

Numerical solutions of nonlinear, simultaneous, partial differential equations can be obtained by using high speed digital computers, but marine fog problems, which are compunded by turbulent winds, require an appropriate closure scheme to describe the physical problem realistically. Because of the physical and mathematical complexities, marine fog analyses are primarily made of open ocean situations.

4. OPEN OCEAN FOG SITUATIONS

Fog situations that originate over the ocean and are advected to coastal regions have been reported in England by Walker and Fox (1942-1946), in the United States by Leipper (1968), in Japan by Magono (1972), and in many other coastal regions of the world. A 48-hour fog event, which occurred along the coast of Massachusetts during the 26-28 January 1975, demonstrates the feasibility of predicting fog events on the basis of weather station information. A number of weather stations are located in the region, as shown in Figure 4. The wind direction, wind speed (in knots), air temperature (in ^{O}C), dew point (in ^{O}C), and visibility (in km) are shown in the subsequent figures for all the reporting stations. The average air temperature in the region before the event was about $3^{O}C$. Warm wind moved into the region from the east and southeast direction at approximately 10 knots during the early morning hours of 26 January 1975 (Fig. 4a). Heavy fog began to appear at the 1500 hour (Fig. 4b), when the average air temperature of the region rose to about $6^{O}C$. The dew

- 13 -

point temperature was lower than the local air temperature. As long as the warm humid air was supplied from the south or southeast direction, fog persisted in spite of substantial dew point depressions (Fig. 4c). The fog began to dissipate in the inland area, when cold dry air moved into the region from the west at the 1200 hour of 28 January 1975 (Fig. 4d). Fog was cleared from the entire region at the 1800 hour (Fig. 4e), when the average air temperature was about 2°C and the wind moved at 15 knots from the west direction. During the 45 hours of the heavy fog period, two observations need to be emphasized: 1) The diurnal effect of radiation heating did not appear to play any significant role in improving visibility, and 2) significant dew point depressions were reported by all the weather stations where the dew point data were recorded.

Advection fog of this type is a major hazard to navigation, and this particular fog event makes it very clear that synoptical meteorology has to be an integral part of the investigation. Mathematical formulation of fog analysis was suggested by Rodhe (1962), Fisher and Caplan (1963), and Zakharova (1972). The turbulent nature of the transport process of the atmospheric air, as discussed by Lumley and Panofsky (1964) and Monin and Yaglom (1971), limited the author's choice of realistic closure schemes for analyzing actual fog situations. Lee et al. (1974) developed a boundary layer model to study the turbulent transport of heat, mass, and momentum. Pepper and Lee (1975) extended this method to investigate advection fog over the ocean. The air-sea interface can be treated as an atmospheric boundary layer that has various roughnesses at the ocean surface. The amount of moisture supply from the ocean depends on the air-water temperature difference as well as

- 14 -

on the spray process resulting from air-wave interactions. In general, fog may form during one of the following situations:

(1) Warm humid air can be cooled to a saturation condition while it is being transported by turbulent winds to a cold region. This was the condition under which the above-mentioned Massachusetts fog was formed as well as the advection fog observed by Magona (1972) at the south shore of Hakkaido, Japan. Marine fog of this type constitutes the most undesirable hazard to navigation, because it may last several days if the synoptical conditions persist. Magono (1972) was able to improve visibility from 150 m to 250 m for five minutes by burning five tons of propane along half of the runway length at the Chitose Airport. This example makes it clear why there is a need to study the scientific and economic feasibility of fog modification.

(2) Moisture may be supplied from a warm ocean to cooler air through evaporation. Fog is formed when radiation cooling drops the air temperature to a condensation condition. Wind accelerates the evaporation process. Turbulent winds often add more moisture to the cool air by evaporating the spray. The more moisture there is in the air, the less degree of radiation cooling is needed to reach saturation conditions. This type of fog often occurs as a nocturnal phenomenon as observed by George (1940) along the Gulf of Mexico, by Mack et al. (1972) along the California Coast, and by Goodman (1976) in San Francisco, California. Radiation cooling is a very important factor in the formation of dense fog in this situation. In other words, when such a moisture supply process occurs in the morning, as observed by Kikuchi (1964) at the Ishikari Bay located on the north shore of Hokkaido, Japan, a thin layer

- 15 -

of the condensed moisture may soon be dissipated by the radiation heat created by the thermal energy of the rising sun.

The dynamics involved in the systems study of predicting fog conditions at sea are relatively well known, but the microphysical phenomenon of moisture supply at the air-sea interface is not completely understood, especially when turbulent winds are involved in the process. Moreover, the effect of radiation cooling can be correctly evaluated only when the amounts of water vapor and/or liquid water in the radiating layer are accurately known. The adjacent water is the source for the moisture that creates a marine fog situation. This is quite different from the situation in which a cloud is formed at a relatively high altitude. Laboratory experiments cannot ignore the problem of moisture supply, simply because the condition is unfamiliar to cloud physicists. Field data have to be collected to provide the maximum amount of information that can be attained in the direction of the wind from both outside and inside of a fog bank.

Detailed discussions of the boundary layer method that is used for predicting marine fog situations at sea are contained in the technical papers included in Appendix B. A computer program for the method is available upon request. Because the evaluation of a moisture supply cannot be made with certainty, the developed program can be used only for a qualitative analysis at the present. The data that are currently available from laboratory experiments and field observations should be used to improve the microphysical models so that the current program can be developed into a practical tool for fog prediction. Moreover, it must be noted that the boundary layer method cannot be applied to fog situations in which the topography

and/or weather fronts cause recirculating flows.

5. FOG FORMATION IN RECIRCULATING FLOW REGIONS

Fog may form along shorelines or in harbors where the wind recirculates as a result of the topography. The importance of recirculating flow as a natural process was first suggested by von Karman (1934). In his autobiography (von Karman, 1967), he stated that the concept of the Karman vortex could not be accepted by the fluid mechanics community until the collapse of the Tacoma-Narrow bridge could not be explained by any other known phenomenon. Consequently, the reluctance of the meteorological community (especially in the restricted area of cloud physics) to investigate the hypothesis that fog may form in the region of recirculating flows is understandable. However, it would be irresponsible to discard the facts, because they cannot be satisfactorily explained by the current knowledge of cloud physicists. The facts are as follows:

(1)   The fog situation observed by Mack et al. (1975) during the expedition of the R/V Acania in the region downwind of Cape Mendocino, California, on 25-27 August 1974 was considered "strange" (Fig. 5).

(2)   The fog situation observed by Gathman (1976) and Larson (1976) during the expedition of the USNS Hays in the region downwind of Nova Scotia, Canada, on 2-3 August 1975 was never explained (Fig. 6 and Table 1).

These two fog situations, which differ from most other reported fogs, are similar in the following respects: 1) In both, the prevailing winds were relatively strong. 2) The wind directions in the fog regions were opposite to those of the prevailing winds. 3) Both fog regions are located on the lee side of topographic obstructions.

A complete analysis of the flow characteristics in a recirculating flow region requires the solution of the complete set of equations shown in Figure 2 without the use of the boundary layer assumption outlined in the technical papers contained in Appendix B. There are two problems. One is to develop a numerical method for stable solutions of a system of nonlinear elliptical differential equations, and the other is to establish a realistic closure scheme in which all the tensor components of turbulence correlation for velocities, temperatures, and water vapor and liquid water concentrations can be considered. The author's effort to resolve the mathematical problem was discussed by Lin et al. (1976). This paper is included in Appendix C. The Strongly Implicit Procedure (SIP) appears to be the most efficient method for analyzing recirculating flow when the turbulence closure scheme is replaced by an equivalent laminar model. A concept of a turbulent recirculating flow can be developed by using the SIP method of Appendix C and the turbulence closure scheme of Appendix B which still needs to be perfected for use in recirculating flow regions. Ability to predict and/or modify fog situations in harbors requires a basic understanding of the recirculating flow affected by topography. This knowledge is not currently available.

6. CONCLUSIONS

1. Fog can be formed by either decreasing the air temperature or increasing the air humidity to a saturation condition. Once the saturation condition is reached, excessive moisture will condense on available aerosols to form fog.

2. Because there is an abundant supply of moisture and condensation nuclei at the air-water interface, marine fog formation undergoes some natural processes

- 18 -

that have not been realistically simulated in conventional cloud chambers.

3. Prediction and modification of marine fog situations cannot be accomplished by considering condensation from the microphysical viewpoint alone, because the interaction between dynamics and microphysics requires the synoptical information of dynamical meteorology and oceanography as well as the micro-physical phenomena of cloud physics.

4. Because there are many possible combinations of natural phenomena in fog formations, a systems study is necessary to obtain a general perspective in analyzing the fog data that are gathered from various locations at different times.

5. A summary of ten reported fog situations is given in Table 2. Eight cases can be simulated by using the boundary layer model. The other two cases, how-ever, can only be explained by using the hypothesis of recirculating flow.

REFERENCES

Asai, T. (1965), "A Numerical Study of the Air-Mass Transformation over the Japan Sea in Winter", J. Meteor. Soc. Japan, 43, 1-7.

Barker, E. H. (1973), "Oceanic Fog: A Numerical Study", EPRF, Naval Postgraduate School, Tech. Paper 6-73, p. 65.

Dankerwerts, P. V. (1951), "Significance of Liquid-Film Coefficients in Gas Absorption", Ind. Eng. Chem., 43, 1460-1467.

Emmons, G. (1947), "Vertical Distributions of Temperature and Humidity over the Ocean between Nantucket and New Jersey", Tech. Report No. 413, Woods Hole Oceanographic Inst., p. 89.

Fisher, E. L., and Caplan, P. (1963), "An Experiment in Numerical Prediction of Fog and Stratus", J. Atmos. Sci., 30, 425-478.

Gathman, S. G. (1976), "The 1975 USNS Hays Fog Cruise", Fourth Ann. Marine Fog Conf., Reno, Nevada, January 6-7, 1976.

George, J. J. (1940), "Fog, Its Causes and Forecasting with Special Reference to Eastern and Southern United States", Bull. Am. Meteor. Soc., 31, 285-291.

Goodman, J. K. (1976), "The Micro-Structure of California Coastal Fog and Stratus", Report No. 76-09, Department of Meteorology, San Jose State University, San Jose, California, p. 35.

Kikuchi, K. (1964), "On Some Coastal Clouds over Ishikari Bay, Hokkaido", J. Meteor. Soc. Japan, 42, 341-353.

Knudson, J. G., and Katz, D. L. (1958), Fluid Mechanics and Heat Transfer, McGraw-Hill, New York, N. Y.

Larson, R. E. (1976), "Radon 222 Measurements During the Nova Scotia Marine Fog Cruise", Fourth Ann. Marine Fog Conf., Reno, Nevada, January 6-7, 1976.

Lee, S. C., Pepper, D. W., Byrne, W. M., and Tai, R. C. (1974), "Heat Mass and Momentum Transfer in Turbulent Boundary Layer Flows", Heat Transfer 1974, 2, 104-108.

Leipper, D. F. (1968), "The Sharp Smog Bank and California Fog Development", Bull. Am. Meteor. Soc., 49, 354-358.

Lin, C. L., and Lee, S. C. (1973), "Transient State Analysis of Separated Flow Around a Sphere", Intl. J. Comp. Fluids, 1, 235-250.

Lin, C. L., and Lee, S. C. (1975), "Collision Efficiency of Water Drops in the Atmosphere", J. Atm. Sci., 32, 1412-1418.

Lin, C. L., and Lee, S. C. (1976a), "Collision Efficiency Analyses", J. Atm. Sci., 33, 873-875.

Lin, C. L., and Lee, S. C. (1976b), "The Effect of Vertical Separation on Droplet Collision Efficiency", J. Atm. Sci., 33, 1826-1827.

Lin, C. L., Pepper, D. W., and Lee, S. C. (1976), "Numerical Methods for Separated Flow Solutions Around a Circular Cylinder", Am. Inst. Aeronaut. and Astronaut., 14, 900-907.

Lumley, J. L., and Panofsky, H. A. (1964), "The Structure of Atmospheric Turbulence", Interscience Publishers, New York, p. 239.

Mack, E. J., Ealie, W. J., Rogers, C. W., Kocmond, W. C., and Pilie, R. J. (1972), "A Field Investigation and Numerical Simulation of Coastal Fog", Tech. Report, No. CJ-5055-M-L, Calspan Corp., p. 136.

Mack, E. J., Pilie, R. J., and Ulrich, K. (1975), "Marine Fog Studies off the California Coast", Tech. Report No. CJ-5607-M-1, Calspan Corp., p. 80.

Magono, C. (1972), "A Warm Fog Dissipation Experiment Utilizing Burning Propane Gas", J. de Recherches Atmospheriques, 6, 343-365.

Mason, B. J. (1971), "The Physics of Clouds", Clearendon Press, Oxford.

McDonald, J. E. (1963), "The Saturation Adjustment in Numerical Modeling of Fog", J. Atm. Sci., 20, 476-478.

Monin, A. S., and Yaglom, A. M. (1971), Statistical Fluid Mechanics, MIT Press, Cambridge, Mass., p. 373-416.

Pepper, D. W., and Lee, S. C. (1975), "Transport Phenomena in Thermally Stratified Boundary Layers", J. Heat Transfer, 97, 60-65.

Rodhe, B. (1962), "The Effect of Turbulence on Fog Formation", Tellus, 24, 49-86.

Silverman, B. A., and Kunkel, B. A. (1970), "A Numerical Model of Warm Fog Dissipation by Hygroscopic Particle Seeding", J. Appl. Meteor., 9, 627-633.

Stone, R. G. (1936), "Fog in the United States", Geograph. Rev., 26, 111-134.

Tag, P. M. (1971), "Results Generated From a One-Dimensional Warm Fog Model Which Simulates Hygroscopic Seeding", NAVWEARSCHFAC Tech. Paper No. 11-71.

Taylor, G. I. (1917), "The Formation of Fog and Mist", Quart. J. Roy. Meteor. Soc., 43, 241-268.

Walker, E. G., and Fox, D. A. (1942-1946), "The Dispersal of Fog From Airfield Runways", Petroleum Warfare Dept., Ministry of Supply, London, England.

von Karman, T. (1934), "Some Aspects of the Theory of Turbulent Motion", Proc. Intern. Congr. Appl. Mech., Cambridge.

von Karman, T. (1967), "The Wind and Beyond", Little Brown, Boston.

Weinstein, A. L. (1973), "Thermal Warm Fog Dissipation - Heat Requirements and Projected Utilization of a System for Travis AFB, California", AFCRL-TR-73-0367, Air Force Cambridge Res. Labs., Bedford, Mass.

Zakharova, I. M. (1972), "A Mathematical Model of the Evaluation of Radiation Fog", AFCRL-72-0720, Air Force Cambridge Res. Labs., Bedford, Mass., p. 25.
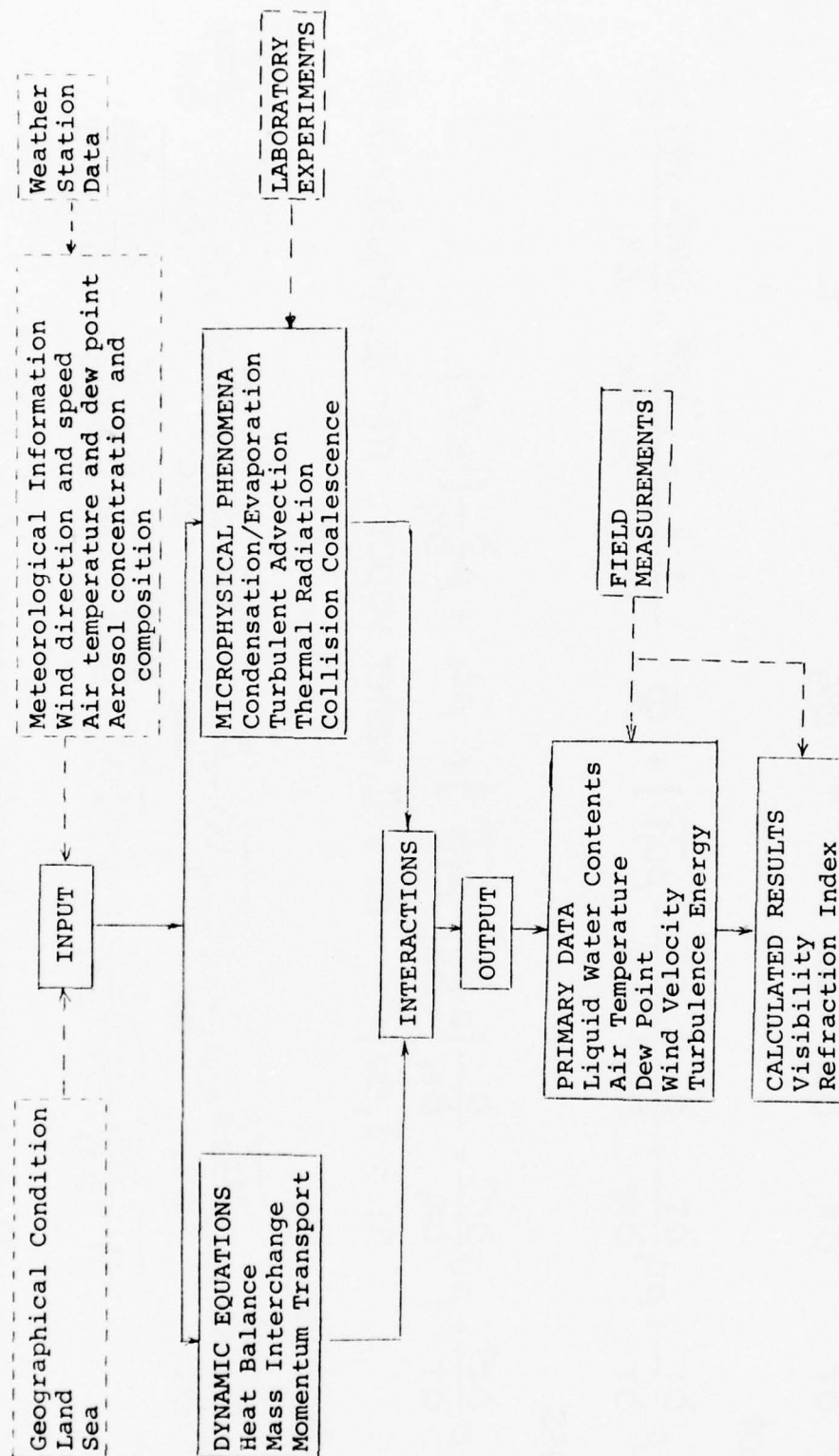
Figure 1. Flow Chart for Marine Fog Analysis

MARINE FOG DYNAMICS

Momentum

$$\rho\frac{\delta u_i}{\delta \tau} + \rho u_j \frac{\delta u_i}{\delta x_j} = \frac{\delta}{\delta x_j}\left[\mu\frac{\delta u_i}{\delta x_j} - \rho\overline{u_i' u_j'}\right] - \frac{\delta p}{\delta x_i} - \epsilon_{ijk}\Omega_j u_k + \frac{\rho g\delta_{i3}}{T_o}\Delta T$$

Heat

$$\rho\frac{\delta T}{\delta \tau} + \rho u_j \frac{\delta T}{\delta x_j} = \frac{\delta}{\delta x_j}\left[\kappa\frac{\delta T}{\delta x_j} - \rho\overline{u_j' T'}\right] + \Phi - \frac{1}{c_p}\left[-L_v \dot{c}_s + \frac{\delta R^{III}}{\delta x_j} + \frac{\delta(R^{I}_4 + R^{II}_4)}{\delta x_j}\right]$$

Mass

$$\rho\frac{\delta c^m}{\delta \tau} + \rho u_j \frac{\delta c^m}{\delta x_j} = \frac{\delta}{\delta x_j}\left[D\frac{\delta c^m}{\delta x_j} - \rho\overline{u_j' c'}\right] + \rho \dot{c}_s + \rho\frac{\delta}{\delta x_j}\left[v_d c^m\right]$$

m = I, air; m = II, water vapor ; m = III, liquid water

Turbulence

$$\rho\frac{\delta \overline{u_i' u_k'}}{\delta \tau} + \rho u_j \frac{\delta \overline{u_i' u_k'}}{\delta x_j} = -\rho\frac{\delta}{\delta x_j}(\overline{u_i' u_j' u_k'}) - \frac{\delta}{\delta x_k}(\overline{p' u_i'}) - \frac{\delta}{\delta x_i}(\overline{p' u_k'}) + \overline{p'\left(\frac{\delta u_i'}{\delta x_k} + \frac{\delta u_k'}{\delta x_i}\right)}$$

$$-\overline{u_j' u_k'}\frac{\delta u_i}{\delta x_j} - \overline{u_j' u_i'}\frac{\delta u_k}{\delta x_j} + \frac{\rho}{T}(\overline{g_i u_k' T'} + \overline{g_k u_i' T'}) + \mu\left(\overline{\frac{\delta u_i' u_k'}{\delta x_j \delta x_j}} - \overline{\frac{\delta u_i'}{\delta x_j}\frac{\delta u_k'}{\delta x_j}}\right)$$

Def. turbulence kinetic energy, $Q = \frac{1}{2}\overline{u_k' u_k'}$

Figure 2   Dynamic Equations

MICROPHYSICAL PROCESSES

Eddy Transport (Pepper & Lee, 1975)

$$K_m = \mu - \rho \overline{w'u'} / \frac{\partial U}{\partial Z} = 0.3 \, \rho \, Q \, \Lambda \left| \frac{\partial U}{\partial Z} \right|$$

$$K_h = \kappa - \rho \overline{w't'} / \frac{\partial T}{\partial Z} = K_m / \sigma_h$$

$$K_c = D - \rho \overline{w'c'} / \frac{\partial c^m}{\partial Z} = K_m / \sigma_c$$

$$K_q = -\rho \overline{w'\left(\frac{P'}{\rho} + Q\right)} / \frac{\partial Q}{\partial Z} = K_m / \sigma_q$$

Radiation Effect (Mack, et al, 1972; Barker, 1973)

$$\frac{\partial R^{III}}{\partial Z} = 1.6 \, \beta \, \sigma \, T_w^4 \, K_\lambda \, C^{III} \, EXP\left[-1.6 K_\lambda \int_Z^{Z_t} C^{III} \, dZ\right]$$

$$R_v^{II}(Zr) = -\sigma \, T_t^4 [1 - \epsilon(Zr, Zt)] - \int_{Zr}^{Zt} \sigma \, T^4 \frac{\partial [1 - \epsilon(Zr, Z)]}{\partial Z} \, dZ$$

$$R_v^{I}(Zr) = \sigma \, T_w^4 [1 - \epsilon(Zr, 0)] + \int_{Zr}^{0} \sigma \, T^4 \frac{\partial [1 - \epsilon(Zr, Z)]}{\partial Z} \, dZ$$

Evaporation Process (Dankerwerts, 1951; Knudson & Katz, 1958)

$$E = \int_0^\infty - D^{II} \left(\frac{\partial c^{II}}{\partial Z}\right)_{Z=0} \frac{1}{\tau} EXP\left[-\frac{\theta}{\tau}\right] d\theta$$

Average contact time $\tau = K_r \dfrac{\mu \, Rex^{0.4}}{\rho U^2}$

Condensation Rate (McDonald, 1963; Asai, 1965)

$$\dot{C}_s = \frac{1}{V} \int \rho U \, c_p \frac{0.622(P_v - P_g) \, R_a T^2}{P \, C_p R_a T^2 + 0.387 L_h^2 P_g} \, dA$$

Precipitation Velocity (Mack, et al, 1972)

$$V_d = 5.3 \times 10^3 \, (W^{III} / N)^{2/3}$$
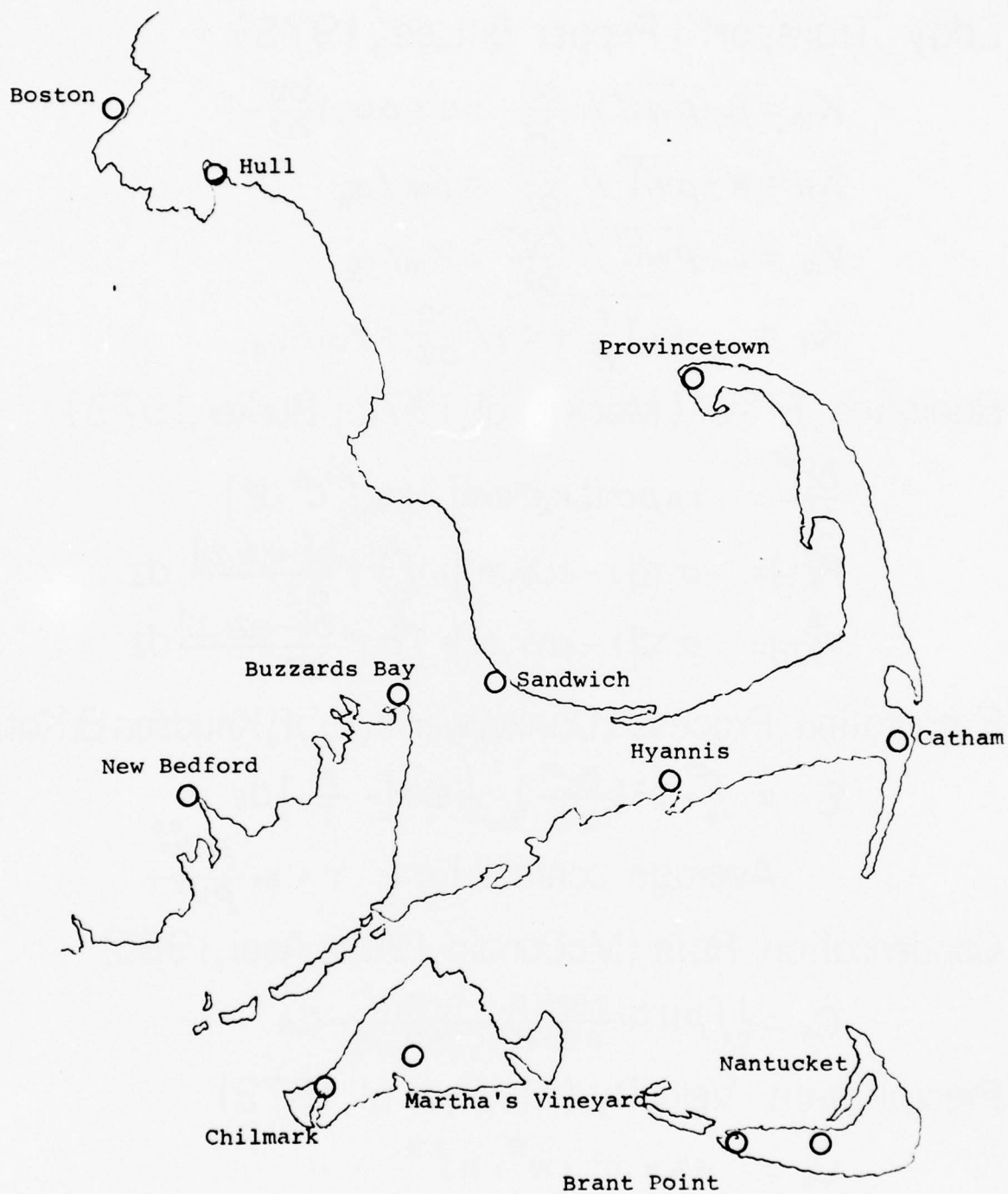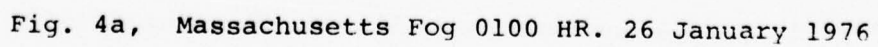
Figure 3   Microphysical Equations

Fig. 4, Weather Stations along Massachusetts Coast

Air Temp. 1°C   Visibility 12 km

Dew Point -1°C ◯—   [Clear]

Wind E SE 10 Knots

Fig. 4a, Massachusetts Fog 0100 HR. 26 January 1976

- 27 -

Air Temp. 6°C   Visibility 0 km

Dew Point 4°C   [Fog]

Wind S 15 Knots

5.0 ⌐ 0.4
3.0 ○ [F]

6.0
[H]

6.5 ○
—

6.0   0.0
—   [F]

8.5   0.0
7.5 ○ [F]

6.5   0.0
3.5 ○ [F]

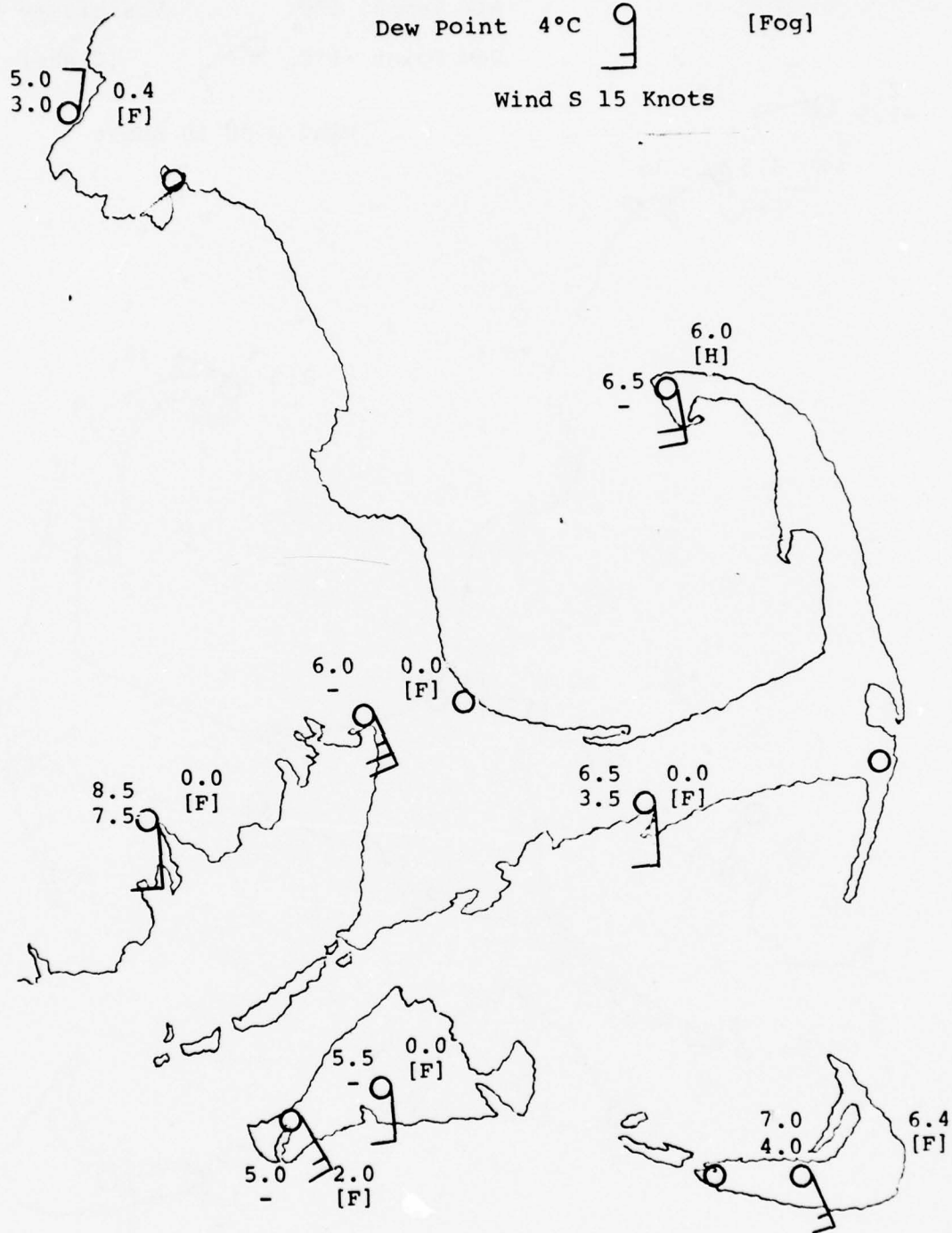5.5   0.0
—   [F]

7.0   6.4
4.0   [F]

5.0   2.0
—   [F]

Fig. 4b, Massachusetts Fog 1500 HR. 26 January 1976

- 28 -

Air Temp. 8°C   Visibility 3 km

Dew Point 7°C   [Fog]

Wind S 15 Knots

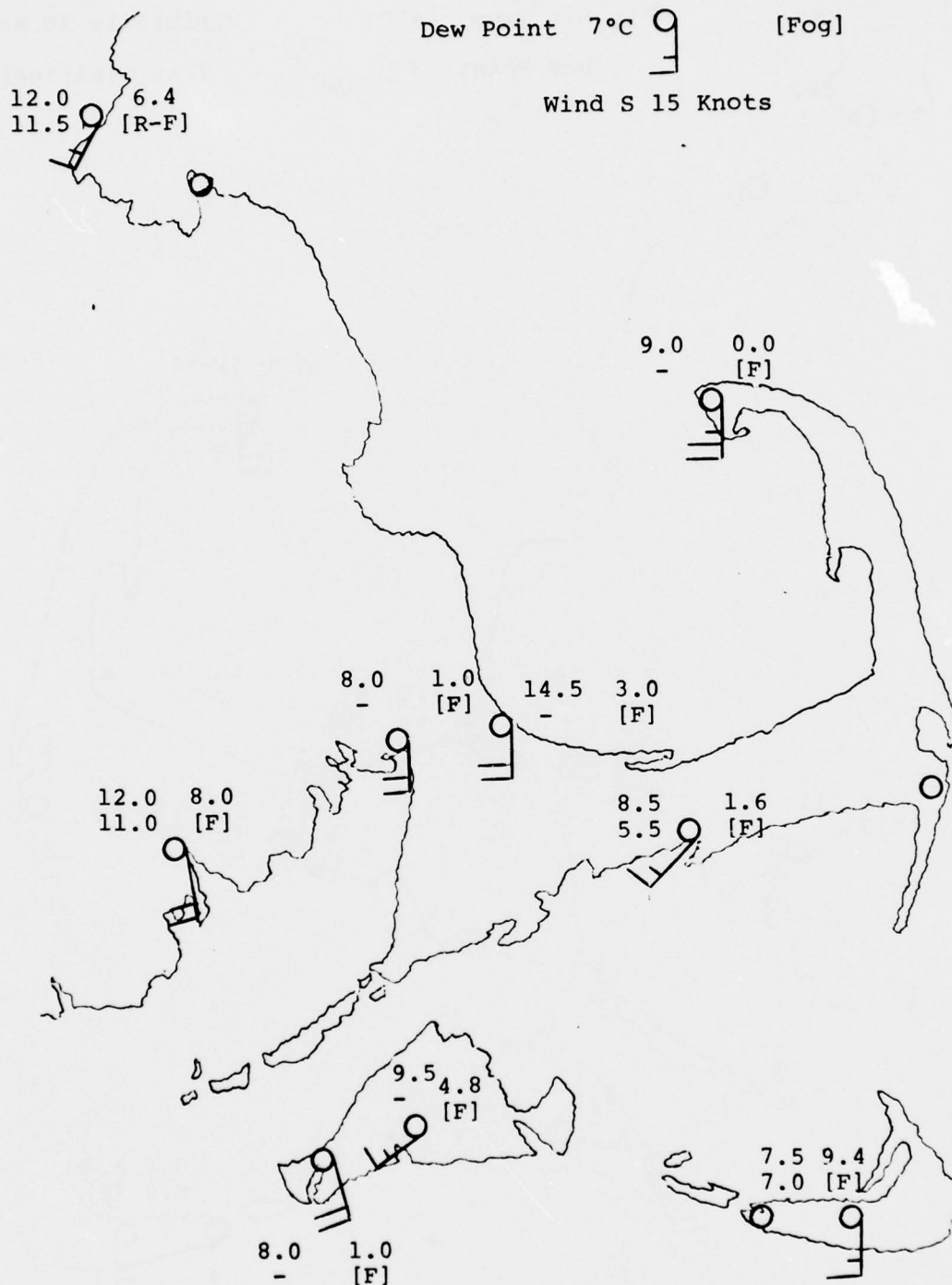12.0   6.4
11.5 [R-F]

9.0   0.0
-     [F]

8.0   1.0
-     [F]

14.5   3.0
-     [F]

12.0   8.0
11.0 [F]

8.5   1.6
5.5 [F]

9.5 4.8
-   [F]

7.5 9.4
7.0 [F]

8.0   1.0
-     [F]

Fig. 4c, Massachusetts Fog 1200 HR. 27 January 1976

Air Temp.   4°C   Visibility 10 km

Dew Point   2°C   [Fog Clearing]

4.5
2.5   29.

3.
11.0 [R-F]
-

2.5   16.   5.5   8.
-                -   [H]

4.0 / 11.   4.5   1.8
2.5   1.5   [F]

4.5   16.
-

9.5 4.8
8.0 [F]

10.0   3.
-      [R]
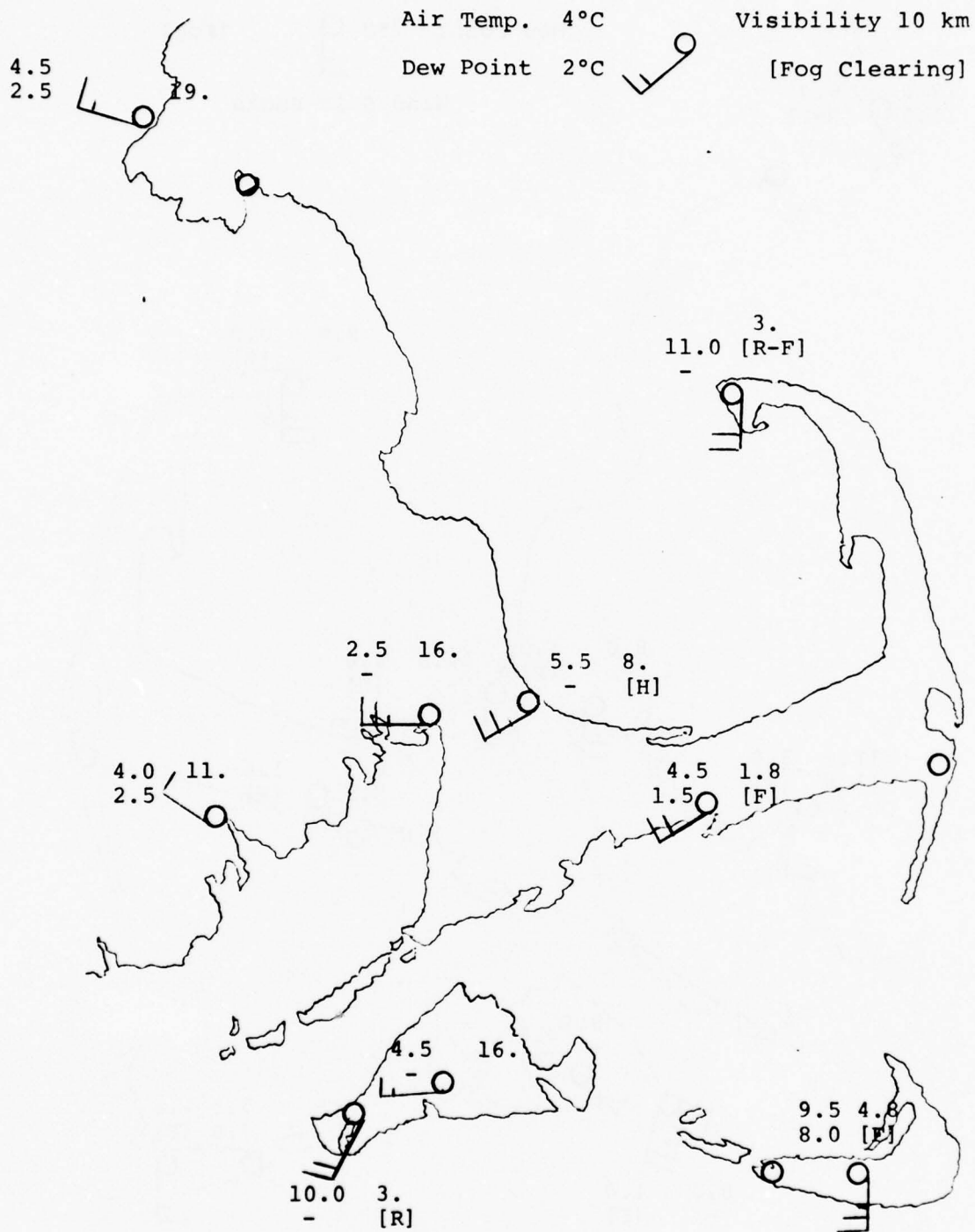
Fig. 4d, Massachusetts Fog 1200 HR. 29 January 1976

- 30 -

Air Temp. 0°C   Visibility 20 km

Dew Point -6°C ⌐⌐─○   [Clear]

Wind W 20 Knots

2.0   24
-5.0

4.5   3.
 ─   [R-F]

0.0   16.
 ─

1.0   13.
 ─

0.0   32.
-6.0

2.0   24.
-6.0
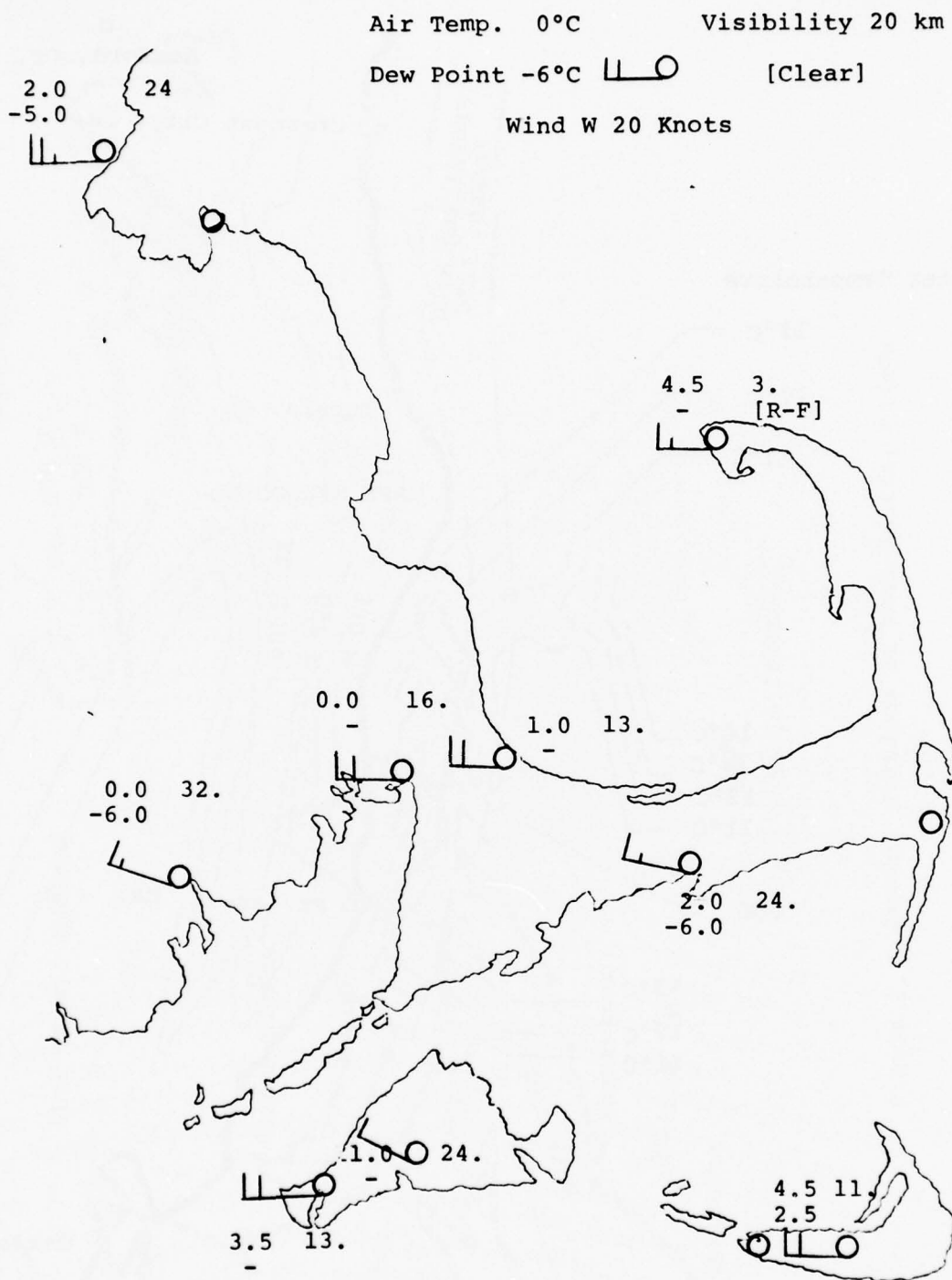
1.0○ 24.
 ─

4.5 11.
2.5

3.5   13.
 ─

Fig. 4e, Massachusetts Fog 1800 HR. 28 January 1976

- 31 -
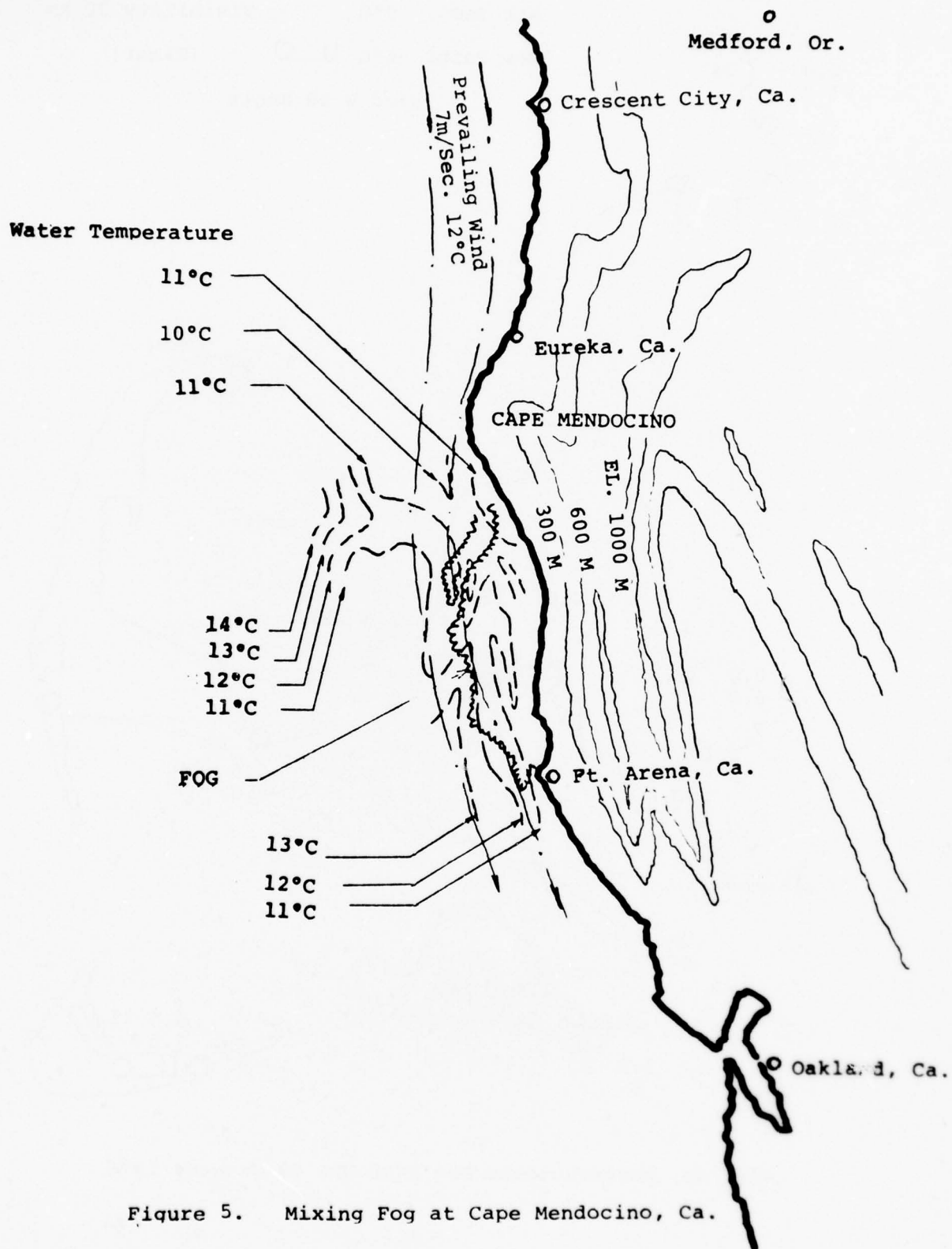
Figure 5.   Mixing Fog at Cape Mendocino, Ca.
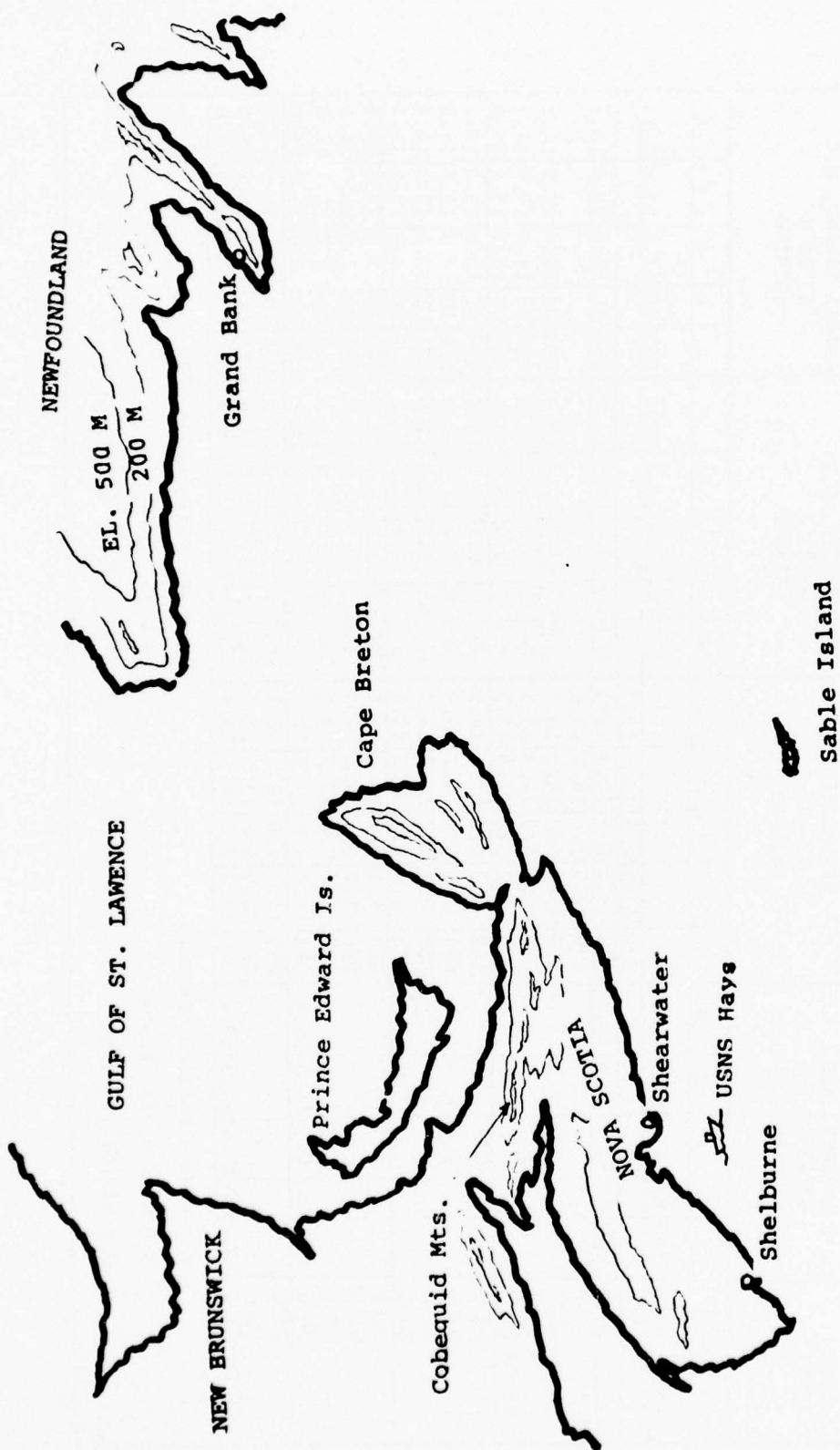
Figure 6. Weather Stations at Nova Scotia, Canada

NEWFOUNDLAND

EL. 500 M
200 M

Grand Bank

GULF OF ST. LAWENCE

Cape Breton

Prince Edward Is.

NEW BRUNSWICK

Cobequid Mts.

NOVA SCOTIA

Shearwater

USNS Hays

Shelburne

Sable Island

TABLE 1

Nova Scotia Fog 2 - 3 August 1975

TIME (LST) MON DAY HR	SHELBURNE, N.S. 43°43'N 65°15'W					USNS-HAYES 43-44N 63-64W					SHEARWATER, N.S. 44°38'N 63°30'W					SABLE ISLAND, N.S. 43°56'N 60°01'W				
	a	b	c	d	e	a	b	c	d	e	a	b	c	d	e	a	b	c	d	e
08 02 0800	200	02	17.4	14.3	13.8						135	04	13.9	14.6	13.4	052	05	17.4	15.6	14.1
1900						156	12.6	6.4	13.8	12.7										
2000	210	03	13.9	16.4	16.1	163	9.8	0.7	13.2	12.3	173	05	20.9	13.9	13.4	082	07	17.4	15.8	14.7
2100						176	6.3	1.2	14.4	13.6	178	02	17.4	13.9	13.4	053	07	17.4	15.5	14.6
2200						122	6.7	5.2	14.7	13.7	⊕	0	0.2	13.7	13.7	059	07	17.4	15.5	14.7
2300						137	6.5	0.9	14.3	13.5	⊕	0	0.4	13.7	13.7	069	08	13.9	15.5	14.8
08 03 0000						130	9.1	2.6	14.4	13.7	⊕	0	0.8	14.7	14.7	073	09	13.9	15.3	14.7
0100						128	5.9	4.6	15.0	14.1	⊕	0	2.2	14.2	14.2	064	10	13.9	15.2	14.6
0200						071	8.6	0.9	14.7	13.9	102	03	0.8	13.9	13.9	058	11	13.9	15.3	14.8
0300						058	8.2	4.7	14.9	14.2	⊕	0	2.2	13.7	13.7	042	09	10.6	15.1	14.7
0400						135	6.6	6.2	14.9	13.6	100	02	2.2	13.9	13.9	043	11	7.0	15.0	14.8
0500						093	18.2	6.5	14.4	13.1	100	03	8.7	14.7	14.5	032	12	7.0	15.2	14.9
0600						096	21.0	6.5	14.0	12.9	054	03	10.4	14.9	14.5	048	15	7.0	15.1	14.8
0700						093	16.7	7.8	14.7	13.3	110	05	10.4	15.5	14.7	048	11	7.0	15.5	15.0
0800	080	04	3.5	15.0	14.8	092	14.7	8.8	13.5	11.9	108	06	12.1	15.8	14.5	058	10	12.1	16.5	15.6
0900						349	11.2	7.0	12.0	10.7	118	07	17.4	17.0	14.9	051	14	13.9	16.4	15.6
1000						*063	8.5	5.6	13.1	12.2	073	05	17.4	15.5	14.5	052	07	1.7	16.1	15.8
08 03 2000	060	08	17.4	15.3	13.2	080	15.2	2.1	14.5	13.8										

(The SHELBURNE column is marked "F O G" across the middle rows.)

a = wind direction, degrees

b = wind speed, knots

c = visibility, Km

d = air temperature, °C

e = dew point, °C

* = 44°54'N 61°21'W

TABLE 2

MARINE FOG MODELING

Dynamic Modeling	Thermodynamic Consideration	Conventional Classification	Observer & Time	Fog Location	Source of Moisture Supply
Boundary Layer Model	Decrease of Local Air Temperature to Dew Point	Tropical-Air fog	Taylor(1917) Summer	Grand Bank Newfoundland Canada	Moisture supply by advection of warm humid air to a cold region
		Advection-sea fog	Stone(1936) Summer	Outer Coast New England USA	
			Emmons(1947) Summer	Off Coast Long Island, NY USA	
			Magono(1972) Summer	Chitose Airport Hokkaido Japan	
	Increase of Local Humidity to Saturation	Steam fog	Kikuchi(1964) Winter Morning	Ishikari Bay Hokkaido Japan	Moisture supply by evaporating from warm water to cold air
		Advection-Radiation fog	George(1940) Autumn Evening	Gulf of Mexico Coast Region USA	
			Mack,et.al.(1972) Evening	California Coast USA	Fog formed by radiative cooling
			USNS Hays 6-8 & 10 Aug.'75	Off Nova Scotia Canada	
Recirculating flow model	Mixing of air masses		R/V ACANIA 25-27 Aug.'74	Cape Mendocino California USA	Moisture supply by evaporation of the ocean surface accelerated by turbulent wind in the recirculating region.
			USNS Hays 2-3 Aug. '75	Nova Scotia Coast Canada	

. Radiation plays an important role in all fog situations, if sufficient moisture is available.
. Moisture supply through spraying and evaporation affected by turbulent wind is yet to be investigat
. Turbulence structure in recirculating flows is not as reasonably established as in boundary layer
  flows.

APPENDIX A

Published Papers Related to

"Collision and Coalescence of

Water Droplets in the Atmosphere"

1. "Transient State Analysis of Separated Flow Around a Sphere",
   International Journal of Computers and Fluids, 1, 235-250, 1973.

2. "Collision Efficiency of Water Drops in the Atmosphere", Journal
   of Atmospheric Science, 32, 1412-1418, 1975.

3. "Collision Efficiency Analyses", Journal of Atmospheric Science, 33,
   873-875, 1976.

4. "The Effect of Vertical Separation on Droplet Collision Efficiency",
   Journal of Atmospheric Science, 33, 1826-1827, 1976.

A1

TRANSIENT STATE ANALYSIS OF SEPARATED FLOW AROUND A SPHERE

C. L. Lin and S. C. Lee

University of Missouri, Rolla, U.S.A.

Abstract—Transient state solutions of the Navier–Stokes equations were obtained for incompressible flow around a sphere accelerating from zero initial velocity to its terminal free falling velocity. By assuming rotational symmetry about the axis in the direction of motion, the Navier–Stokes equations and the continuity equation were simplified in terms of vorticity and stream function. The instantaneous acceleration of the falling sphere was calculated by considering the difference between the gravitational force and the drag force in a transient state. A set of implicit finite difference equations was developed. In order to obtain accurate information around the body, an exponential transformation along the radial direction was used to provide finer meshes in the vicinity of the surface of the sphere. The vorticity equation was solved by an alternating direction implicit (ADI) method while the stream function equation was solved by a successive over-relaxation (SOR) method. Simultaneous solutions were obtained. Transient state solutions were compared with steady state solutions for Reynolds numbers up to 300. Separations first occurred at a Reynolds number 20 for steady state flows and at Reynolds numbers 22·46 and 28·24 for transient state flows with terminal Reynolds numbers of 100 and 300, respectively. Separation angles, sizes of separation regions, and drag coefficients were calculated for both steady and unsteady states. Good agreement was obtained with existing experimental data in the steady state.

NOMENCLATURE

a lattice spacing in radial direction
A location of grid point in the positive z direction
b lattice spacing in angular direction
B location of grid point in the positive θ direction
C location of grid point in the negative z direction
C_D total drag coefficient
C_{DF} drag coefficient due to skin friction
C_{DP} drag coefficient due to surface pressure
d diameter of sphere
D location of grid point in the negative θ direction
g gravitational acceleration
l wake length
0 location of grid point, the origin
p static pressure at surface of sphere
P static pressure in free stream
r radial distance
r_∞ radial distance of outer boundary
R radius of sphere
$(Re)_i$ local Reynolds number
t time

235

A2

$T.R.$ terminal Reynolds number
 U terminal free stream velocity
 U_s local free stream velocity
 z dimensionless radial coordinate
 θ angular spherical coordinate
 Ψ stream function
 ω vorticity
 μ dynamic viscosity
 v kinematic viscosity
 ρ density of the medium
 ρ_s density of the sphere

INTRODUCTION

CURRENT INTEREST in the motions of small particles in the atmosphere has lead to a large number of extensive investigations of flow around spherical bodies. Approximate solutions for steady state laminar flow at very low Reynolds numbers ($Re \leq 1$) have been obtained by Stokes[1] and Oseen[2]. Stokes assumed that the inertia force was negligible. Oseen used a small perturbation technique to linearize the equation of motion. The exact solution to Oseen's linearized equation was obtained by Goldstein[3]. Based on Goldstein's analysis, the flow pattern around a spherical body was then calculated in detail by Tomotika and Aoi[4] and Pearcey and McHugh[5]. Improvement of these analyses was made by Proudman and Pearson[6] for the purpose of covering higher Reynolds number regions. However, from the experimental work of Maxworthy[7], this improvement was found to be valid only for Reynolds numbers below 1·3. In order to analyze the flow patterns in the steady state, where the inertia force cannot be ignored, numerical solutions of the nonlinear Navier–Stokes equations were obtained by Jenson[8] for Reynolds numbers up to 40. With modern computers, Hamielec et al.[9] improved Jenson's analysis for Reynolds numbers up to 100 and Le Clair et al.[10] refined the numerical computation to cover the Reynolds number region up to 400. Le Clair et al.'s results agree well with the empirical relations of Pruppacher and Steinberger[11] and Beard and Pruppacher[12]. Numerical solution of the unsteady state Navier–Stokes equations was obtained by Rimon and Cheng[13]. However, when the steady state was approached, Rimon and Cheng's results differed from those of Le Clair et al. for separation angle in the Reynolds number range between 10 and 20, for surface pressure distributions for all of the cases studied ($Re \leq 300$), and for surface vorticity distributions in the separated flow region for Reynolds numbers greater than 100. Rimon and Cheng's method was used by Shafrir and Tzvi[14], with an improved boundary condition, for terminal Reynolds numbers up to 104. Shafrir and Tzvi's solutions gave closer agreement with Le Clair et al.'s results than those of Rimon and Cheng. Experimental data of Taneda[15] also seems to support Le Clair et al.'s findings. This study was initiated to develop a new method for transient state analysis to evaluate the flow pattern around an accelerating particle of spherical shape.

THEORETICAL ANALYSIS

The governing equations for an incompressible flow around a spherical body with rotational symmetry in the flow direction may be written as follows:

$$E^2\Psi = r \sin\theta\,\omega \tag{1}$$

A3

The question of whether 130 is the critical Reynolds number in a laminar flow around

$T.R.$ terminal Reynolds number
   U terminal free stream velocity
   U_s local free stream velocity
   z dimensionless radial coordinate
   θ angular spherical coordinate
   Ψ stream function
   ω vorticity
   μ dynamic viscosity
   v kinematic viscosity
   ρ density of the medium
   ρ_s density of the sphere

INTRODUCTION

CURRENT INTEREST in the motions of small particles in the atmosphere has lead to a large number of extensive investigations of flow around spherical bodies. Approximate solutions for steady state laminar flow at very low Reynolds numbers ($Re \leq 1$) have been obtained by Stokes[1] and Oseen[2]. Stokes assumed that the inertia force was negligible. Oseen used a small perturbation technique to linearize the equation of motion. The exact solution to Oseen's linearized equation was obtained by Goldstein[3]. Based on Goldstein's analysis, the flow pattern around a spherical body was then calculated in detail by Tomotika and Aoi[4] and Pearcey and McHugh[5]. Improvement of these analyses was made by Proudman and Pearson[6] for the purpose of covering higher Reynolds number regions. However, from the experimental work of Maxworthy[7], this improvement was found to be valid only for Reynolds numbers below 1·3. In order to analyze the flow patterns in the steady state, where the inertia force cannot be ignored, numerical solutions of the nonlinear Navier–Stokes equations were obtained by Jenson[8] for Reynolds numbers up to 40. With modern computers, Hamielec et al.[9] improved Jenson's analysis for Reynolds numbers up to 100 and Le Clair et al.[10] refined the numerical computation to cover the Reynolds number region up to 400. Le Clair et al.'s results agree well with the empirical relations of Pruppacher and Steinberger[11] and Beard and Pruppacher[12]. Numerical solution of the unsteady state Navier–Stokes equations was obtained by Rimon and Cheng[13]. However, when the steady state was approached, Rimon and Cheng's results differed from those of Le Clair et al. for separation angle in the Reynolds number range between 10 and 20, for surface pressure distributions for all of the cases studied ($Re \leq 300$), and for surface vorticity distributions in the separated flow region for Reynolds numbers greater than 100. Rimon and Cheng's method was used by Shafrir and Tzvi[14], with an improved boundary condition, for terminal Reynolds numbers up to 104. Shafrir and Tzvi's solutions gave closer agreement with Le Clair et al.'s results than those of Rimon and Cheng. Experimental data of Taneda[15] also seems to support Le Clair et al.'s findings. This study was initiated to develop a new method for transient state analysis to evaluate the flow pattern around an accelerating particle of spherical shape.

THEORETICAL ANALYSIS

The governing equations for an incompressible flow around a spherical body with rotational symmetry in the flow direction may be written as follows:

$$E^2\Psi = r \sin \theta \, \omega \qquad (1)$$

A3

$$r \frac{\partial \omega}{\partial t} + \frac{\partial \Psi}{\partial r} \frac{\partial}{\partial \theta} \left(\frac{\omega}{r \sin \theta} \right) - \frac{\partial \Psi}{\partial \theta} \frac{\partial}{\partial r} \left(\frac{\omega}{r \sin \theta} \right) = \frac{v}{\sin \theta} E^2 (r \sin \theta \, \omega) \tag{2}$$

where $E^2 = \dfrac{\partial^2}{\partial r^2} + \dfrac{\sin \theta}{r^2} \dfrac{\partial}{\partial \theta} \left(\dfrac{1}{\sin \theta} \dfrac{\partial}{\partial \theta} \right)$;

ω and Ψ are the vorticity and stream function, respectively; (r, θ) and t denote space and time variables, respectively. The instantaneous acceleration of a falling sphere can be obtained from the difference between the gravitational and drag forces:

$$\frac{dU_s}{dt} = \left(1 - \frac{\rho}{\rho_s} \right) g - \frac{3}{8} \frac{\rho}{\rho_s} \frac{U_s^2}{R} C_D \tag{3}$$

Introducing the characteristic quantities of length R and velocity U_s, the stream function, vorticity and the sphere velocity can be non-dimensionalized by

$$\Psi' = \frac{\Psi}{U_s R^2}$$

$$\omega' = \frac{\omega R}{U_s} \tag{4}$$

$$(Re)_s = \frac{2 R U_s}{v}$$

The independent variables t, r and θ then become

$$t' = \frac{t v}{R^2}$$

$$r' = \frac{r}{R} \tag{5}$$

$$\theta' = \theta$$

Since the flow field variations take place more rapidly in the close vicinity of the sphere than in regions at large distances from the sphere, it is convenient to transform the radial coordinate by an exponential function

$$e^z = \frac{r}{R} \tag{6}$$

The non-dimensionalized governing equations then become (dropping the primes for simplicity):

$$\Sigma^2 \Psi - \omega e^{3z} \sin \theta = 0 \tag{7}$$

$$\frac{\partial \omega}{\partial t} + \frac{(Re)_s}{2 e^{2z}} \left[\frac{\partial \Psi}{\partial z} \frac{\partial F}{\partial \theta} - \frac{\partial \Psi}{\partial \theta} \frac{\partial F}{\partial z} \right] - \frac{1}{\sin \theta \, e^{3z}} \Sigma^2 G + \frac{\omega}{(Re)_s} \frac{d(Re)_s}{dt} = 0 \tag{8}$$

$$\frac{d(Re)_s}{dt} = \frac{2 g R^3}{v^2} \left(1 - \frac{\rho}{\rho_s} \right) - \frac{3}{16} \frac{\rho}{\rho_s} (Re)_s^2 C_D \tag{9}$$

A 4

where $F = \dfrac{\omega}{e^z \sin \theta}$

$G = \omega e^z \sin \theta$

$$\Sigma^2 = \frac{\partial^2}{\partial z^2} - \frac{\partial}{\partial z} + \sin \theta \frac{\partial}{\partial \theta} \left(\frac{1}{\sin \theta} \frac{\partial}{\partial \theta} \right)$$

Equations (7), (8) and (9) may be solved *simultaneously* for the stream function, Ψ, the vorticity, ω, and the instantaneous Reynolds number, $(Re)_s$, in terms of the independent variables of t, r and θ.

FINITE DIFFERENCE EQUATIONS

Numerical solutions can be obtained by using central difference and forward difference approximations for the space and time coordinates, respectively. The finite difference equations may be written as follows:

1. *Stream function*

The stream function equation (7) may be written in the following finite difference form, which can be solved by a successive over-relaxation (SOR) method:

$$\Psi_A \lambda_A + \Psi_B \lambda_B + \Psi_C \lambda_C + \Psi_D \lambda_D + \Psi_0 \lambda_0 - (\omega e^{3z} \sin \theta)_0 = 0 \qquad (10)$$

where $\lambda_A = \dfrac{1}{2a} \left(\dfrac{2}{a} - 1 \right)$

$\lambda_B = \dfrac{1}{2b} \left(\dfrac{2}{b} - \cot \theta_0 \right)$

$\lambda_C = \dfrac{1}{2a} \left(\dfrac{2}{a} + 1 \right)$

$\lambda_D = \dfrac{1}{2b} \left(\dfrac{2}{b} + \cot \theta_0 \right)$

$\lambda_0 = 2 \left(\dfrac{1}{a^2} + \dfrac{1}{b^2} \right)$

with $a = \Delta z$ and $b = \Delta \theta$. The subscripts A, B, C, D and 0 refer to the locations of the grid points in space as shown in Fig. 1.

2. *Vorticity*

The vorticity equation (8) may be written as two finite difference equations which can be solved by an alternating directional implicit (ADI) scheme:

(1) The first half time-step, $(n + \frac{1}{2})$, is given in the θ direction as

$$\omega_B{}^{n+\frac{1}{2}} \zeta_B + \omega_0{}^{n+\frac{1}{2}} \zeta_0 + \omega_D{}^{n+\frac{1}{2}} \zeta_D + \zeta = 0 \qquad (11)$$

where $\zeta_B = \dfrac{(Re)_s}{16abe^{3z} \sin \theta_B} \left[\Psi_A{}^{n+1} - \Psi_C{}^{n+1} + \Psi_A{}^n - \Psi_C{}^n \right] - \dfrac{\sin \theta_B}{\sin \theta_0 \, e^{2z}} \left[\dfrac{1}{b^2} - \dfrac{\cot \theta_0}{2b} \right]$

$\zeta_D = - \dfrac{(Re)_s}{16abe^{3z} \sin \theta_D} \left[\Psi_A{}^{n+1} - \Psi_C{}^{n+1} + \Psi_A{}^n - \Psi_C{}^n \right] - \dfrac{\sin \theta_D}{\sin \theta_0 \, e^{2z}} \left[\dfrac{1}{b^2} + \dfrac{\cot \theta_0}{2b} \right]$

A 5

$$\zeta_0 = \frac{2}{\Delta t} + \frac{2}{b^2 e^{2z}}$$

$$\zeta = -\frac{2\omega_0^n}{\Delta t} - \frac{(Re)_s}{16abe^{2z}}[\Psi_B^{n+1} - \Psi_D^{n+1} + \Psi_B^n - \Psi_D^n][F_A^n - F_C^n]$$

$$\qquad - \frac{1}{\sin\theta_0 e^{3z}}\left[\frac{G_A^n - 2G_0^n + G_C^n}{a^2} - \frac{G_A^n - G_C^n}{2a}\right] + \frac{\omega_0^n}{(Re)_s}\left[\frac{d(Re)_s}{dt}\right]^n$$

(2) The second half time-step, $(n + 1)$, is given in the z direction as

$$\omega_A^{n+1}\xi_A + \omega_0^{n+1}\xi_0 + \omega_C^{n+1}\xi_C + \xi = 0 \qquad (12)$$

where $\xi_A = -\dfrac{(Re)_s}{16abe^{3z+a}\sin\theta_0}[\Psi_B^{n+1} - \Psi_D^{n+1} + \Psi_B^n - \Psi_D^n] - \dfrac{1}{e^{2z-a}}\left[\dfrac{1}{a^2} - \dfrac{1}{2a}\right]$

$$\xi_C = \frac{(Re)_s}{16abe^{3z-a}\sin\theta_0}[\Psi_B^{n+1} - \Psi_D^{n+1} + \Psi_B^n - \Psi_D^n] - \frac{1}{e^{2z+a}}\left[\frac{1}{a^2} + \frac{1}{2a}\right]$$

$$\xi_0 = \frac{2}{\Delta t} + \frac{2}{a^2 e^{2z}}$$

$$\xi = -\frac{2\omega_0^{n+\frac{1}{2}}}{\Delta t} + \frac{(Re)_s}{16abe^{2z}}[\Psi_A^{n+1} - \Psi_C^{n+1} + \Psi_A^n - \Psi_C^n][F_B^{n+\frac{1}{2}} - F_D^{n+\frac{1}{2}}]$$

$$\qquad - \frac{1}{\sin\theta_0 e^{3z}}\left[\frac{G_B^{n+\frac{1}{2}} - 2G_0^{n+\frac{1}{2}} + G_D^{n+\frac{1}{2}}}{b^2} - \cot\theta_0\frac{G_B^{n+\frac{1}{2}} - G_D^{n+\frac{1}{2}}}{2b}\right]$$

$$\qquad + \frac{\omega_0^{n+\frac{1}{2}}}{(Re)_s}\left[\frac{d(Re)_s}{dt}\right]^n$$

The superscripts n, $n + \frac{1}{2}$ and $n + 1$ designate the present, the first-half and the second-half time steps, respectively. The term $(d(Re)_s/dt)^n$ denotes the slope of the instantaneous Reynolds number at the present time step and $(Re)_s$ is the average value of $(Re)_s^n$ and $(Re)_s^{n+1}$.
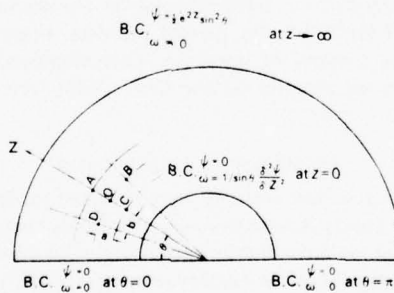
· Fig. 1. Schematic diagram for boundary conditions and nomenclatures used in finite difference equations.

A6

3. *Instantaneous Reynolds number*

The instantaneous Reynolds number can be calculated by using two successive numerical techniques as given by Conte[16].

(1) The Reynolds number at the $(n + 1)$th time step may be estimated by the Adams–Bashforth prediction formula:

$$(Re)_s^{n+1} = (Re)_s^n + \frac{\Delta t}{24} [55f^n - 59f^{n-1} + 37f^{n-2} - 9f^{n-3}] \qquad (13)$$

(2) The estimation may then be refined by the Adams–Moulton correction formula:

$$(Re)_s^{n+1} = (Re)_s^n + \frac{\Delta t}{24} [9f^{n+1} + 19f^n - 5f^{n-1} + f^{n-2}] \qquad (14)$$

where f^n denote the slope of the instantaneous Reynolds number at the nth time step.

BOUNDARY CONDITIONS

The initial condition is given such that the sphere begins to fall when the surrounding medium is not yet disturbed:

$$t = 0: \qquad \Psi = 0, \qquad \omega = 0, \qquad (Re)_s = 0, \qquad \text{everywhere} \qquad (15)$$

The boundary conditions are such that, for all time intervals, the axis of symmetry remains undisturbed; the surface velocity is zero; and the free stream denotes a uniform flow velocity for the sphere. The dimensionless form of the boundary conditions, as shown schematically in Fig. 1, may be written as:

$$0 < t < \infty: \qquad \Psi = 0, \qquad \omega = 0, \qquad \text{at } \theta = 0 \text{ for all } z$$

$$\Psi = 0, \qquad \omega = 0, \qquad \text{at } \theta = \pi \text{ for all } z$$

$$\Psi = 0, \qquad \omega = \frac{1}{\sin \theta} \frac{\partial^2 \Psi}{\partial z^2}, \qquad \text{at } z = 0 \text{ for all } \theta$$

$$\Psi = \tfrac{1}{2} e^{2z} \sin^2 \theta, \qquad \omega = 0, \qquad \text{at } z \to \infty \text{ for all } \theta \qquad (16)$$

Numerical solutions may then be obtained by solving the stream function equation, the vorticity equation and the Reynolds number equation *simultaneously* for a given size sphere falling from zero initial velocity to its terminal velocity. No special problems were encountered in applying the ADI method to the present problem, either in the interior or at the boundaries. However, the amount of computer time employed, while modest for low Reynolds number (five to ten minutes on the CDC 7600) increases substantially at the larger Reynolds numbers.

NUMERICAL SOLUTIONS

Solutions for stream function and vorticity were obtained for both steady and unsteady states. Figure 2 shows the steady state solutions for Reynolds numbers of 5, 20, 40, 100, 200 and 300. It can be seen that the recirculation region begins to develop at Reynolds number 20 and increases its size as the Reynolds number increases. Moreover, the vorticity gradient increases very rapidly with Reynolds numbers at the surface of the sphere. Figure 3 shows the transient state solutions for a falling sphere at terminal Reynolds numbers (T.R.) of 100
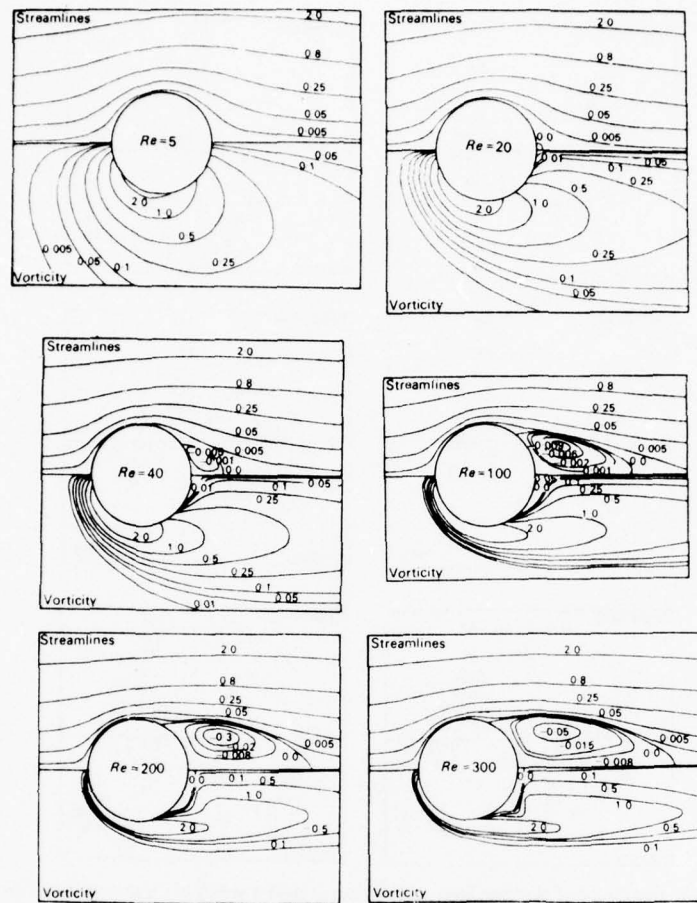
Fig. 2. Distributions of streamlines and vortices around a sphere for steady state flow.

and 300, with local Reynolds numbers $(Re)_s$ of 5, 40 and 90. It is noted that, at the same local Reynolds number, the recirculating region at $T.R. = 100$ is larger than that at $T.R. = 300$. Comparison between the steady state and the transient state solutions is shown in Fig. 4. It is evident that a smaller recirculating region occurs in accelerating flow in comparison with the fully developed steady state flow at the same local Reynolds number.

DRAG EVALUATION

The drag force of a falling sphere consists of the skin friction drag and pressure drag: The skin friction drag coefficient can be calculated through the vorticity as:

$$C_{DF} = \frac{8}{(Re)_s} \int_0^\pi \omega|_{z=0} \sin^2 \theta \, d\theta \tag{17}$$

A8

C. L. Lin and S. C. Lee
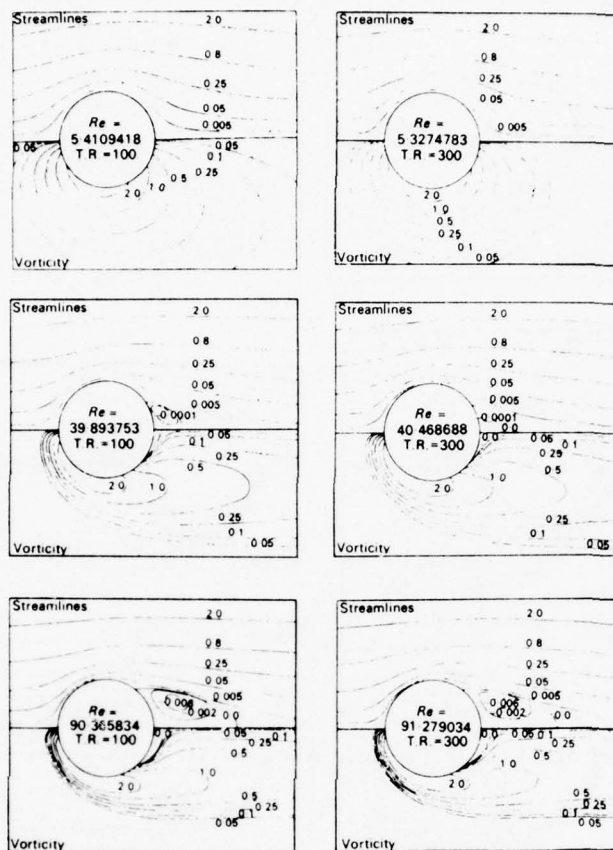
Fig. 3. Distributions of streamlines and vortices around a sphere for transient state flow.

The pressure drag coefficient can be obtained through the vorticity and stream function as:

$$C_{DP} = \int_0^\pi \frac{p - P}{\frac{1}{2}\rho U_s^2} \sin 2\theta \, d\theta \qquad (18)$$

where

$$\frac{p - P}{\frac{1}{2}\rho U_s^2} = 1 + \frac{4}{(Re)_s} \left\{ \int_0^\infty \left[2 \frac{\partial \omega}{\partial \theta}\bigg|_{\theta=0} + \frac{1}{(Re)_s} \frac{\partial}{\partial t} \left(e^z (Re)_s \left(1 - \frac{1}{e^{2z} \sin \theta} \frac{\partial \Psi}{\partial \theta}\bigg|_{\theta=0} \right) \right) \right] dz \right.$$
$$\left. + \int_0^\theta \left(\frac{\partial \omega}{\partial z} + \omega \right)\bigg|_{z=0} d\theta + \frac{1 - \cos \theta}{(Re)_s} \frac{d(Re)_s}{dt} \right\}$$

Figures 5 and 6 show the vorticity and pressure distributions, respectively, at the surface of the sphere at various local Reynolds numbers for both steady state and unsteady state

A9
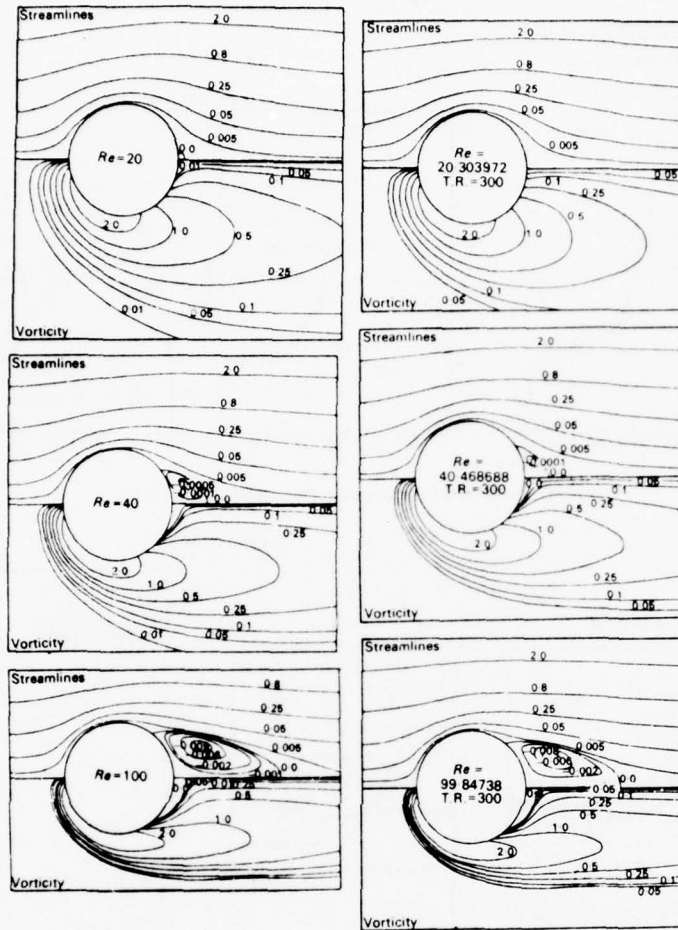
Fig. 4. Comparisons of streamlines and vortices around a sphere between steady state flow and transient state flow.

flows. The total drag coefficient, as shown in Fig. 7, was calculated by summing the skin friction drag and the pressure drag. It can be seen that the drag coefficient in the steady state agrees well with existing experimental data as given by Schlichting[17]. An empirical relation for the steady state drag coefficient is proposed as:

$$C_D = \frac{24}{Re} [1 + 0.2207\, Re^{1/2} + 0.0125\, Re],\qquad(19)$$

for Reynolds numbers up to 1000. Available formulae for calculating the drag coefficient are listed in Table 1 for reference. Transient state drag coefficients were also calculated for terminal Reynolds numbers of 100 and 300 and are shown by broken lines in Fig. 7.

A10
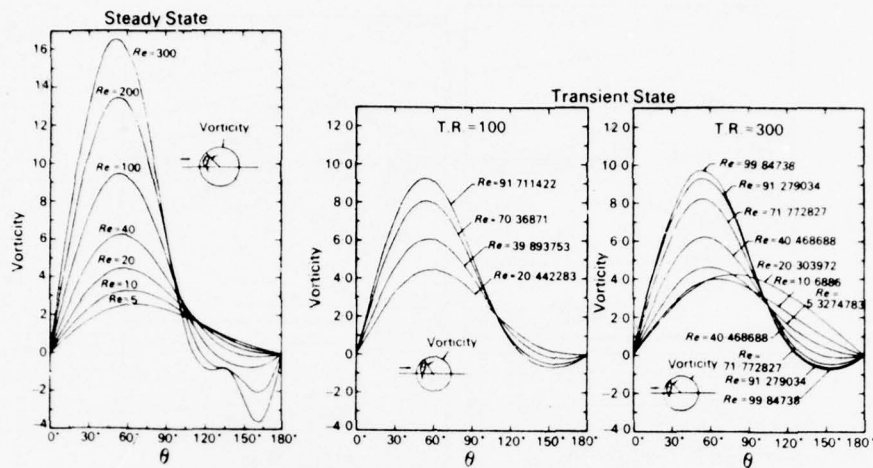
Fig. 5. Vorticity distributions on the surface of a sphere.
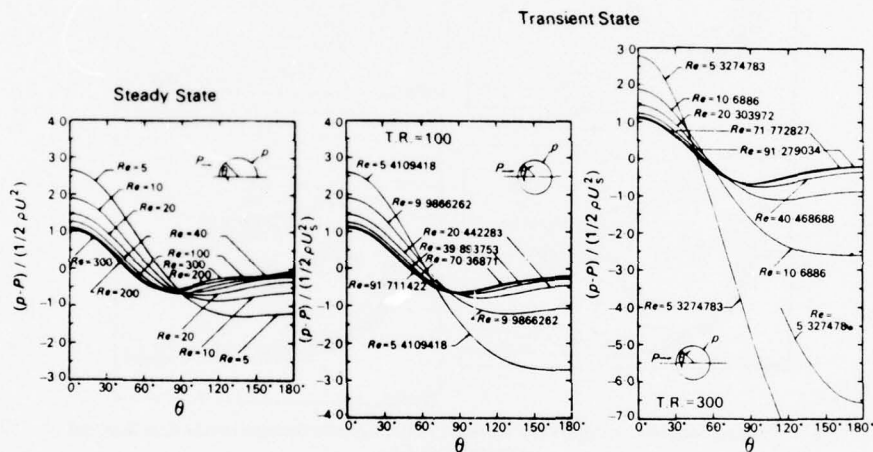
Fig. 6. Pressure distributions on the surface of a sphere.

FLOW SEPARATION

Comparisons with experimental data for separation angle and wake length are shown in Figs. 8 and 9, respectively. The steady state solutions indicate that flow separation occurs at a Reynolds number of 20. The unsteady solutions indicate that separation occurs at Reynolds numbers 22·46 and 28·24 for terminal Reynolds numbers of 100 and 300, respectively. Taneda reported that oscillations of the separated flow region were observed for terminal Reynolds numbers greater than 130. Preliminary results of the numerical solutions also indicated some oscillatory behavior; however this was later confirmed to be the result of numerical instability.

A11

Table 1. Formulae for calculating steady state drag coefficient

Name	Year	Drag coefficient, C_D	Reynolds no.
Stokes	1851	$\dfrac{24}{Re}$	$Re \approx 0$
Osen	1910	$\dfrac{24}{Re}\left[1 + \dfrac{3}{16}Re\right]$	$Re \leq 1$
Goldstein	1929	$\dfrac{24}{Re}\left[1 + \dfrac{3}{16}Re - \dfrac{19}{1280}Re^2 + \dfrac{71}{20480}Re^3 - \dfrac{30179}{34406400}Re^4 + \dfrac{122519}{560742400}Re^5\right]$	$Re \leq 1$
Proudman and Pearson	1957	$\dfrac{24}{Re}\left[1 + \dfrac{3}{16}Re + \dfrac{9}{160}Re^2 \ln(Re/2)\right]$	$Re \leq 1\cdot3$
		$\dfrac{24}{Re}[1 + 0\cdot102\, Re^{0\cdot95}]$	$0\cdot001 \leq Re \leq 2$
Pruppacher and Steinberger	1968	$\dfrac{24}{Re}[1 + 0\cdot115\, Re^{0\cdot80}]$	$2 < Re \leq 10$
		$\dfrac{24}{Re}[1 + 0\cdot102\, Re^{0\cdot955}]$	$0\cdot2 \leq Re \leq 2$
Beard and Pruppacher	1969	$\dfrac{24}{Re}[1 + 0\cdot115\, Re^{0\cdot802}]$	$2 < Re \leq 20$
		$\dfrac{24}{Re}[1 + 0\cdot189\, Re^{0\cdot632}]$	$20 < Re \leq 200$
Present result		$\dfrac{24}{Re}[1 + 0\cdot2207\, Re^{1/2} + 0\cdot0125\, Re]$	$1 \leq Re \leq 1000$
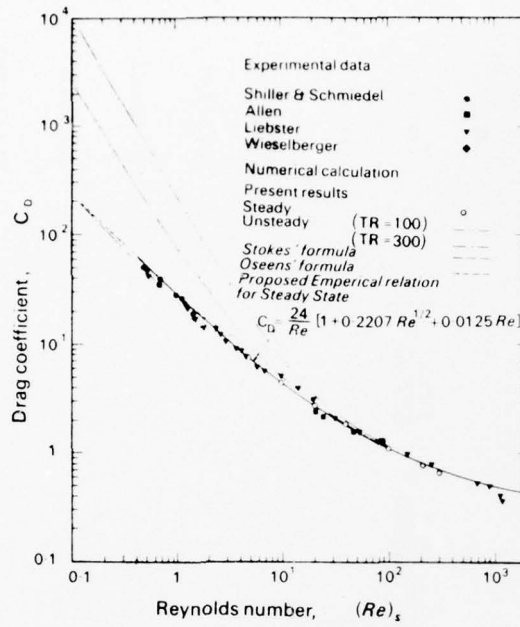
Fig. 7. Drag coefficient vs. Reynolds number for a sphere.
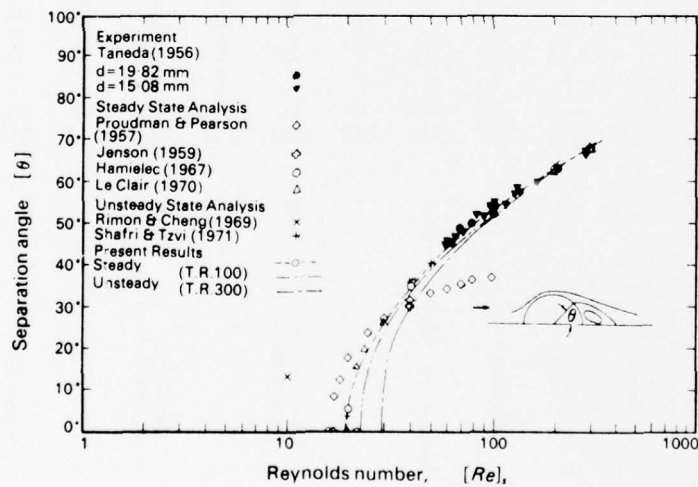
Fig. 8. Separation angle vs. Reynolds number around a sphere.

A13
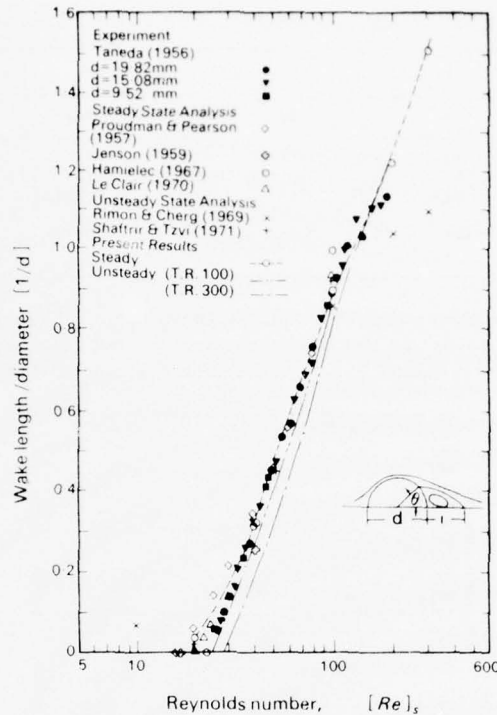
Fig. 9. Wake length vs. Reynolds number around a sphere.

EFFECTS OF STEP SIZE AND OUTER BOUNDARY ON NUMERICAL CALCULATIONS

Numerical instability usually leads to divergence of the numerical solution. However, under certain conditions an unstable or oscillatory solution may be misinterpreted as describing a physical phenomenon. The transient state analysis for separated flow around a sphere is one such example. In this case, the oscillation is largely due to the choice of step size.

The grid sizes Δz, $\Delta\theta$, Δt are considered to be sufficiently small, when a decrease of the step size no longer affects the solution, viz., to some prescribed tolerance. Table 2 shows the mesh sizes chosen in this study. It is necessary to point out that the required mesh size can be a function of the terminal Reynolds number. The mesh sizes of $\Delta z = 0 \cdot 1$ and $\Delta\theta = 6°$ were originally chosen for all Reynolds numbers and stable solutions were reached for all cases with terminal Reynolds numbers less than 100. However, at terminal Reynolds numbers of 200 and 300, the calculated flow patterns in the wake region of the sphere fluctuated within certain finite limits. The dashed lines in Fig. 10 depict the variation of wake length and separation angle, with respect to time, at various terminal Reynolds numbers ranging between 40 and 300. Experimental data obtained by Taneda[17] also

Table 2. Step sizes and outer boundaries used in numerical computations

				Re			
	5	10	20	40	100	200	300
a	0·1	0·1	0·1	0·1	0·05	0·03	0·03
b	6°	6°	6°	6°	6°	3°	3°
t	0·01	0·01	0·02	0·03	0·03	0·002–0·03	0·001–0·03
$\dfrac{r_\infty}{R}$	54·6	54·6	54·6	20·08	14·88	12·43	12·43

showed such an oscillatory motion at terminal Reynolds numbers larger than 130. In order to have a reasonable assurance that this phenomenon was not caused by numerical instability, the mesh size was reduced to $\Delta z = 0.03$ and $\Delta \theta = 3°$. The solid lines in Fig. 10 show
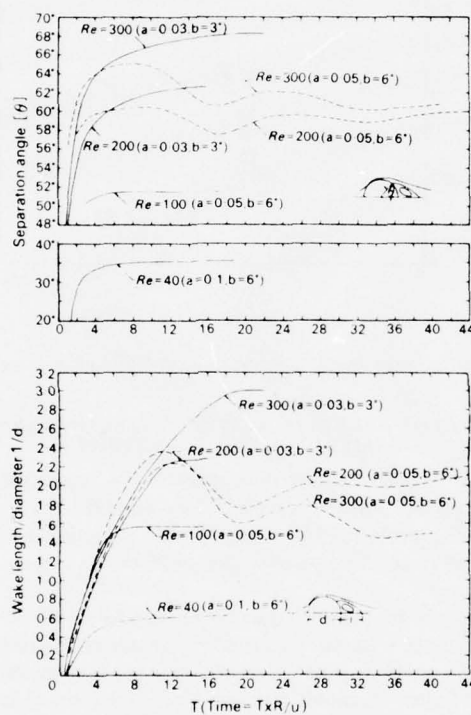
Fig. 10. Effects of step sizes on numerical instability at steady state.
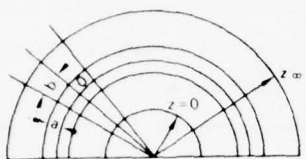
that the solutions are stable even for the cases with terminal Reynolds numbers of 200 and 300 if the mesh sizes are sufficiently small. It is therefore necessary to conclude that the oscillatory phenomenon obtained in the present solution with larger values of Δz and $\Delta \theta$ is due to numerical instability.

A15

The question of whether 130 is the critical Reynolds number in a laminar flow around a sphere cannot be answered in this study; the analysis assumes rotational symmetry which may prevent the development of a realistic asymmetric flow pattern. It is felt that the critical Reynolds number can only be determined numerically by analyzing the complete three dimensional transient flow field around a spherical body.

The accuracy of the numerical solution is also affected by the location of the outer boundary. Theoretically, the limit of the outer boundary is at infinity. Unfortunately, such a limit cannot be used in numerical computations. Some large but finite distance from the sphere therefore has to be assumed. The distance is determined in such a way that further increases in the outer boundary do not affect the solution. Table 3 indicates the effect on the

Table 3. Effect of outer boundary on steady state drag calculations

$Re = 5-40$: $a = 0\cdot1$, $b = 6°$
$Re = 100$: $a = 0\cdot05$, $b = 6°$

| | Re | | | | | | | |
	5		20		40		100	
Z_∞	1·8	4	1·8	4	1·8	3	1·8	2·7
$\dfrac{r_\infty}{R}$	6·049	54·598	6·049	54·598	6·049	20·086	6·049	14·880
C_{DP}	2·8687	2·5172	1·1012	1·0195	0·7230	0·6744	0·5243	0·4969
C_{DF}	5·5002	4·8751	1·8872	1·7848	1·1811	1·1303	0·6679	0·6180
C_D	8·3689	7·3923	2·9884	2·8043	1·9041	1·8047	1·1922	1·1149

solution of the choice of the outer boundary location. As the Reynolds number increases, the effect of the outer boundary, on the accuracy of the numerical solution, gradually decreases while the effect of decreasing step size becomes more important.

CONCLUSION

A transient state analysis has been formulated for separated flow around a sphere. The analytical results agree well with available experimental data and other analytic solutions when the steady state is approached. The transient development of the separation region is found to be a function of the local Reynolds number. In the steady state, flow separation occurs at a Reynolds number of 20. In the transient, flow separation occurs at local Reynolds numbers of 22·46 and 28·24 for accelerating spheres with terminal Reynolds numbers of 100 and 300, respectively.

The drag coefficient of a sphere moving at a constant velocity is usually determined from an empirical formula. Based on the comparison between analytical and experimental results, a simple relation is obtained for calculating the drag coefficient of a sphere moving uniformly. This expression applies in the Reynolds number range between one and one thousand.

A16

The critical Reynolds number for laminar instability could not be determined. With the assumption of rotational symmetry it was not possible to confirm the experimental observation that laminar instability occurs at a critical Reynolds number of approximately 130.

REFERENCES

1. G. G. Stokes, On the effect of the internal friction of fluids on the motion of pendulums, *Camb. Phil. Trans.* **9**, 8 (1851).
2. C. W. Oseen, Uber die Stokessche Formel und uber die verwandte Aufgabe in der Hydrodynamik, *Arkiv for Mathematik, Astronomi och Fys.* **6**, No. 29 (1910).
3. S. Goldstein, The forces on a solid body moving through viscous fluid, *Proc. Roy. Soc.*, Lond. **A123**, 216 (1929).
4. S. Tomotika and T. Aoi, The steady flow of viscous fluid past a sphere and circular cylinder at small Reynolds numbers, *Quart. J. Mech. Appl. Math.* **3**, 140 (1950).
5. T. Pearcey and B. McHugh, Calculation of viscous flow around spheres at low Reynolds numbers, *Phil. Mag.* **46**, 783 (1955).
6. I. Proudman and J. R. A. Pearson, Expansions at small Reynolds numbers for the flow past a sphere and a circular cylinder, *J. fluid Mech.* **2**, 237 (1957).
7. T. Maxworthy, Accurate measurement of sphere drag at low Reynolds numbers, *J. fluid Mech.* **23**, 369 (1965).
8. V. G. Jenson, Viscous flow round a sphere at low Reynolds numbers ($Re \leq 40$), *Proc. Roy. Soc.*, Lond. **A249**, 346 (1959).
9. A. E. Hamielec, T. W. Hoffman and L. L. Ross, Numerical solution of the Navier–Stokes equation for flow past spheres, *A.I. Chem. Eng. J.* 212 (1967).
10. B. P. LeClair, A. E. Hamielec and H. R. Pruppacher, A numerical study of the drag on a sphere at low and intermediate Reynolds numbers, *J. atmos. Sci.* **27**, 308 (1970).
11. H. R. Pruppacher and E. R. Steinberger, An experimental determination of the drag on sphere at low Reynolds number, *J. appl. Phys.* **39**, 9, 4129 (1968).
12. K. V. Beard and H. R. Pruppacher, A determination of the terminal velocity and drag of small water drops by means of a wind tunnel, *J. atmos. Sci.* **26**, 1066 (1969).
13. Y. Rimon and S. I. Cheng, Numerical solution of a uniform flow over a sphere at intermediate Reynolds number, *Phys. Fluids* **12**, 949 (1969).
14. U. Shafrir and G. C. Tzvi, A numerical study of collision efficiencies and coalescence parameters for droplet pairs with radii up to 300 microns, *J. atmos. Sci.* **28**, 741 (1971).
15. S. Taneda, Studies on wake vortices: Experimental investigation of the wake behind a sphere at low Reynolds numbers, *Rep. Res. Inst. appl. Mech., Kyushu Univ.* **4**, 16, 99 (1956).
16. S. D. Conte, *Elementary Numerical Analysis.* McGraw-Hill, New York (1965).
17. H. Schlichting, *Boundary Layer Theory*, 6th Edn. McGraw-Hill, New York (1968).

Collision Efficiency of Water Drops in the Atmosphere

C. L. LIN AND S. C. LEE

*Department of Mechanical and Aerospace Engineering and Graduate Center for Cloud Physics Research,
University of Missouri-Rolla 65401*

A18

Collision Efficiency of Water Drops in the Atmosphere

C. L. Lin and S. C. Lee

*Department of Mechanical and Aerospace Engineering and Graduate Center for Cloud Physics Research,
University of Missouri-Rolla 65401*

ABSTRACT

A study has been made of the growth through collision of water drops in the atmosphere. The method of superposition of flow fields obtained from the numerical solution of the Navier-Stokes equations was used for the calculations, and only inertia, gravity and drag force were considered.

The calculated linear collision efficiency is significantly less than the geometric collision efficiency between a large collector drop and a small collecting drop because of the effect of hydrodynamic forces. The linear collision efficiency is substantially higher than the geometric collision efficiency between similarly sized drops because of the wake effect.

To verify the validity of the calculations, the analytical results were compared with available experimental data. Satisfactory agreement was obtained for most drop sizes. It is concluded that in the absence of electricity and turbulence the dominant factor in the formation of precipitation is the collisional growth of similarly sized drops.

1. Introduction

The method of growth of water drops in the atmosphere can be classed as two types: condensational and collisional. Condensational growth, in which water vapor condenses on atmospheric aerosols, is the dominant mechanism for the growth of water drops with radii $\leq 20 \, \mu m$. The Wegener-Bergeron-Findeisen process, in which the ice crystal is growing at the expense of supercooled water droplets in clouds as discussed in standard textbooks such as Fleagle and Businger (1970), is also considered as condensational growth of ice crystals. Collisional growth, in which accretion processes operate, is responsible for the growth of water drops with radii $> 20 \, \mu m$. This study is concerned with the collisional growth of water drops, because it is directly related to the understanding of the precipitation phenomenon in clouds as well as to the scavenging process of pollutants.

Analytical studies of collisional efficiency have been made by using modified Stokes flow solutions, modified Oseen flow solutions, or available numerical solutions of the Navier-Stokes equations. Owing to the nonlinear nature of the flow field surrounding a relatively large drop, which is responsible for the collisional growth, considerable discrepancy occurs in the literature for the calculated collision efficiency. Extensive effort has been made to improve the calculation procedures for collision efficiency by improving the empirical relations for drag coefficients. Based on an improved method developed by Lin and Lee (1973) for flow field calculations, this study shows that the unsatisfactory flow field surrounding a moving water drop is responsible for the high order of magnitude of the discrepancy in collision efficiency, while the improvement of drag formulas can only account for a very small percentage of the discrepancy existing in the literature.

2. Historical background

Collision takes place when one moving drop (or collector drop), whose movement is caused by gravitational or other forces, collides with other drops (or collecting drops) which happen to be in its path. To examine the probability of collision, the following equation for linear collision efficiency is used:

$$Y_c = y_c/R. \qquad (1)$$

Here R is the radius of the collector drop, and y_c is the radius of the collisional cross-sectional area within which any collecting drop of radius r will collide with the collector drop. Fig. 1 shows schematically the nomenclature used in this study. Ideally, the collisional cross-sectional radius should be equal to the sum of the radii of the collector and the collecting drops if the drops are not surrounded by air. The nondimensionalized form of this ideal collision cross-sectional radius is known as the geometric collision efficiency. However, as a result of the forces generated by the relative motion between the water drop and the air, laboratory observations of linear collision efficiency often differ substantially with the geometric collision efficiency. These phenomena were reported by Telford *et al.* (1955), Schotland and Kaplin (1956), Telford and Thorndike

(1961), Woods (1965), and Beard and Pruppachar (1968). To understand the physical processes of the collisional growth of water drops, many investigators have conducted theoretical studies along one or the other of the following two approaches.

a. Evaluation of forces between two drops

Hocking (1959) analyzed the Stokes equations and calculated the force exerted between two drops to determine collision efficiency. Davis and Sartor (1967) and Hocking and Jonas (1970) extended Hocking's approach to include rotation of the water drops. However, because they assumed that the inertial force is negligibly small in Stokes equations, their approach can only apply to cases of practically zero Reynolds number (Re≈0). For freely falling water drops in a standard atmosphere, the drop sizes and terminal falling velocities vs Reynolds numbers are shown in Fig. 2. It can be seen that a 30 μm drop has a free fall velocity of 10 cm s^{-1} that corresponds to a Reynolds number of 0.4. The effect of inertial force on collision efficiency was considered by Klett and Davis (1973) using a modified Oseen's equation made by Carrier (1953). Their results indicated that the collision efficiency is considerably larger for approximately equal size drops. However, due to the inherital limitation of the Oseen's equation, this method is only valid for relatively small drops.

b. Superposition of flow field

Langmuir (1948) suggested that the flow field around a single drop could be superposed on the flow field of another drop to determine the relative motion between the two drops. Pearcey and Hill (1956) developed this approach by using Goldstein's (1929) solution of Oseen's (1910) linearized equations for flow around a spherical drop at a very low Reynolds number (Re<1). Shafrir and Neiburger (1963), Shafrir (1965) and Neiburger (1967) improved the superposition approach by using Jenson's (1959) method to obtain solutions of the Navier-Stokes equations for an intermediate Reynolds number range (Re<20). Shafrir and Tzvi (1971) extended the Reynolds number range (Re<104) by using Rimon and Cheng's (1969) method with a modified boundary condition. Beard and Grover (1974) utilized the flow field calculated by LeClair et al. (1970), and obtained the collision efficiency for raindrops colliding with micron size particles. Since the particle is assumed much smaller than the raindrops, the existence of the particle does not alter the flow field around the raindrop (collector). Consequently, no superposition is necessary if the radius ratio between the particle and the raindrop is less than 10%.

A brief summary of the literature is shown in Fig. 3. It is noted that the collision efficiency determined from existing theories does not seem to be consistent. For example, the calculated collision efficiency between a
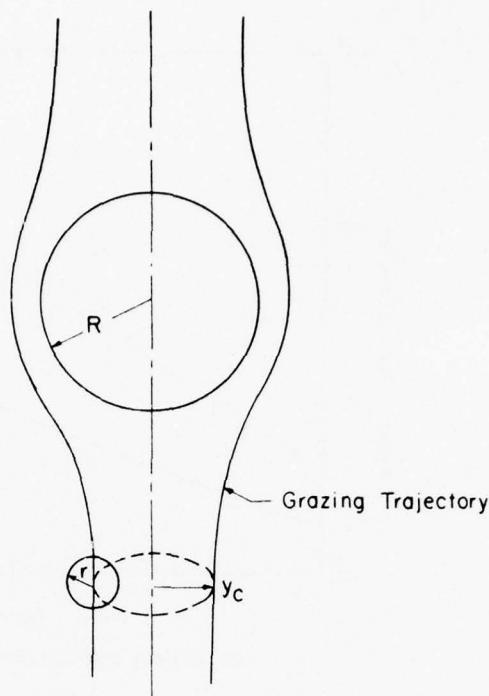

FIG. 1. Nomenclature.

20 μm collector drop and a 19 μm collecting drop varies from 0 to 2. To resolve some of these discrepancies, the available literature was re-examined. Hocking's approach, which appears to be limited to very small drops, is not practical when applied to pollutant scavenging and weather modification. Langmuir's approach does not appear to have any size restriction for most atmospheric applications provided that the solution of the Navier-Stokes equations can be accurately determined. The availability of high-speed digital computers makes it possible both scientifically and economically to meet this requirement. Le Clair et al. (1970) and Lin and Lee (1973) obtained numerical solutions for flows around spherical drops at steady and transient states, respectively. The accuracy of their solutions has been verified by experimental data on drag coefficients, separation angles, and wake lengths. This study uses Langmuir's approach by superpositioning the flow fields obtained from Lin and Lee's (1973) numerical solution of the Navier-Stokes equations.

3. Analysis

Water drops in the atmosphere may be influenced by many parameters, such as gravity, inertia, turbulence, updraft and electrical charge. To understand the significance of each parameter on droplet growth, laboratory experiments have to be conducted in a
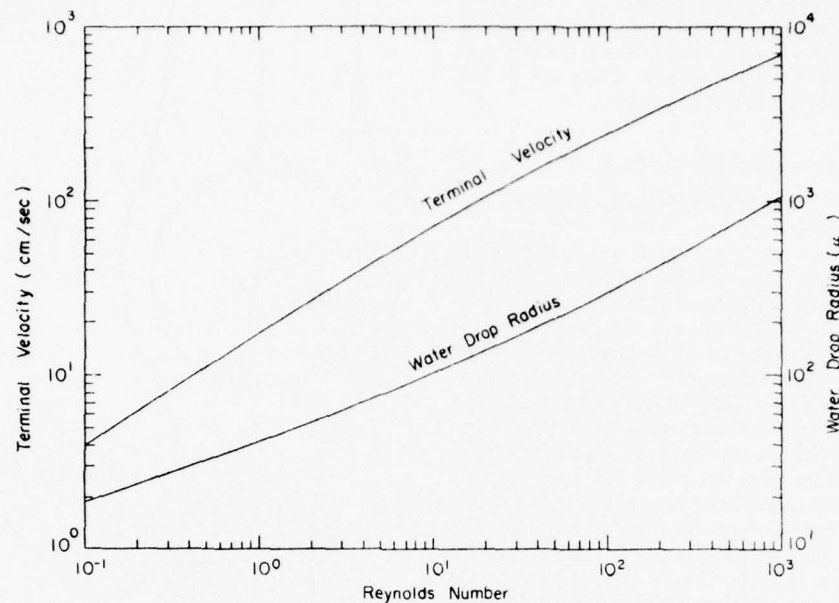
A20

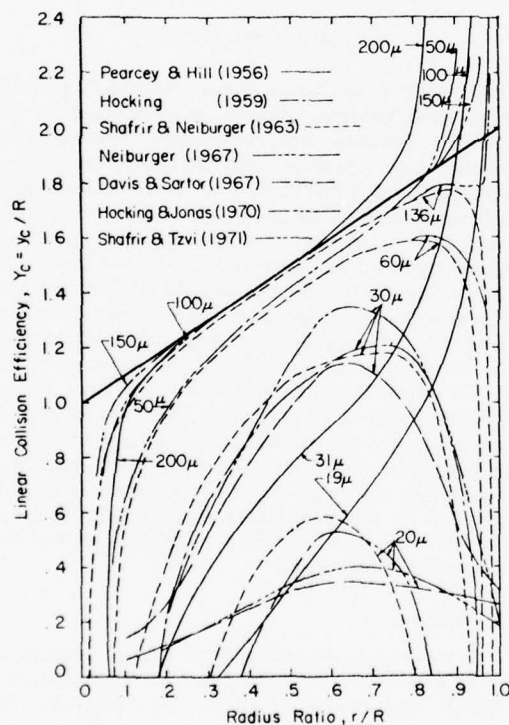FIG. 2. Water drop size and terminal velocity vs Reynolds number.

FIG. 3. Survey of literature on collision efficieny as a function of radius ratio.

controlled environment. Analytical studies are being established so that the effect on droplet growth by each parameter can be verified with experimental data. With a well-established knowledge concerning each individual parameter, the overall effect on droplet *growth by the combination of the many physical* parameters actually existing in the atmosphere can then be investigated.

If one considers an environment where only gravity, inertia and drag forces are significant, the equations of motion of a freely falling drop can be written as

$$\frac{d\mathbf{V}_L}{dt} = \mathbf{g} - \left(\frac{C_D\,\mathrm{Re}}{24}\right)_L \frac{6\pi\mu R}{M_L}(\mathbf{V}_L - \mathbf{U}_s), \qquad (2)$$

$$\frac{d\mathbf{V}_s}{dt} = \mathbf{g} - \left(\frac{C_D\,\mathrm{Re}}{24}\right)_s \frac{6\pi\mu r}{M_s}(\mathbf{V}_s - \mathbf{U}_L), \qquad (3)$$

in which the subscripts L and s designate the larger collector drop and the smaller collecting drop, respectively. The drop velocity is $\mathbf{V}$ and the flow field velocity $\mathbf{U}$. The mass of the water drop is M, the gravitational acceleration is $\mathbf{g}$, and μ is the dynamic viscosity. The drag coefficient C_D is given by Oseen (1910) for the Reynolds number region of $0 < \mathrm{Re} \leqslant 1.6$ as

$$C_D = \frac{24}{\mathrm{Re}}(1 + \tfrac{3}{16}\,\mathrm{Re}), \qquad (4)$$

and by Lin and Lee (1973) for the Reynolds number

A 21

region of $1.6 < \text{Re} \leqslant 1000$ as

$$C_D = \frac{24}{\text{Re}}(1 + 0.2207\,\text{Re}^{\frac{1}{2}} + 0.0125\,\text{Re}). \qquad (5)$$

The Reynolds number is evaluated by using the relative velocity between the drop and its surrounding flow field, i.e.,

$$(\text{Re})_L = \frac{2\rho|\mathbf{V}_L - \mathbf{U}_s|R}{\mu}, \qquad (6)$$

$$(\text{Re})_s = \frac{2\rho|\mathbf{V}_s - \mathbf{U}_L|r}{\mu}, \qquad (7)$$

in which ρ is the density of the medium in which the water drop is traveling.

To calculate the position of each drop, Eqs. (2) and (3) are integrated numerically in both vertical and horizontal directions. The vertical direction is along the axis connecting the center of the collector drop and the center of gravity of the earth. The horizontal direction is normal to the vertical direction from the center of the collector drop toward the vertical axis of the collecting drop. The integration is performed in two steps as discussed by Conte (1965). The first step is an estimation which uses the Adams-Bashforth's prediction formula

$$\mathbf{V}^{n+1} = \mathbf{V}^n + \frac{\Delta t}{24}\left[55\left(\frac{d\mathbf{V}}{dt}\right)^n - 59\left(\frac{d\mathbf{V}}{dt}\right)^{n-1}\right.$$
$$\left. + 37\left(\frac{d\mathbf{V}}{dt}\right)^{n-2} - 9\left(\frac{d\mathbf{V}}{dt}\right)^{n-3}\right], \quad (8)$$

in which the subscripts n, $n+1$, ..., denote the time steps of n, $n+1$, ..., respectively. The velocity at the $(n+1)$st time step is refined by the Adams-Moulton

correction formula

$$\mathbf{V}^{n+1} = \mathbf{V}^n + \frac{\Delta t}{24}\left[9\left(\frac{d\mathbf{V}}{dt}\right)^{n+1} + 19\left(\frac{d\mathbf{V}}{dt}\right)^n\right.$$
$$\left. -5\left(\frac{d\mathbf{V}}{dt}\right)^{n-1} + \left(\frac{d\mathbf{V}}{dt}\right)^{n-2}\right]. \quad (9)$$

By integrating $\mathbf{V}$ with respect to time again, the position of each drop can be determined. These processes of integration are repeated by assuming the distance of the initial separation between the collector and the collecting drops of given sizes. Collision is considered to take place if the closest distance between the two drops is less than 1% of the smaller collecting drop radius. An initial vertical separation distance of 54 radii of the larger collector drop is used because the flow pattern calculations indicate that the flow fields are not noticeably disturbed by the presence of each other. The initial horizontal separation distance is the variable to be determined. The largest initial horizontal separation distance, which results in collision between the collector and the collecting drops, is known as the radius of the collisional cross-sectional area, y_c.

4. Results and discussion

The collision trajectory of a collector drop and a smaller collecting drop is shown in Fig. 4. For a collector drop of 30 μm to collide with a collecting drop of 9 μm, the collisional cross-sectional radius is about 25 μm. On the other hand, the 30 μm collector drop can only collide with a 3 μm collecting drop within a collisional cross-sectional radius of 1.5 μm. The hydrodynamic force in the vicinity of the frontal surface of the collector drop pushes the collecting drop away from its falling axis. The collecting drop, as a result of its own inertia, tends to maintain its own course. A larger collecting
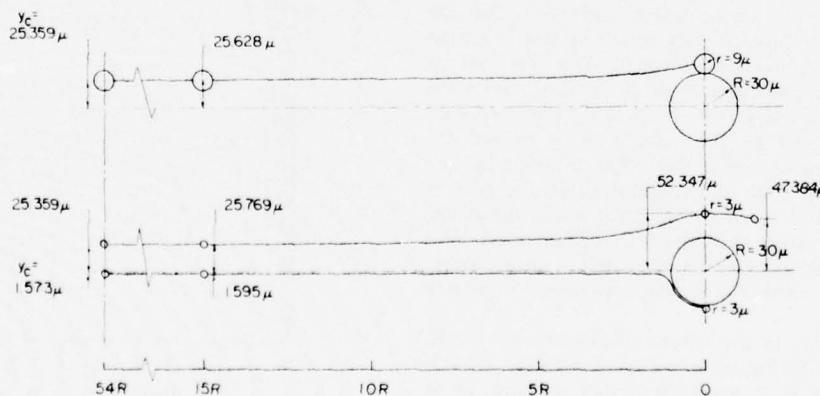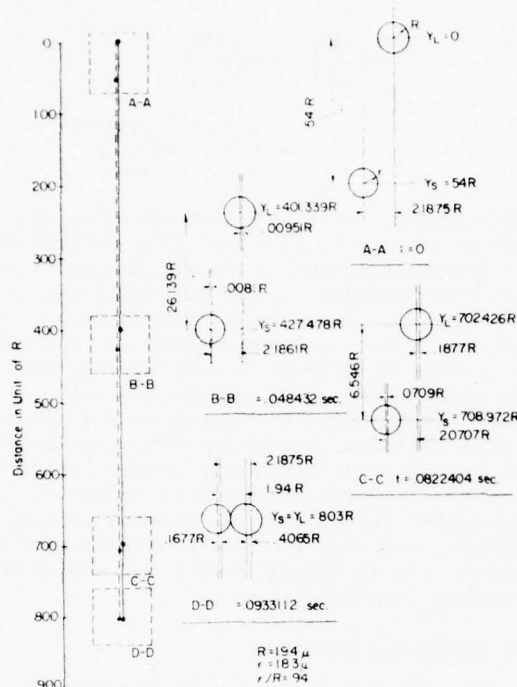

FIG. 4. Collisional trajectories.

FIG. 5. Collision of a pair of water drops.

stantially when the collector drop $\geqslant 30\ \mu$m. This value differs from the results of some previous investigators. A comparison of theoretical results with some available experimental data is shown in Fig. 7 for the case of a 75 μm collector drop. It can be seen that the agreement is satisfactory for most of the radius ratio regions except for those drops of approximately equal size. Re-examination of the theoretical results indicates that the vertical distance traveled by a pair of drops of approximately equal size is very long before the collector drop can catch up with the collecting drop. Although this particular situation exists often in nature, conventional laboratory apparatus is limited by its physical dimensions and prevents this phenomenon from being experimentally observed.

Comparison is also made with the analytical results of Klett and Davis (1973) for a collector drop of 70 μm. It is noted that all calculated collisional efficiencies are large for high radius ratios. However, the Klett and Davis results appear to be substantially smaller than available experimental data.
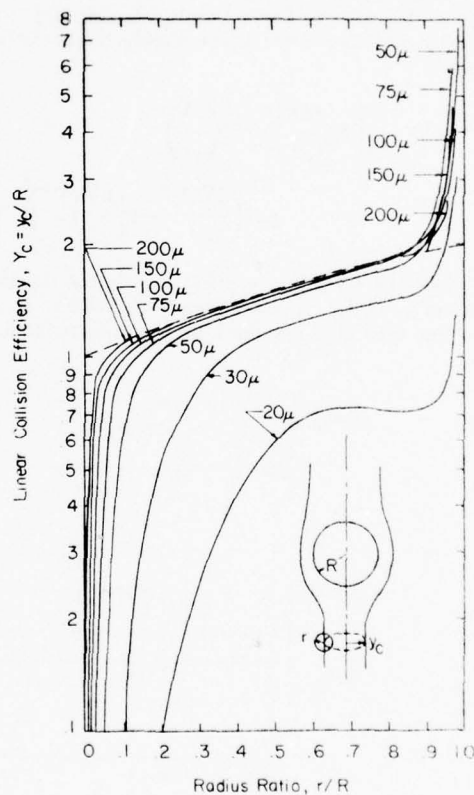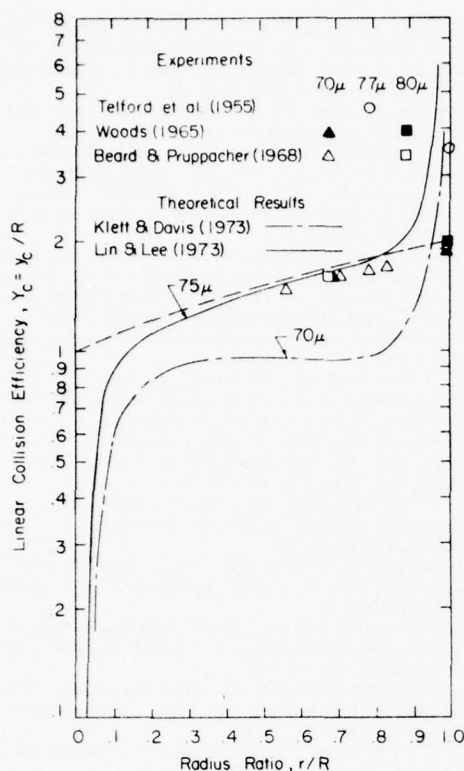
drop possesses a greater inertia and thereby has a larger collisional cross-sectional radius.

The relative position of two drops of approximately equal size is shown in Fig. 5. For a collector drop of 194 μm to collide with a collecting drop of 183 μm, the collisional cross-sectional radius is 425 μm. In other words, for a pair of water drops with a radius ratio of 0.94, the linear collision efficiency is 2.19, which is larger than the geometric collision efficiency of 1.94. The reason for the high collision efficiency is that the disturbed air in the back of the collecting drop drags the collector drop into its wake region. The disturbed air in the front of the collector drop, in turn, pushes the collecting drop away from it. Because the horizontal distance traveled by the collector drop toward the collecting drop is larger than that traveled by the collecting drop from the collector drop, the pair of drops will collide even though their initial horizontal separation is larger than the sum of their radii. This condition is sometimes referred to as the wake capture phenomenon, which is one of the important processes in precipitation.

The variation of the linear collision efficiency with drop radius ratio for various sizes of collector drops is shown in Fig. 6. It should be noted that the linear collision efficiency is relatively high for drops of approximately equal size. The numerical value increases sub-

FIG. 6. Calculated collision efficiency.

FIG. 7. Comparison between theory and experiment.

tion appears to be the collisional growth of drops of water of approximately equal size. Further investigations to include additional atmospheric parameters, such as electric charges, updraft and turbulence, can be developed by a similar approach for applications to more complicated atmospheric problems.

APPENDIX

Effect of Drag Force on Collision Efficiency

A water drop in the atmosphere is surrounded by air, which produces a drag force when the drop travels with a certain velocity. Calculation of collision efficiency requires a knowledge of the drag force of various drop sizes at different velocities. Consequently, a dimensionless drag coefficient is given as a function of Reynolds
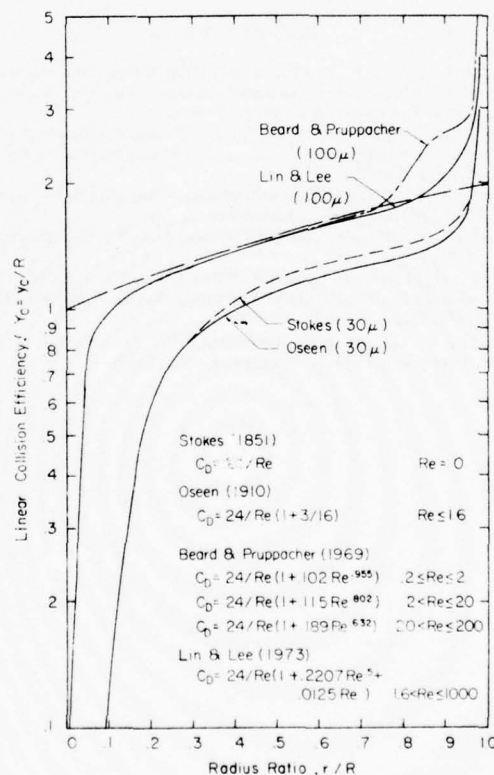
5. Conclusion

The linear collision efficiency of a pair of water drops in the atmosphere has been calculated by using the method of superposition. Based on the flow fields obtained from the numerical solution of the Navier-Stokes equations, collision trajectories between drops of various sizes were determined by considering only gravity, inertia and drag forces. For cases of large collector drops and small collecting drops, the linear collision efficiency is significantly less than the geometric collision efficiency, because the hydrodynamic force upstream of the collector drop pushes the small collecting drops away from its falling axis. For cases of collector and collecting drops of similar sizes, the linear collision efficiency is substantially higher than the geometric collision efficiency, because the low pressure created by the viscous forces downstream of the collecting drop drags the collector drop into its wake. The theoretical result has been compared with existing data from laboratory experiments. Satisfactory agreement between the theoretical and experimental results indicates that the theory is basically sound. In an atmospheric environment, where only inertia, gravity and drag forces are significant, the dominant factor in forming precipita-

FIG. 8. Effect of drag equation.

numbers. At a Reynolds number region between 0 and 1, it is not absolutely certain that the drag coefficient actually follows the Stokes drag formula or Oseen's drag formula. To examine the actual derivation of the linear collision efficiency caused by the uncertainty of the chosen drag relation, Fig. 8 shows the comparison of the Stokes and Oseen's drag on linear collision efficiency calculations for a 30 μm collector drop. It is obvious that the drag formula does not affect the trend of the linear collision efficiency. A maximum deviation of 10% could be expected in the vicinity of drop radius ratio of 0.75. For larger drops, evaluations of collision efficiencies were made by using Beard and Pruppacher's formulas as well as Lin and Lee's formula based on the same flow field data for a drop radius of 100 μm. Fig. 8 shows that no appreciable difference can be found in linear collision efficiency for radius ratios ≤ 0.7. In the region where the sizes of collecting drops are approaching the size of the collector drop, no drag formula can cause the decrease of collision efficiency as reported in some early investigations. Step changes in the drag formula are the only cause of the irregularities of the collision efficiency curve, and these are not readily explainable in natural phenomena.

REFERENCES

Beard, K. V., and H. R. Pruppacher, 1968: An experimental test of the theoretically calculated collision efficiency of cloud drops. J. Geophys. Res., 73, 6407–6414.

——, and S. N. Grover, 1974: Numerical collision efficiencies for small raindrops colliding with micron size particles. J. Atmos. Sci., 31, 543–550.

Carrier, G. F., 1953: On slow viscous flow. Final Report, Contract Nonr-653(00), Brown University, 31 pp.

Conte, S. D., 1965: Elementary Numerical Analysis. McGraw-Hill, 278 pp.

Davis, M. H., and J. D. Sartor, 1967: Theoretical collision efficiencies for small cloud droplets in Stokes flow. Nature, 215, 1371–1372.

Fleagle, R. G., and J. A. Businger, 1970: An Introduction to Atmospheric Physics. Academic Press, 346 pp.

Goldstein, S., 1929: The forces on a solid body moving through viscous fluid. Proc. Roy. Soc. London, A123, 216–235.

Hocking, L. M., 1959: The collision efficiency of small drops. Quart. J. Roy. Meteor. Soc., 85, 44–50.

——, and P. R. Jonas, 1970: The collision efficiency of small drops. Quart. J. Roy. Meteor. Soc., 96, 722–728.

Jenson, V. G., 1959: Viscous flow round a sphere at low Reynolds numbers [Re≤40]. Proc. Roy. Soc. London, A249, 346–366.

Klett, J. D., and M. H. Davis, 1973: Theoretical collision efficiencies of cloud droplets at small Reynolds numbers. J. Atmos. Sci., 30, 107–117.

Le Clair, B. P., A. E. Hamielec and H. R. Pruppacher, 1970: A numerical study of the drag on a sphere at low and intermediate Reynolds numbers. J. Atmos. Sci., 27, 308–315.

Langmuir, I., 1948: The production of rain by a chain reaction in cumulus clouds at temperature above freezing. J. Meteor., 5, 175–192.

Lin, C. L., and S. C. Lee, 1972: Drag and ventilation of water drops in clouds. Trans. Amer. Geophys. Union, 53, 999–1000.

——, and ——, 1973: Transient state analysis of separated flow around a sphere. Intern. J. Comp. Fluids, 1, 235–250.

Neiburger, M., 1967: Collision efficiency of nearly equal cloud drops. Mon. Wea. Rev., 95, 917–920.

Oseen, C. W., 1910: Über die Stokessche Formel und über die verwandte Aufgabe in der Hydrodynamik. Ark. Math. Astron. Fys., 6, No. 29.

Pearcey, T., and G. W. Hill, 1956: A theoretical estimate of the collection efficiencies of small droplets. Quart. J. Roy. Meteor. Soc., 83, 77–92.

Rimon, Y., and S. I. Cheng, 1969: Numerical solution of an uniform flow over a sphere at intermediate Reynolds number. Phys. Fluids, 12, 949–959.

Schotland, R. M., and E. J. Kaplin, 1956: The collision efficiency of cloud droplets. Sci. Rept. No. 1, Dept. Meteor. Oceanogr., New York University.

Shafrir, U., 1965: Some nonlinear effects in the collision efficiency problem. J. Geophys. Res., 70, 4491–4500.

——, and M. Neiburger, 1963: Collision efficiencies of two spheres falling in a viscous medium. J. Geophys. Res., 68, 4141–4147.

——, and G. C. Tzvi, 1971: A numerical study of collision efficiencies and coalescence parameters for droplet pairs with radii up to 300 microns. J. Atmos. Sci., 28, 741–751.

Telford, J. W., and N. S. Thorndike, 1961: Observations of small drop collisions. J. Appl. Meteor., 18, 382–387.

——, —— and E. G. Bowen, 1955: The coalescence between small water drops. Quart. J. Roy. Meteor. Soc., 81, 241–250.

Woods, J. D., 1965: The collision and coalescence of water droplets. Ph.D. thesis, University of London.

Reply: Collision Efficiency Analyses

C. L. LIN AND S. C. LEE

*Department of Mechanical and Aerospace Engineerng and Graduate Center for Cloud Physics Research,
University of Missouri-Rolla 65401*

11 December 1975

In response to Dr. Klett's comment on the article of Lin and Lee (1975), it is necessary to keep the following subjects in focus.

1. The purpose of a scientific article

A scientific article is being published for the purpose of clarifying a situation which is being confused by conflicting results. Figs. 1 and 2 show the situation on linear collision efficiencies today for a collector drop of approximately $70\,\mu$m and $30\,\mu$m, respectively. It is evident that the method of superposition used by Lin and Lee (1975) and the method of force evaluation used by Klett and Davis (1973) provide better agreement in comparison with the results in earlier studies. To argue for the better accuracy of one method over the other does not serve any constructive purpose, because both are approximate in nature. [This has been pointed

out by Lin and Lee (1975) as well as by the original authors of these methods, Langmuir (1948) and Hocking (1959).] Improvement by Lin and Lee (1973) in computation techniques can only minimize the inaccuracy which is caused by the inability of obtaining mathematical solutions of the Navier–Stokes equations applying to a flow field that consists of two or more drops of various sizes. Similarly, modification of Oseen's linearization technique by compromising with Stokes' approach, as discussed by Carrier (1953) and Klett and Davis (1973), is not a solution of the nonlinear Navier–Stokes equations which govern flow fields of continuum media at non-zero Reynolds numbers. A $70\,\mu$m radius water drop falling in air at steady state gives a Reynolds number of approximately 4, and a $30\,\mu$m drop of approximately 0.4. When the flow field is being disturbed by another drop which occurs before all collisions, the assumption of steady-state flow phenomenon
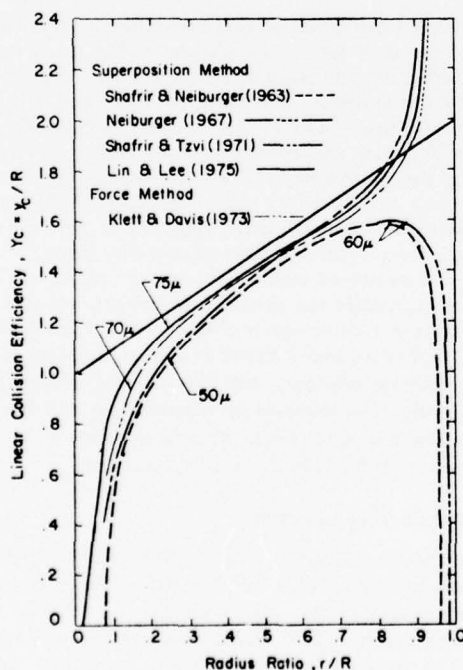

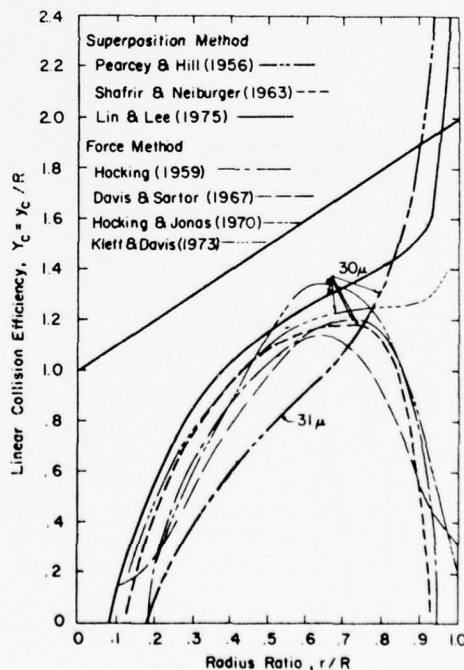FIG. 1. Linear collision efficiency for collector drop radius of approximately 70 μm.

FIG. 2. Linear collision efficiency for collector drop radius of approximately 30 μm.

A26

is in question, not to mention the credibility of super-position or linearization. It would be a worse alternative if this discussion were to leave the impression that the problems caused by superposition could be eliminated by some kind of compromise between two linearization techniques.

2. A curve on linear collision efficiency

In Fig. 7 of Lin and Lee (1975), a curve on collision efficiency E by Klett and Davis (1973) was used as linear collision efficiency Y_c for comparison between theory and experiment. The comparison showed that the numerical values in the analytical result of Klett and Davis were less than those of Lin and Lee, which agreed well with available experimental data. This was a mistake by Lin and Lee. The result of Klett and Davis was presented as collision efficiency not as linear collision efficiency. A sincere apology is extended to Klett and Davis for the hasty addition of that particular curve. Our explanation here is not to find an excuse about what was done but to present the circumstances of turning a good intention to a poor relation. The manuscript of Lin and Lee was prepared before the article of Klett and Davis appeared in the Journal. The question in doubt, at that time, was "whether the wake capture phenomenon increases or decreases collision efficiency." Most earlier publications (Davis and Sartor, 1967; Shafrir and Neiburger, 1963; Hocking
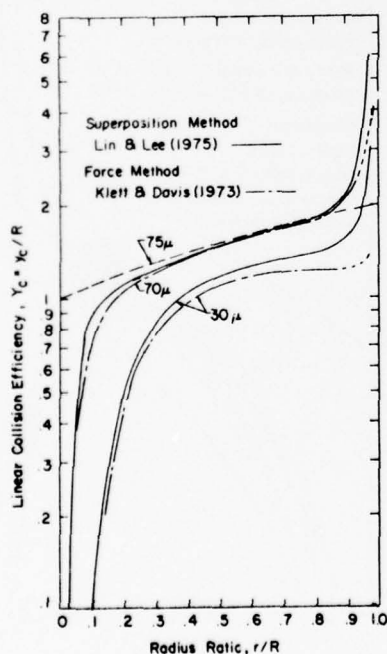

FIG. 3. Comparison of linear collision efficiencies obtained by superposition and force methods.
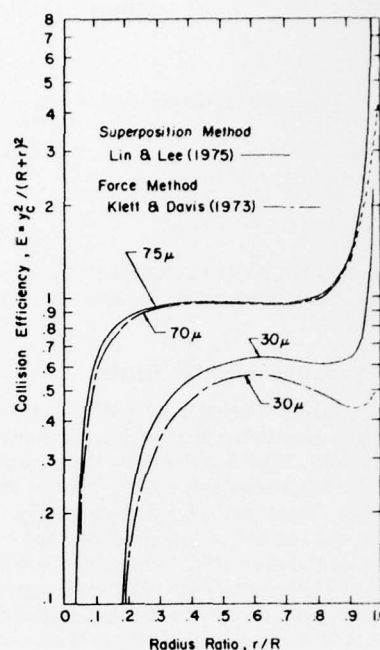

FIG. 4. Comparison of collision efficiencies obtained by superposition and force methods.

and Jonas, 1970) indicated that the collision efficiencies tended to go to zero as the droplet radius ratios approached unity. Lin and Lee found that the trend was exactly the opposite. The trend of Klett and Davis agreed with that of Lin and Lee and was quickly added to Fig. 7 during the revision of their article for supporting the controversy. It was not conceivable that those two curves, which were calculated from two completely different methods, could be in agreement within a few percent at a time when earlier studies had discrepancies ranged almost between zero and infinity. In order to clarify the situation on collision efficiency analyses, the positive aspect of these two articles needs to be emphasized and is shown in Figs. 3 and 4 for the linear collision efficiency and the collision efficiency, respectively. The methods of superposition and force evaluation are approximations which produce comparable results for collision efficiency analyses.

3. Oseen's drag equation

The Oseen's drag equation was given as Eq. (4) by Lin and Lee (1975). A table inserted in Fig. 8 of the article misprinted the same equation by omitting a Reynolds number. This was an oversight by Lin and Lee. The thoroughness of Dr. Klett in reading this article is to be commended. We appreciate his promptness in bringing it to our attention.

A27

REFERENCES

Carrier, G. F., 1953: On slow viscous flow. Final Report, Contract Nonr-653(00), Brown University, 31 pp.

Davis, M. H., and J. D. Sartor, 1967: Theoretical collision efficiencies for small cloud droplets in Stokes flow. *Nature*, **215**, 1371–1372.

Hocking, L. M., 1959: The collision efficiency of small drops. *Quart. J. Roy. Meteor. Soc.*, **85**, 44–50.

——, and P. R. Jonas, 1970: The collision efficiency of small drops. *Quart. J. Roy. Meteor. Soc.*, **96**, 722–728.

Klett, J. D., and M. H. Davis, 1973: Theoretical collision efficiencies of cloud droplets at small Reynolds numbers. *J. Atmos. Sci.*, **30**, 107–117.

Langmuir, I., 1948: The production of rain by a chain reaction in cumulus clouds at temperature above freezing. *J. Meteor.*, **5**, 175–192.

Lin, C. L., and S. C. Lee, 1973: Transient state analysis of separated flow around a sphere. *Intern. J. Comput. Fluids*, **1**, 235–250.

——, and ——, 1975: Collision efficiency of water drops in the atmosphere. *J. Atmos. Sci.*, **32**, 1412–1418.

Neiburger, M., 1967: Collision efficiency of nearly equal cloud drops. *Mon. Wea. Rev.*, **95**, 917–920.

Pearcey, T., and G. W. Hill, 1956: A theoretical estimate of the collection efficiencies of small droplets. *Quart. J. Roy. Meteor. Soc.*, **83**, 77–92.

Shafrir, U., and M. Neiburger, 1963: Collision efficiencies of two spheres falling in a viscous medium. *J. Geophys. Res.*, **68**, 4141–4147.

——, and G. C. Tzvi, 1971: A numerical study of collision efficiencies and coalescence parameters for droplet pairs with radii up to 300 microns. *J. Atmos. Sci.*, **28**, 741–751.

$$F_m = -(\partial P/\partial X) \qquad \text{(A-1)}$$

$$R(Z) = \beta \sigma T_w^{\ 4} \exp\left(-1.6 k_\lambda \int_{z_b}^{z_t} \rho \omega^m dZ\right) \qquad \text{(A-11)}$$

The Effect of Vertical Separation on Droplet Collision Efficiency

(Reply to Comments by Cataneo and Semonin)

C. L. LIN[1] AND S. C. LEE

Department of Mechanical and Aerospace Engineering and Graduate Center for Cloud Physics Research, University of Missouri-Rolla 65401

16 March 1976

The experimental data of Cataneo *et al.* (1971) and the analytical results of Lin and Lee (1975) appear to be in excellent agreement on collision efficiency, which

is the nondimensionalized distance of the maximum horizontal separation between two free-falling drops. However, an apparent discrepancy exists with regard to the amount of their vertical separation that may affect the collision efficiency. Upon reexamining the two
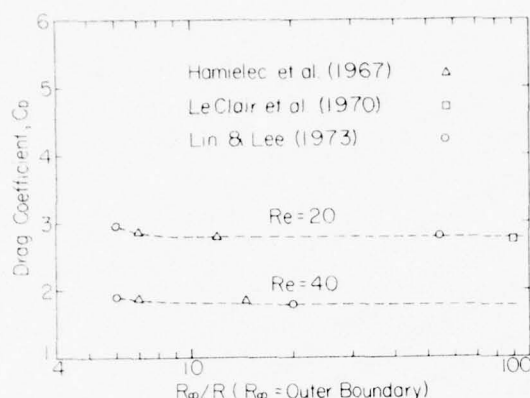
[1] Present affiliation: National Aviation Facilities Experimental Center, Atlantic City, N. J. 08405.

FIG. 1. Effect of outer boundary on drag coefficient calculations for a spherical drop of radius R.

papers, the following distinctions are noted:

1) The study of Lin and Lee (1975) was undertaken to determine collision efficiency by using a vertical separation distance, which is critical for the accuracy of the calculation. A maximum horizontal separation distance, which will result in the collision of two falling drops of approximately equal size, occurs within the range of 54 radii of the vertical separation distance. In other words, the effect on collision efficiency calculations becomes insignificant when the vertical separation distance is larger than 54 radii. It is necessary to point out that this hypothesis was only indirectly evaluated through the effect on the drag coefficient by assuming various sizes of the outer boundary, which approximates the location of the undisturbed flow field in numerical calculations. Detailed discussions of the effect of the outer boundary on drag coefficient calculations have been published by Hamielec et al. (1967), LeClair et al. (1970) and Lin and Lee (1973). Fig. 1 illustrates the test range of Cataneo et al. (1971). Reynolds numbers Re of 20 and 40 are approximately equal to free-falling drops with radii of 140 and 180 μm, respectively. It can be seen that the assumption of 54 radii appears to be a conservative estimate for drag coefficient evaluations.

2) In the experiment of Cataneo et al. (1971) for drops of equal size, the wake effect of the collecting drop was observed at a vertical separation distance >100 diameters because the collector drop was noticeably accelerated. In order to compare their observation with the theoretical value of 54 radii that is used in collision efficiency calculations, it is necessary to ask whether the maximum horizontal separation distance is smaller or larger than the critical limit determined from the collision efficiency. In other words, although the wake length may be longer than 100 diameters, the effect on the calculated collision efficiency becomes insignificant, as long as the radius of the wake is less than the maximum horizontal separation distance that determines the collision efficiency.

The excellent agreement on collision efficiency between the experiment of Cataneo et al. (1971) and the theory of Lin and Lee (1975) indicates that the hypothesis is reasonable. Direct verification of this hypothesis is desirable; however, a numerical investigation of the vertical separation is impractical because too much computer time is required for calculating streamfunctions and vorticities of an extraordinarily large flow field and for evaluating by the method of superposition the change of vertical separation from two seemingly undisturbed flow fields. Experimental investigations may be more realistic if existing facilities are used to measure photographically the horizontal separation simultaneously with the vertical separation.

REFERENCES

Cataneo, R., J. R. Adam and R. G. Semonin, 1971: Interactions of equal-sized droplets due to the wake effect. J. Atmos. Sci., 28, 416–418.

Hamielec, A. E., T. W. Hoffmann and L. L. Ross, 1967: Numerical solution of the Navier-Stokes equations for flow past spheres. Amer. Inst. Chem. Eng. J., 13, 212–219.

LeClair, B. P., A. E. Hamielec and H. R. Pruppacher, 1970: A numerical study of the drag on a sphere at low and intermediate Reynolds numbers. J. Atmos. Sci., 27, 308–315.

Lin, C. L., and S. C. Lee, 1973: Transient state analysis of separated flow around a sphere, Intern. J. Comput. Fluids, 1, 235–250.

——, ——, 1975: Collision efficiency of water drops in the atmosphere. J. Atmos. Sci., 32, 1412–1418.

A30

APPENDIX B

Published Papers Related to

"Fog Situations Over the Ocean"

1. "Heat, Mass and Momentum Transfer in Turbulent Boundary Layer Flows", Heat Transfer 1974, 2, 104-108, 1974.

2. "Transport Phenomena in Thermally Stratified Boundary Layers", Journal of Heat Transfer, 97, 60-65, 1975.

B1

FC3.3   HEAT MASS AND MOMENTUM TRANSFER IN TURBULENT BOUNDARY LAYER FLOWS

S.C. Lee, D.W. Pepper, W.M. Byrne, and R.C. Tai
University of Missouri, Rolla, U.S.A.

Abstract

An analytical method using turbulence energy to study the transfer of heat mass and momentum in a turbulent boundary layer was developed. This approach considers the history of the turbulent motion by treating the eddy viscosity as a dependent variable to be determined as a function of locations in a turbulent flow field. A systematic comparison with experimental data was made. The same empirical constants established in an incompressible self-preserved turbulent flow along a flat plate were also applicable to accelerating and decelerating flows with suction and blowing as well as for boundary layer flows with heat and mass transfer.

NOMENCLATURE

C, c: Species concentration, mgs/cc
D : Turbulence dissipation, m^2/sec^2
F : Dimensionless blowing parameter
g : Gravitational acceleration, m/sec^2
H, h: Enthalpy, m^2/sec^2
K : Kinetic energy of turbulence, m^2/sec^2
P : Turbulence production, m^2/sec^2
p : Static pressure, $newton/m^2$
p^+ : Dimensionless pressure gradient
Pr : Prandtl number
Re : Reynolds number
Ri : Richardson number
St : Stanton number
T : Temperature, $°k$
U, u: Velocity component in x-direction, m/sec
U^* : Friction velocity, m/sec
V, v: Velocity component in y-direction, m/sec
x : Horizontal distance, m
y : Vertical distance, m
y^+ : Dimensionless vertical distance
$\alpha's$: Coefficients of the generalized equation
β : Coefficient in the modified law of the wall
δ : Boundary layer thickness
ϵ : Exchange coefficient, $newton-sec/m^2$
κ : Von Karman's universal constant
μ : Dynamic viscosity, $newton-sec/m^2$
ν : Kinematic viscosity, m^2/sec
ρ : Density, $newton-sec^2/m^4$
σ : Dimensionless constant
τ : Shear stress, $newton/m^2$
Φ : Generalized flow parameter
ψ : Stream function, $newton-sec/m^2$
ω : Normalized stream function

Subscript

C : Concentration
H : Energy
K : Kinetic energy of turbulence
M : Momentum
W : Wall
O : Initial x location
∞ : Free stream

INTRODUCTION

One of the most commonly observed phenomena occurring in many practical problems is the transfer of heat, mass, and momentum. Most frequently this phenomenon is encountered in turbulent flows which are governed by the Reynolds Equations. Analytical solutions of the Reynolds equations are only theoretically possible if the turbulent stresses are known. In order to close the Reynolds equations, Boussinesq /1/ related the turbulent shear stress with the average velocity gradient by introducing an "eddy viscosity," also known as a "momentum exchange coefficient." It is the precise form of this "eddy viscosity" that becomes the subject of many phenomenalogical theories. Prandtl /2/ used momentum as a transferable quantity resulting in a mixing length which was considered as the average distance between turbulent eddies in analogy to the mean free path between molecules in kinetic theory. Taylor /3/ used the vorticity as a transferable quantity and also derived a similar length parameter. Nevertheless, neither Prandtl nor Taylor could give a workable relation for this length parameter because of the lack of a universal constant. Von Karman /4/ conducted a series of experiments through which a length parameter was found to be linearly proportional to the ratio of the first and second derivatives of the average velocity. He named his value of proportionality the "universal constant" which was applicable to some turbulent flow problems. Earlier efforts in establishing a workable phenomenological theory of turbulence were discussed in detail by Hinze /5/. It is evident that the mixing length approach did not provide the necessary mechanism to take the history of turbulence into account. The use of the turbulence kinetic energy equation to complete the Reynolds equations was first proposed by Kolmogorov /6/ and discussed in standard textbooks, such as Townsend /7/, Hinze /5/, Monin and Yaglom /8/ and many others. Kolmogorov /6/ and Prandtl /9/ independently suggested that the turbulent shear stress related to the turbulence kinetic energy's one-half power. This model has been the basis of calculation procedures by Glushko /10/ and Spalding /11/. A simpler model was suggested by Nevzglajdov /12/ in which the turbulent shear stress related linearly to the turbulence kinetic energy. The latter model was used by Bradshaw et al /13/ and Lee and Harsha /14/ for boundary layer flows and free turbulent flows, respectively. Figure 1 shows the correlation of the Nevzglajdov model with the experimental data of Klebanoff /15/ and Schon and Mery /16/. It is evident that the linear relation between turbulent shear stress and turbulence kinetic energy describes realistically the physical phenomenon. Lee et al /17/ applied the Nevzglajdov model successfully in studying heat mass and momentum transfer in free mixing flows. This paper is to extend the same approach to boundary layer flows.

The second half-time step is an implicit finite-difference equation in the Z direction

$$E_{i,j} = \frac{4}{Re}\left[\frac{1}{(\Delta Z)^2} + \frac{1}{(\Delta\theta)^2}\right] + \frac{a^2 e^{2aZ}}{\Delta t} \qquad (19c)$$
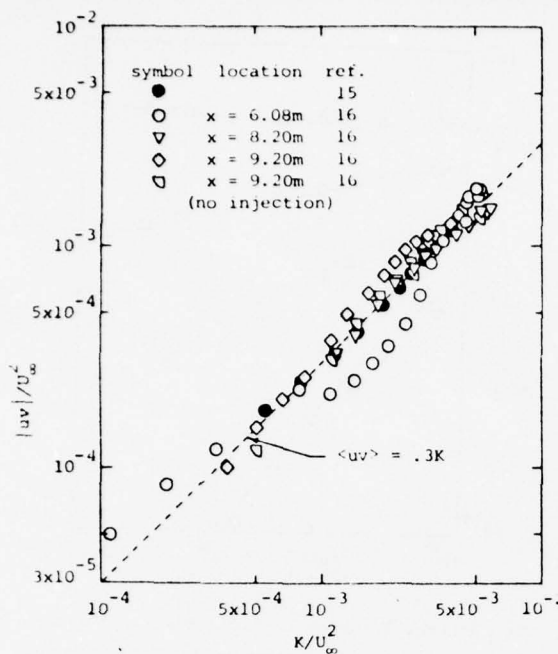
Fig. 1: Data Correlation of Nevzglajdov Model

ANALYSIS

The mathematical formulation of heat, mass, and momentum transfer in turbulent boundary layer flows was given by Patankar and Spalding /18/. The use of Nevzglajdov model to relate the turbulent shear stress and the turbulence kinetic energy was discussed by Lee and Harsha /14/. The validity of using constant turbulent Prandtl and Schmidt numbers was examined by Lee et al /17/. A brief summary of the analytical approach of the turbulence kinetic energy method for various boundary layer flow problems can be outlined as follows:

Governing Equations

For two-dimensional, steady state, boundary layer flows, the continuity, momentum, turbulence kinetic energy, mean-flow energy and species concentration equations may be written as:

$$\frac{\partial}{\partial x} \rho U + \frac{\partial}{\partial y} \rho V = 0 \tag{1}$$

$$\rho U \frac{\partial U}{\partial x} + \rho V \frac{\partial U}{\partial y} = \frac{\partial}{\partial y} \epsilon_M \frac{\partial U}{\partial y} - \frac{\partial p}{\partial x} \tag{2}$$

$$\rho U \frac{\partial K}{\partial x} + \rho V \frac{\partial K}{\partial y} = \frac{\partial}{\partial y} \epsilon_k \frac{\partial K}{\partial y} + P_K - D_K \tag{3}$$

$$\rho U \frac{\partial H}{\partial x} + \rho V \frac{\partial H}{\partial y} = \frac{\partial}{\partial y} \epsilon_H \frac{\partial H}{\partial y} + (\epsilon_K - \epsilon_H) \frac{\partial K}{\partial y} +$$
$$+ \frac{\epsilon_M - \epsilon_K}{2} \frac{\partial U}{\partial y}^2 \tag{4}$$

$$\rho U \frac{\partial C}{\partial x} + \rho V \frac{\partial C}{\partial y} = \frac{\partial}{\partial y} \epsilon_C \frac{\partial C}{\partial y} \tag{5}$$

where U and V are the time-average velocity com-

ponents in the x and y directions, respectively; ρ is the density; p is the static pressure, K is the kinetic energy of turbulence; H is the stagnation enthalpy; and C is the species concentration. Using the Nevzglajdov model as modified by Lee and Harsha /14/, the turbulent shear stress, τ, can be related to the turbulence kinetic energy, K, as

$$\tau = - < \rho vu > = 0.3 \rho K \frac{\partial U}{\partial y} / \left| \frac{\partial U}{\partial y} \right| \tag{6}$$

The exchange coefficients may then be defined as:

Momentum:

$$\epsilon_M = -<\rho vu> / \frac{\partial U}{\partial y} = 0.3 \, \rho K / \left| \frac{\partial U}{\partial y} \right| \tag{7}$$

Turbulence Kinetic Energy:

$$\epsilon_K = -<\rho vK> / \frac{\partial K}{\partial y} = \epsilon_M / \sigma_K \tag{8}$$

Mean-Flow Energy:

$$\epsilon_H = -<\rho vh> / \frac{\partial H}{\partial y} = \epsilon_M / \sigma_H \tag{9}$$

Species Concentration:

$$\sigma_C = -<\rho vc> / \frac{\partial C}{\partial y} = \epsilon_M / \sigma_C \tag{10}$$

where the lower letter case designates the fluctuating components. σ_K is the equivalent Prandtl number which is approximately equal to 0.7 determined by Lee et al /17/. σ_H is the turbulent Prandtl number with a numerical value of 0.75 obtained experimentally by Arya /19/. σ_C is the turbulent Schmidt number with a numerical value of 0.75 given by Fleagle and Bussinger /20/ for air and water vapor mixture in the atmosphere. The turbulence production term, P_K, consists of the shear generated turbulence due to the mean motion and the buoyancy generated turbulence due to flow stratification. As used by Plate /21/, the production term may be written as

$$P_K = \epsilon_M (\frac{\partial U}{\partial y})^2 - \epsilon_H \frac{g}{T} \frac{\partial T}{\partial y} = \epsilon_M (1 - \frac{Ri}{\sigma_H}) (\frac{\partial U}{\partial y})^2 \tag{11}$$

with g designating the gravitational acceleration and Ri designating the Richardson number. The dissipation term, D_K, was first used by Glushko /10/ and later modified by Byrne /22/ as

$$D_K = 1.8 \rho K^{3/2}/\delta \qquad \text{for } y > \delta/4 \tag{12}$$

$$D_K = (\delta/4y) \, 1.8 \rho K^{3/2}/\delta \quad \text{for } y \leq \delta/4 \tag{13}$$

where δ is the boundary layer thickness. Byrne's expression is in close agreement with that of Bradshaw et al /13/ for the region near the wall boundary.

Numerical Method

Except the continuity, all governing differential equations are parabolic. Transforming to streamline coordinates, (x, ψ), the system of equation can be solved with the numerical method developed by Spalding and Patankar /23/ modified by Lee and Harsha /14/. The generalized parabolic equation takes the form:

$$\frac{\partial \Phi}{\partial x} + (\alpha_1 + \alpha_2 \omega) \frac{\partial \Phi}{\partial \omega} = \frac{\partial}{\partial \omega} (\alpha_3 \frac{\partial \Phi}{\partial \omega}) + \alpha_4 \tag{14}$$

105   B3

Table 1: Coefficient of α_4 of Eq. (14)

ϕ	α_4
U	$-\dfrac{1}{\rho U}\dfrac{\partial p}{\partial x}$
K	$\dfrac{\rho U \epsilon_M}{(\psi_\infty - \psi_w)^2}(1-\dfrac{Ri}{\sigma_H})(\dfrac{\partial U}{\partial \omega})^2 - \dfrac{D_K}{\rho U}$
H	$\dfrac{\partial}{\partial \omega}\{\dfrac{\rho U \epsilon_M}{(\psi_\infty - \psi_w)^2}[(\dfrac{1}{\sigma_K} - \dfrac{1}{\sigma_H})\dfrac{\partial K}{\partial \omega} + (1 - \dfrac{1}{\sigma_H})\dfrac{\partial}{\partial \omega}(\dfrac{U^2}{2})]\}$
C	0

where ω is the normalized streamfunction with ω equal to zero or unity at the wall boundary, ψ_w, or the free stream boundary, ψ_∞, respectively. The coefficients α_1, α_2, and α_3 can be expressed as

$$\alpha_1 = -\frac{\partial \psi_w}{\partial x}/[\psi_\infty - \psi_w]$$

$$\alpha_2 = -[\frac{\partial \psi_\infty}{\partial x} - \frac{\partial \psi_w}{\partial x}]/[\psi_\infty - \psi_w] \qquad (15)$$

$$\alpha_3 = \frac{\epsilon_M}{\sigma_\phi}\frac{\rho U}{[\psi_\infty - \psi_w]^2}$$

where $\sigma_\phi = 1$, σ_K, σ_H or σ_C for $\phi = U$, K, H, or C, respectively. The coefficient α_4 for various values of ϕ is given in Table 1.

Boundary Conditions

Standard boundary conditions are being used at the free stream boundary as well as at the wall boundary. However, in the laminar sublayer adjacent to
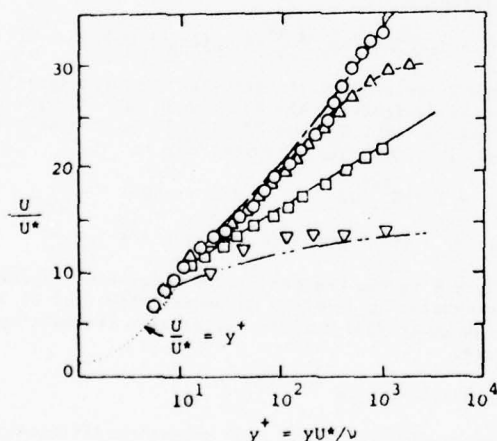
Fig. 2: Friction Velocity in Turb. Boundary Layer

V_w/U^*	P^+	eq. (16)	exp.	ref.
0.122	0.0	— · —	O	25
0.122	-.017	- - - -	△	25
0.0	0.0	———	□	24
-.072	0.0	— ·· —	▽	24
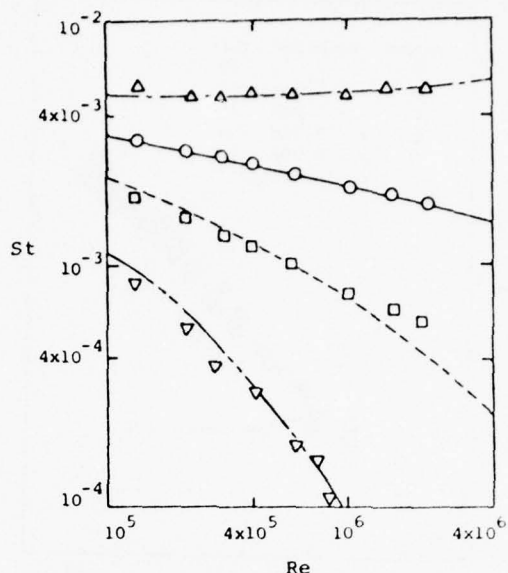
Fig. 3: Heat Transfer in Turb. Boundary Layer

F	eq. (17)	exp.	ref.
-.0046	— · —	△	28
0.0	———	O	28
.0038	- - - -	□	28
.0096	— ·· —	▽	28

the wall boundary, the turbulent shear stress decreases rapidly to zero while the laminar shear stress increases to the value of the wall shear, τ_w. Defining an "effective shear stress" as the summation of the local laminar and turbulent shear stresses, an "effective turbulence kinetic energy" can be introduced to satisfy the linear relation of the Nevzglajdov model. Using the "slip value" approach of Spalding and Patankar /23/, the friction velocity, U^*, can be related to the local velocity, U, by a modified "Law of the Wall":

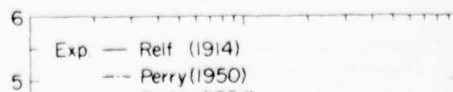$$\frac{U}{U^*} = [2.5 \ln y^+ + \beta][1 + \frac{V_w}{4U^*}(2.5 \ln y^+ + \beta)] \quad (16)$$

where $U^* = [\tau_w/\rho]^{1/2}$, $y^+ = yU^*/\nu$,

$\beta = 4.9 - 10\frac{V_w}{U^*} + 4[(y^+)^{.5}-15(y^+)^{-.5}]P^+$

$+ 5.2\frac{Ri}{\sigma_H}\frac{y}{U^*}\frac{\partial U}{\partial y}$

correlation of Eq. (16) with the experimental data of Rotta /24/ and Julien et al /25/ is shown in Figure 2 for boundary layer blowing and suction under the influence of pressure gradient, P^+. Consideration of thermal stratifications was based on the suggestion of Lumley and Panofsky /26/, where Ri is the Richardson number. In heat transfer studies, either the Nusselt number or the Stanton number is being used. Modifying the expression of Reichardt /27/, the Stanton number, St, becomes:

$$St = \frac{(U^*/U_\infty)^2}{\sigma_H + (U^*/U_\infty)[(Pr-\sigma_H)a + 4(1-\sigma_H)]} \quad (17)$$

where $a = \frac{U^*}{\nu}\int_0^\infty [(1+\frac{\epsilon_M}{\mu})(1+\frac{Pr}{\sigma_H}\frac{\epsilon_M}{\mu})]^{-1} dy$

NT

Exp — Relf (1914)
-- Perry (1950)

$$\frac{U^\star}{U_\infty} = [0.0296\ Re^{-0.21}(1+Re^{0.32F}+0.5Re^{0.64F^2})]^{1/2}$$

with $F = (\rho V)_w/(\rho U)_\infty$

For the case of σ_H equal to 0.75 and Pr equal to 0.72, a is approximately equal to 0.96. Correlation of Eq. (17) with the experimental data of Moffat and Kays /28/ is shown in Figure 3.
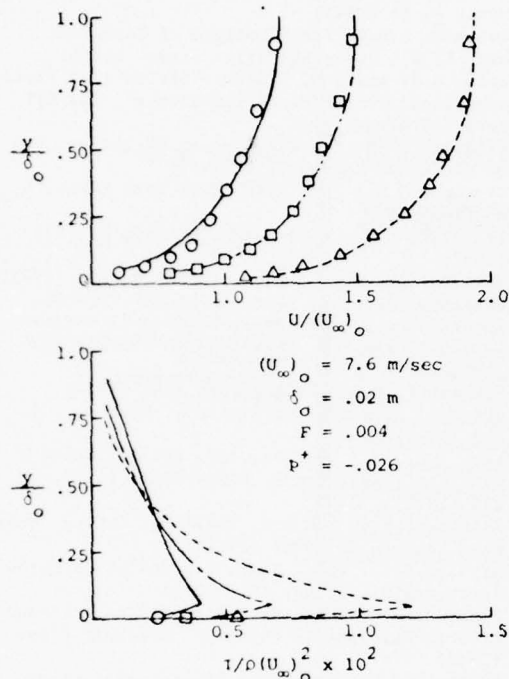
$(U_\infty)_o = 7.6$ m/sec

$\delta_o = .02$ m

$F = .004$

$P^+ = -.026$

Fig. 4: Velocity and Shear Stress Distributions

x/δ_o	theory	exp.	ref.
18.8	——	O	30
28.3	—·—·	□	30
37.7	-----	△	30

RESULTS AND DISCUSSION

Application of the turbulence kinetic energy method was made systematically to a number of engineering problems. Tai /29/ analyzed turbulent boundary layer flows along a flat plate and compared with the experimental data of Klebanoff /15/. Byrne /22/ analyzed turbulent boundary layer flows with blowing and suction under the influence of favorable and adverse pressure gradients and compared with the experimental data of Julien /30/ and Bradshaw /31/. Figure 4 shows one of Byrne's comparisons for boundary layer blowing with favorable pressure gradient. Good agreement was obtained between Byrne's analytical results and Julien's experimental data in velocity profiles. Only sheer stress at the wall was measured. As expected, the maximum sheer stress for the blowing case occurred at a small distance away from the wall. Pepper /32/ analyzed thermally stratified boundary layer in the atmosphere and compared his results with some available wind tunnel data. Figure 5 shows the comparison of Pepper's analytical results with Arya's /19/ experimental data on a
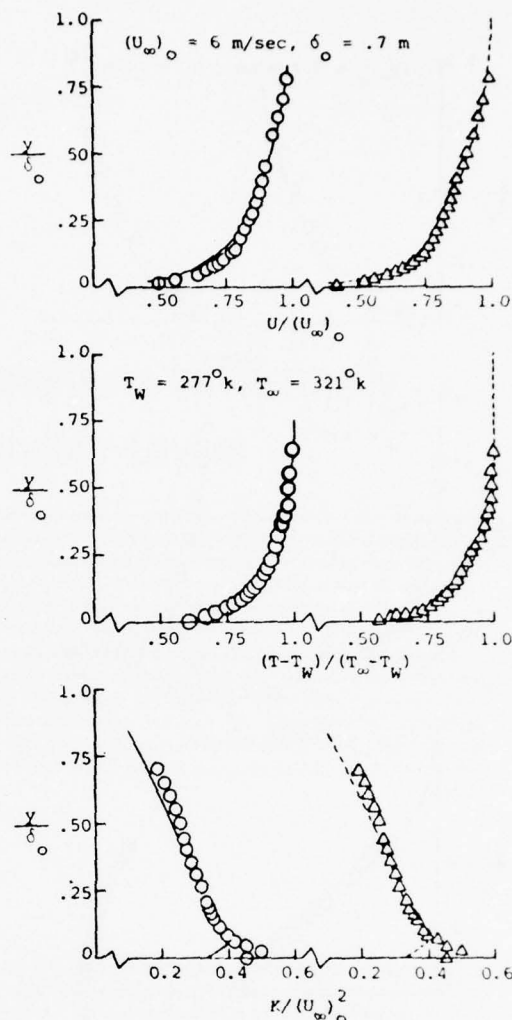
$(U_\infty)_o \approx 6$ m/sec, $\delta_o = .7$ m

$T_W = 277^\circ k$, $T_\infty = 321^\circ k$

Fig. 5: Velocity, Temperature, and Turb. Energy

x/δ_o	theory	exp.	ref.
13.1	——	O	19
16.6	----	△	19

stable atmosphere boundary layer (cold surface). Good agreement was obtained for velocity, temperature and turbulence energy profiles. Figure 6 shows the comparison of Pepper's results with Malhotra's /33/ experimental data on a simulated pollutant (ammonia) diffusion process in an unstable atmosphere. Good agreement was obtained for velocity, temperature and concentration distributions.

CONCLUSION

The turbulence kinetic energy equation was used to complete the Reynolds equations for studying the heat mass and momentum transfer in turbulent boundary layer flows. By calculating the eddy viscosity everywhere in the flow field, a set of uniquely determined empirical constants was established for boundary layer flows along a flat plate with zero pressure gradient, for accelerating and decelerating flows with suction and blowing, as
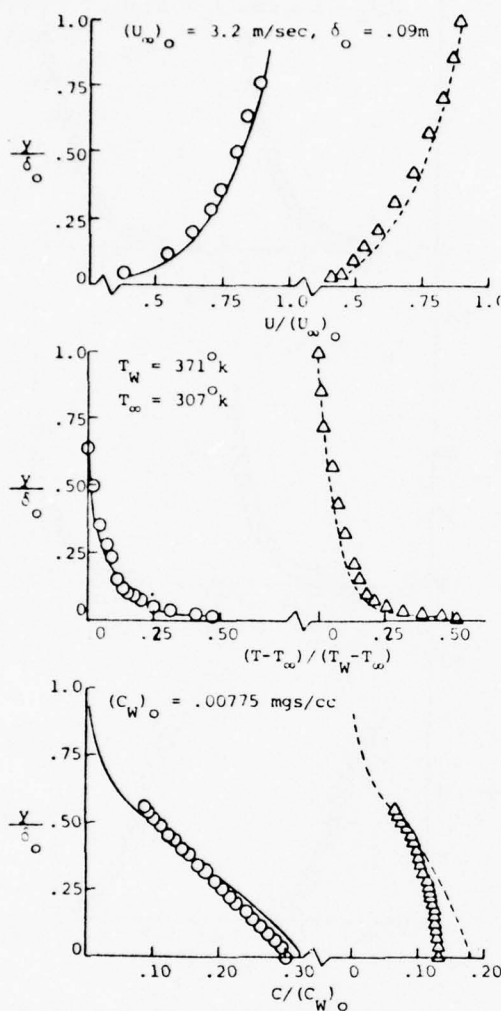
Fig. 6: Velocity, Temperature, and Concentration

x/δ_0	theory	exp.	ref.
10	——	O	33
20	----	Δ	33

well as for heating and cooling of the wall bound-
aries. This approach gives realistic solutions
not only to the engineering design parameters of
wall shear and surface heat transfer but also to the
the meteorological parameters which may be used for
studying pollutant diffusion in the atmospheric
boundary layer.

REFERENCES

/1/ Boussinesq, J.: Mem. Prés Par Div. Savants à
    L´acad. Sci. Paris, 23, 46 (1877)
/2/ Prandtl, L.: A. Angew. Math. U. Mech., 5, 136
    (1925)
/3/ Taylor, G.I.: Phil. Trans. Roy. Soc. London,
    215A, 1 (1915)
/4/ Von Kármán, Th.: Nachr. Akad. Wiss. Göttingen,
    Math. Phys. Kl., 58 (1930)
/5/ Hinze, J.O.: "Turbulence". McGraw-Hill (1959)
/6/ Kolmogorov, A.N.: Izv. Akad. Nauk. SSSR Ser.
    Phys., 6, 56 (1942)
/7/ Townsend, A.A.: "The Structure of Turbulent
    Shear Flow". Cambridge Univ. Press. (1956)
/8/ Monin, A.S. and A.M. Yaglom: "Statistical Fluid
    Mechanics: Mechanics of Turbulence". The MIT
    Press (1971)
/9/ Prandtl, L.: Nachr. Akad. Wiss. Göttingen, Van
    den Loeck und Ruprecht, 6 (1945)
/10/ Glushko, G.S.: Izv. Akad. Nauk SSSR Mekh., 4,
    13 (1965)
/11/ Spalding, D.B.: Appl. Mech. Review, 20, 735
    (1967)
/12/ Nevzglajdov, V.: J. Phys. (USSR) 9, 235 (1945)
/13/ Bradshaw, P., D.H. Ferris, and N.P. Atwell:
    J. Fluid Mech., 28, 593 (1967)
/14/ Lee, S.C. and P.T. Harsha: AIAA Journal, 8,
    1026 (1970)
/15/ Klebanoff, P.S.: NACA Report 1247 (1954)
/16/ Schon, J.P. and P. Mery: Atmos. Environ., 5,
    299 (1971)
/17/ Lee, S.C., P.T. Harsha, J.E. Auiler, and C.L.
    Lin: Proc. Heat Trans. Fluid Mech. Inst., 13,
    215 (1972)
/18/ Patanker, S.V. and D.B. Spalding: Int. J. Heat
    Mass Trans., 10, 1389 (1967)
/19/ Arya, S.P.S.: Proc. Symp. Air Pollution Turbu-
    lence and Diffusion, 191 (1971)
/20/ Fleagle, R.G. and J.A. Businger: "An Introduc-
    tion to Atmospheric Physics". Academic Press
    (1963)
/21/ Plate, E.J. "Aerodynamic Characteristics of
    Atmospheric Boundary Layers". U.S. Atomic En-
    ergy Commission Office of Information Service
    (1971)
/22/ Byrne, W.M., Jr.: Ph.D. Dissertation, Univer-
    sity of Missouri-Rolla (1970)
/23/ Spalding, D.B. and S.V. Patankar: "Heat and
    Mass Transfer in Turbulent Boundary". Chem.
    Rubber Co. Press (1968)
/24/ Rotta, J.C.: Jahrbuch 1970 der DGLR, 91 (1971)
/25/ Julien, H.L., W.M. Kays, and R.J. Moffat: J.
    Heat Trans., 93, 373 (1971)
/26/ Lumley, J.L. and H.A. Panofsky: "The Structure
    of Atmospheric Turbulence". Inter-Science Pub.
    (1964)
/27/ Reichardt, H.: Rept. Max-Planck Inst. für
    Störmungsforschung, 3, 1 (1950)
/28/ Moffat, R.J. and W.M. Kays: Int. J. Heat Mass
    Trans., 11, 1547 (1968)
/29/ Tai, R.C.: M.S. Thesis, University of Missouri
    Rolla (1969)
/30/ Julien, H.L.: Ph.D. Dissertation, Stanford
    University (1969)
/31/ Bradshaw, P.: J. Fluid Mech., 29, 625 (1967)
/32/ Pepper, D.W.: Ph.D. Dissertation, University
    of Missouri-Rolla (1973)
/33/ Malhotra, R.C.: Ph.D. Dissertation, Colorado
    State University (1962)

D. W. Pepper[1]

Post-doctoral Fellow.

S. C. Lee

Professor.

Department of Mechanical and Aerospace
Engineering and Graduate Center of Cloud
Physics Research,
University of Missouri-Rolla,
Rolla, Mo.

Transport Phenomena in Thermally Stratified Boundary Layers

Studies of heat, mass, and momentum transfer are made to analyze the formation of marine fogs in thermally stratified boundary layers in the atmosphere. The governing partial differential equations of continuity, momentum, temperature, and concentration are used to describe the transport phenomena. An additional equation of turbulence energy is introduced to account for the development of the turbulent motions. Simultaneous solution of this system of equations allows the turbulent exchange coefficients to be treated in the same way as all other dependent parameters. Verification of the theoretical approach is made by comparing the numerical predictions with wind tunnel simulations of neutral, stable, and unstable atmospheres. Application of the theory is extended to the investigation of the formation of advection fog over cold ocean surfaces. In addition to the established criteria obtained from wind tunnel data, the fog model takes into consideration the radiation and sedimentation of fog droplets as well as condensation and evaporation of liquid water.

1 Introduction

Considerable effort has been made in recent years to understand transport phenomena in thermally stratified boundary layers. Adequate knowledge in this area is valuable for predicting the diffusion process of air pollutants in the lower atmosphere as well as for forecasting air-water circulation for weather conditions. Many physical parameters are involved in atmospheric transport processes, such as wind, temperature, and concentration of the diffusing medium as well as the geographical terrain. Studies of atmospheric motions, however, are hindered by the turbulence generated from the interactions of all these related parameters. Moreover, as a result of the random motion of turbulence eddies, field measurements are often insufficient for formulating a reliable mathematical model.

Simulations of atmospheric boundary layers are usually accomplished by wind tunnel modeling and numerical computations. A detailed survey of the literature concerning field measurements, laboratory simulations, and numerical predictions is given by Pepper [1].[2] Although many questions have been raised as to whether atmospheric turbulence can be realistically simulated in a wind

tunnel, no definite answer is readily available. As a consequence, it appears necessary to develop a realistic model to numerically analyze transport phenomena which not only can be verified by wind tunnel experiments but may also be used for predicting atmospheric motions.

Mathematical analyses of turbulent transport processes are discussed by Hinze [2], Monin and Yaglom [3], and Lumley and Panofsky [4]. Based upon their studies, transport phenomena are normally treated by phenomenological and statistical theories. While physically more realistic than phenomenological models, the use of statistical description requires a large volume of carefully sampled experimental data which are not currently available. Phenomenological theory is based principally upon mixing length theories and turbulence kinetic energy approaches. The mixing length models, based upon the concept developed by Prandtl [5], incorporate rather simple yet successful empirical relations to account for the Reynolds shear stress term in the equations of motion. The use of turbulence kinetic energy to complete the Reynolds equations, first proposed by Kolmogorov [6], is discussed in textbooks by Townsend [7], Hinze [2], Monin and Yaglom [3], Tennekes and Lumley [8], and many others. Following the suggestions of Kolmogorov [6] and Prandtl [5], the turbulent shear stress is related to the turbulence kinetic energy's one-half power. This model is the basis of calculational procedures used by Glushko [9], Patankar and Spalding [10], and Gosman, et al. [11]. A simpler relationship is suggested by Nevzglajdov [12] in which the turbulent shear stress is linearly related to the turbulence kinetic energy. This concept has been successfully used by Bradshaw, et al. [13] and Lee and Harsha [14] in analyzing boundary layer and free tur-

bulent flows, respectively.

In lieu of the many different approaches used in closing the differential equations governing turbulent flows, it is necessary to investigate the validity of all available models before conducting an analysis. By using the experimental data of Klebanoff [15] and the neutral wind tunnel data of Schon and Mery [16] as a basis of comparison, it was possible to analyze the three methods of closure that are shown in Fig. 1. The disarray of data points in the Prandtl mixing length model indicates that the mixing length parameter requires modification for each particular problem. The Kolmogorov model, while more adequate than the Prandtl mixing length model, begins to show some scattering in the near wall regions of the boundary layer. The Nevzglajdov model, on the other hand, is simple and gives relatively less scattering for the same data. Similar conclusions are also drawn by Harsha and Lee [17] for free turbulent flows.

The approach adopted in this study attempts to make optimum use of the current advancement in numerical techniques coupled with presently available experimental data for the purpose of realistically predicting atmospheric motions with a minimum of empiricism. Comparison of the numerical results with wind tunnel simulations under various conditions of thermal stratification is to be discussed. Application of the present approach is being made to study the formation and dissipation of marine fog over the ocean.

2 Analysis

The basic equations, which describe the atmospheric boundary layer, consist of continuity, momentum, temperature, and concentration. For two-dimensional, steady-state boundary layer flows, the governing equations may be written as

$$\frac{\partial}{\partial X}\rho U + \frac{\partial}{\partial Z}\rho W = 0 \tag{1}$$

$$\rho U\frac{\partial U}{\partial X} + \rho W\frac{\partial U}{\partial Z} = \frac{\partial}{\partial Z}\left(\mu\frac{\partial U}{\partial Z} - \rho\overline{u'u'}\right) + F_m \tag{2}$$

$$\rho U\frac{\partial T}{\partial X} + \rho W\frac{\partial T}{\partial Z} = \frac{\partial}{\partial Z}\left(\alpha\frac{\partial T}{\partial Z} - \rho\overline{w'T'}\right) + F_h \tag{3}$$

$$\rho U\frac{\partial C^m}{\partial X} + \rho W\frac{\partial C^m}{\partial Z} = \frac{\partial}{\partial Z}\left(D\frac{\partial C^m}{\partial Z} - \rho\overline{w'c'}\right) + F_c{}^m \tag{4}$$

in which U and W are the time-average velocity components in the X and Z directions, respectively; ρ is the density; C^m is the concentration for species m; T is the mean temperature; the primes denote fluctuating quantities; μ, α, and D are the dynamic viscosity, thermal diffusivity and species diffusivity, respectively;
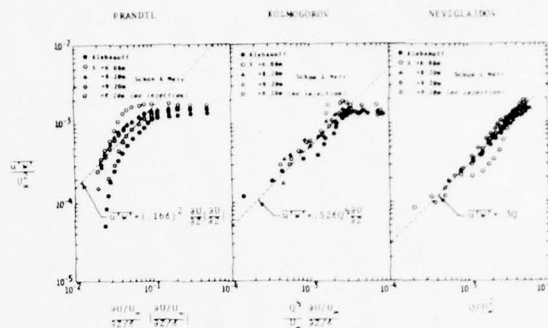

Fig. 1 Data correlation with turbulence models

and F_m, F_h, and $F_c{}^m$ are the source terms of momentum, energy, and concentration, respectively. Detailed discussion of the source terms is given in the Appendix. Closure of this system of equations is accomplished by using the Boussinesq [18] approximation and the Nevzglajdov [12] model, as modified by Lee and Harsha [14], the apparent turbulence kinetic energy, Q, can be related to the laminar and the turbulent shear stresses as

$$\mu\frac{\partial U}{\partial Z} - \rho\overline{u'w'} = 0.3\ \rho Q\frac{\partial U}{\partial Z}\bigg/\left|\frac{\partial U}{\partial Z}\right| \tag{5}$$

It is to be noted that the magnitude of Q is contributed by the shear stresses of the eddy motions in the turbulent layer, the molecular motions in the laminar sublayer, and both laminar and turbulent motions in the transition layer. An additional governing equation for the apparent turbulence kinetic energy is written as

$$\rho U\frac{\partial Q}{\partial X} + \rho W\frac{\partial Q}{\partial Z} = -\frac{\partial}{\partial Z}\left[\rho\overline{w'\left(\frac{P'}{\rho} + Q\right)}\right] + F_q \tag{6}$$

where F_q is the source term for the production and dissipation of turbulence kinetic energy.

Introducing the apparent Prandtl and Schmidt numbers as discussed by Lee, et al. [19], the exchange coefficients of momentum, heat, concentration and turbulence become

$$K_m = \mu - \rho\overline{u'w'}\bigg/\frac{\partial U}{\partial Z} = 0.3\ \rho Q\bigg/\left|\frac{\partial U}{\partial Z}\right| \tag{7}$$

$$K_h = \alpha - \rho\overline{w'T'}\bigg/\frac{\partial T}{\partial Z} = K_m/\sigma_h \tag{8}$$

Nomenclature

a = empirical constant

C^m = concentration of species m

c' = concentration fluctuation

c_p = specific heat at constant pressure

C_s = rate of formation of liquid water

D = coefficient of molecular diffusion

D_q = dissipation of turbulence kinetic energy

$F_c{}^m$ = source term for concentration equation

F_h = source term for temperature equation

F_m = source term for momentum equation

F_q = source term for turbulence kinetic energy

g = gravitational acceleration

K_c = exchange coefficient of concentration

K_h = exchange coefficient of heat

K_m = exchange coefficient of momentum

K_q = exchange coefficient of turbulence kinetic energy

k_s = mass absorption coefficient

L_h = latent heat of vaporization

P = static pressure

P' = pressure fluctuation

P_q = production of turbulence kinetic energy

Q = kinetic energy of turbulence

R = radiation energy

R_a = gas constant of air

R_i = gradient Richardson number

R_f = flux Richardson number

T = mean temperature

t' = temperature fluctuation

U = mean velocity in the X-direction

u' = velocity fluctuation in the X-direction

V_d = sedimentation velocity of fog droplets

W = mean velocity in the Z-direction

w' = velocity fluctuation in the Z-direction

X = horizontal distance

Z = vertical distance

α = thermal diffusivity

β = emissivity

δ = boundary layer thickness

μ = dynamic viscosity

ρ = density

σ = Stefan-Boltzmann constant

σ_c = turbulent Schmidt number

σ_h = turbulent Prandtl number

σ_q = equivalent Prandtl number

$$K_c = D - \overline{\rho u'c'} \Big/ \frac{\partial C}{\partial Z} = K_m/\sigma_c \qquad (9)$$

and

$$K_q = -\overline{\rho u'\left(\frac{P'}{\rho} + Q\right)} \Big/ \frac{\partial Q}{\partial Z} = K_m/\sigma_q \qquad (10)$$

respectively, in which σ_h is the apparent Prandtl number with a numerical value of 0.75, obtained experimentally by Arya [20] for a simulated stable atmosphere, σ_c the apparent Schmidt number, equal to 0.75 as given by Fleagle and Businger [21], and σ_q the equivalent Prandtl number, which is approximately equal to 0.70 as determined by Lee, et al. [22]. Both Prandtl and Schmidt numbers were allowed to vary from 0.4 to 1.0 under various conditions of thermal stability but proved to be insignificant in altering the results to any appreciable degree. For lack of any reliable functional relation to account for the variation in the apparent Prandtl and Schmidt numbers, σ_h and σ_c were assumed to be constant in the study.

Using the concept of exchange coefficients, the governing equations of momentum, heat, mass, and turbulence are parabolic type. The system of equations can be simultaneously solved for the dependent variables of velocity, temperature, concentration, and turbulence using the numerical procedure of Patankar and Spalding [10]. It should be noted that the exchange coefficients are determined locally from the apparent turbulence kinetic energy which is a function of the space coordinates. The detailed numerical scheme and all necessary boundary conditions are given by Pepper [1]. For the purpose of testing the predictability, the developed method is verified with wind tunnel data before being applied to atmospheric problems.

3 Verification With Wind Tunnel Data

Verification of the present model is made by using available experimental data. Comparison with wind tunnel data is made under conditions similar to neutral, stable, and unstable atmospheric boundary layers. While a number of experimental investigations
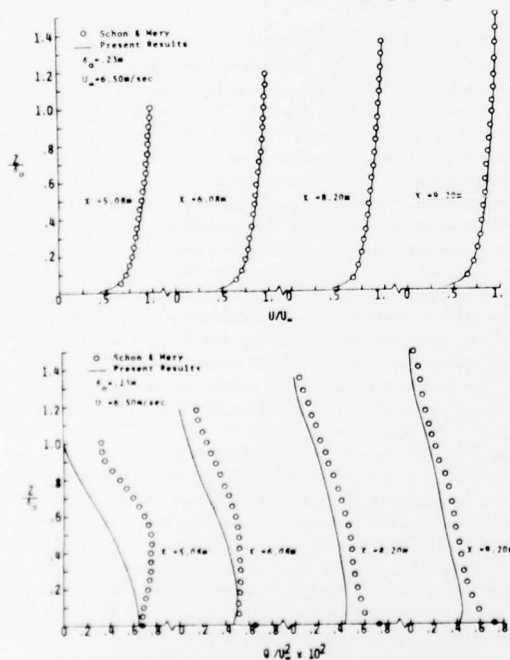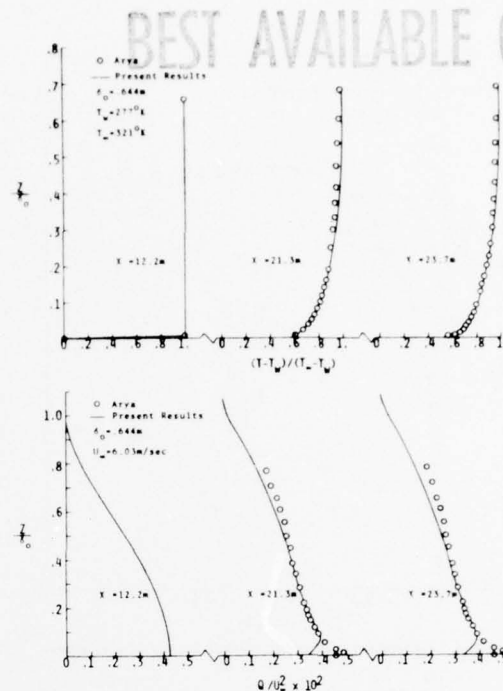

Fig. 3 Comparison of results for a stable atmosphere

Fig. 2 Comparison of results for a neutral atmosphere

have been made under neutral atmospheric conditions in meteorological wind tunnels, only a few cases contain turbulence kinetic energy data which are pertinent to the exchange coefficient model employed here. Similar investigations of experimental work in thermally stratified boundary layers disclose even less available data.

Preliminary investigations are made in a neutral atmosphere by comparing the predicted results with the wind tunnel simulation of Schon and Mery [16] as shown in Fig. 2. The subscript, o, denotes initial conditions. A nondimensional apparent turbulence kinetic energy profile, based upon measurements by Klebanoff [15], is used to generate the initial profile in the numerical scheme. The discrepancy between measured and predicted turbulence kinetic energy is due to the use of the Klebanoff profile which is for fully developed flow, while the initial profile for the Schon and Mery case is still a developing flow. However, the necessity of predicting various atmospheric conditions, without having measured turbulence data as the initial profile, limits our choice to Klebanoff's data for all studied cases. The good agreement in velocity profile comparison indicates that a fully developed turbulent profile for average velocity does not necessarily mean that the turbulence is in equilibrium.

Investigations of stably stratified atmosphere are made by comparing the predicted temperature and turbulence profiles with the wind tunnel simulation data of Arya [20], as shown in Fig. 3. The initial temperature distribution is assumed to be uniform. The Klebanoff turbulence kinetic energy distribution, similar to that for the neutral case, is used for the initial profile. The underprediction of turbulence kinetic energy occurs within 10 percent of the boundary layer near the surface. This discrepancy suggests that the Nevzglajdov model is questionable in the close vicinity of the wall boundary, if the measurements are truly reliable. Once outside this region of the calculated maximum turbulence kinetic energy, the predicted profiles begin to agree with the experimental data. Because the gradient Richardson number, R_i, serves as a quantitative measure of the thermal stratification, the distribution of R_i is plotted as a function of Z/δ in Fig. 4. Although a discrep-
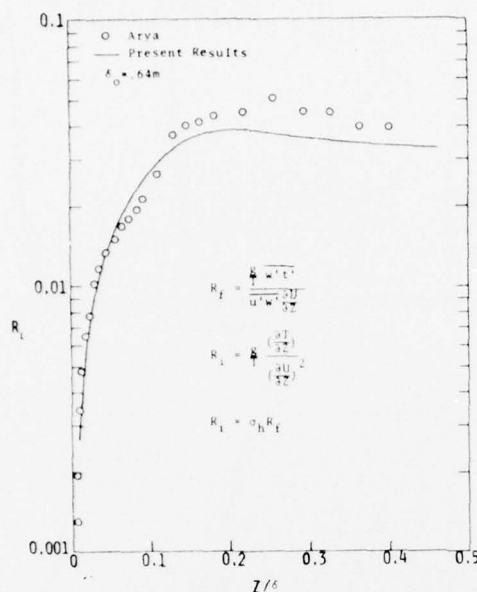
Fig. 4 Richardson number comparison for stable atmosphere

Fig. 6 Schematics of advection fog over the ocean

ancy occurs in the turbulence kinetic energy comparison, the Richardson number predictions agree well with Arya's data even in the lower 10 percent of the boundary layer. The gradient Richardson number, R_i, is related to the flux Richardson number, R_f, by the ratio of the momentum exchange coefficient to the heat exchange coefficient.

Investigations of unstably stratified atmospheres are made by comparing the predicted temperature and concentration profiles

with the wind tunnel simulation data of Malhotra and Cermak [23] as shown in Fig. 5. Using the measured profiles at a distance of 0.3 m downstream of a simulated source ($X_s = 0.3$ m) as the initial concentration and temperature profiles, the predicted results agree well with the measured data throughout the flow field. No turbulence data are available for comparison even though the standard Klebanoff profile is used as the initial turbulence in the numerical scheme. Predictions, with reasonable accuracy for time averaged quantities of velocity, temperature, and concentration, appear to be possible using an approximate initial profile for turbulence; if the turbulence energy is being balanced simultaneously with the momentum, heat, and mass, consistently throughout a thermally stratified atmospheric boundary layer. Extension of this method is being made to predict the formation of advection fog occurring over cold sea surfaces.

4 Advection Fog Formation

Because of insufficient information regarding ocean fogs, few studies are available in the literature. However, studies on land fog and coastal fog have been made by Mack, et al. [24], Fisher and Caplan [25], Zdunkowski and Trask [26], and Barker [27]. Consideration of the microphysical processes of condensation, radiation, and sedimentation in developing the advection fog model is based on the current information used for land and coastal fog studies.

Fig. 6 shows schematically the formation of advection fog as warm moist air blows over an aqueous surface with continuously decreasing isotherms. As a result of the transfer of thermal energy between air and ocean, the air temperature near the ocean surface is lowered until the dew point temperature is reached. This process results in the condensation of water vapor into small liquid droplets, if it is assumed that sufficient number of sea salt particles are available as condensation nuclei. A brief outline of the saturation adjustment procedure, developed by McDonald [28] and Asai [29] is given in the Appendix.

Fig. 7 shows the effect of wind velocity on fog development. Wind velocities of 3 and 6 m/s are used for analyzing an atmospheric boundary layer with a thickness of 943 m. Lines of constant temperature, seen to be emitting from the surface, arise from the continuous cooling of the surface, as shown for the wind velocity of 6 m/s case. A similar trend is also found in the wind velocity of 3 m/s case. Defining the fog boundary as the limit where the liquid water content approaches zero, it is noted that an increase in wind velocity results in a decrease of the fog layer height. Moreover, fog only forms in the region where a stable thermal stratification occurs. This result can be qualitatively verified from field ob-

Fig. 5 Comparison of results for an unstable atmosphere

servations. Leipper [30] observed that for a period of two days, fog formed very rapidly when the temperature distribution of a stable atmosphere occurred near the ocean's surface. Liquid water condensed out continuously to form fog particles as long as the stable stratification persisted. Until the temperature distribution near the ocean's surface returned to a neutral atmosphere on the third day, fog began to dissipate. Visibility started to improve on the fourth day as the temperature inversion region lifted up from the ocean surface to the lower atmosphere. Fog became stratus cloud on the fifth day when the lower atmosphere returned to neutral condition.

5 Conclusion

An analytical investigation of turbulent diffusion in thermally stratified boundary layers is made by using a phenomenological theory based upon the apparent turbulence kinetic energy. The exchange coefficient of momentum is determined based on the modified Nevzglajdov model which relates the local shear stress with the local turbulence energy. The exchange coefficient of heat and mass are determined by relating them with the exchange coefficient of momentum through Prandtl and Schmidt numbers. These coefficients can only be evaluated simultaneously with other dependent variables of velocity, temperature, and concentration. Verification of this method is made by using wind tunnel simulations of thermally stratified atmosphere. Predictions for actual conditions can only be quantitatively verified when more completed field data are made available. This study demonstrates that the development of a realistic model for predicting the transport phenomena between atmospheric and aqueous surface layers needs close cooperation among researchers in many disciplinary areas.

Acknowledgments

References

1 Pepper, D. W., "Numerical Simulation of Heat, Mass, and Momentum Transfer in an Atmospheric Boundary Layer," PhD dissertation, Dept. of Mech. and Aero. Engr., Univ. of Mo.-Rolla, Rolla, Mo., 1973, p. 184.

2 Hinze, J. O., Turbulence, McGraw-Hill, New York-Toronto-London, 1959, p. 586.

3 Monin, A. S., and Yaglom, A. M., Statistical Fluid Mechanics, Nauka Press, Moscow, English Translation, MIT Press, 1971, p. 769.

4 Lumley, J. L., and Panofsky, H. A., The Structure of Atmospheric Turbulence, Interscience Publishers, New York-London-Sydney, 1964, p. 239.

5 Prandtl, L., "Uber Die Ausgebildete Turbulenz," Z. angew. Math. Mech., Vol. 5, 1925, pp. 136-139.

6 Kolmogorov, A. M., "Equations of Turbulent Motion of an Incompressible Fluid," Izv. Akad. Mauk. SSSR Ser. Phys., Vol. 6, 1942, pp. 56-58.

7 Townsend, A. A., The Structure of Turbulent Shear Flow, Cambridge Univ. Press, 1956, p. 315.

8 Tennekes, H., and Lumley, J. L., A First Course in Turbulence, MIT Press, Cambridge, Mass., 1972, p. 300.

9 Glushko, G. S., "Turbulent Boundary Layer on a Flat Plate in an Incompressible Fluid," NASA TT F-10, 080, English translation, Izv. Akad. Nauk SSSR Ser. Mek., No. 4, 1965, pp. 13-23.

10 Patankar, S. V., and Spalding, D. B., "A Finite Difference Procedure for Solving the Equations of the Two-Dimensional Boundary Layer," Intl. J. of Heat and Mass Transfer, Vol. 10, 1967, pp. 1389-1411.

11 Gosman, A. D., Pun, W. M., Runchal, A. K., Spalding, D. B., and Wolfshtein, M., Heat and Mass Transfer in Recirculation Flows, Academic Press, London, 1969, p. 338.

12 Nevzglajdov, V., "A Phenomenological Theory of Turbulence," J. of Phys., USSR, Vol. 9, 1945, pp. 235-243.

13 Bradshaw, P., Ferris, D. H., and Attwell, M. P., "Calculation of Boundary Layer Development Using the Turbulent Energy Equation," J. of Fluid Mech., Vol. 28, Part 3, 1967, pp. 593-616.

14 Lee, S. C., and Harsha, P. T., "Use of Turbulent Kinetic Energy in Free Turbulent Mixing Studies," AIAA J., Vol. 8, No. 6, 1970, pp. 1026-1032.

15 Klebanoff, P. S., "Characteristics of Turbulence in a Boundary Layer With Zero Pressure Gradient," NACA Rept., 1247, 1955, p. 19.

16 Schon, J. P., and Mery, P., "A Preliminary Study of the Simulation of Neutral Atmospheric Boundary Layer Using Air Injection in a Wind Tunnel," Atmos. Environ., Vol. 5, 1974, pp. 299-311.

17 Harsha, P. T., and Lee, S. C., "Correlation Between Turbulent Shear Stress and Turbulent Kinetic Energy," AIAA J., Vol. 8, No. 8, 1970, pp. 1508-1510.

18 Boussinesq, T. V., "Theorie de l'ecoulement Tourbillant," Mem. Prepar. div. Sav., Vol. 23, 1877, p. 46.

19 Lee, S. C., Pepper, D. W., Byrne, W. M., and Tai, R. C., "Heat Mass and Momentum Transfer in Turbulent Boundary Layer Flows," Proceedings Fifth International Heat Transfer Conference, Tokyo, Japan, Vol. II, 1974, pp. 104-108.

20 Arya, S. P. S., "Structure of Stably Stratified Turbulent Boundary Layer," Tech. Report CER68-69SPSA10, Fluid Dyn. and Diffusion Lab., Colo. State Univ., Fort Collins, Colo., 1968, p. 157.

21 Fleagle, R. G., and Businger, J. A., An Introduction to Atmospheric Physics, Academic Press, 1963, p. 346.

22 Lee, S. C., Harsha, P. T., Auiler, J. E., and Lin, C. L., "Heat Mass and Momentum Transport in Free Turbulent Mixing," Proc. Heat Transf. Fluid Mech. Inst., 1972, pp. 215-230.

23 Malhotra, R. C., and Cermak, J. E., "Mass Diffusions in Neutral and Unstably Stratified Boundary Layer Flows," Intl. J. of Heat and Mass Transfer, Vol. 7, 1964, pp. 169-186.

24 Mack, E. J., Eadie, W. J., Rogers, C. W., Kocmond, W. C., and Pilie, R. J., "A Field Investigation and Numerical Simulation of Coastal Fog," Cornell Aero. Lab., CAL No. CJ-5055-M-1, Project Fog Drops Annual Summary Rep., 1972, p. 136.

25 Fisher, E. L., and Caplan, P., "An Experiment in Numerical Prediction of Fog and Stratus," J. Atmos. Sci., Vol. 20, 1963, pp. 425-437.

26 Zdunkowski, W. G., and Trask, D. C., "Application of a Radiative-Conductive Model to the Simulation of Nocturnal Temperature Changes Over Different Soil Types," J. Appl. Meteor., Vol. 10, No. 5, 1971, pp. 937-948.

27 Barker, E. H., "Oceanic Fog, a Numerical Study," EPRF, Naval Postgraduate School, Tech. Paper 6-73, 1973, p. 65.

28 McDonald, J. E., "The Saturation Adjustment in Numerical Modeling of Fog," J. Atmos. Sci., Vol. 20, 1963, pp. 276-478.

29 Asai, T., "A Numerical Study of the Air-Mass Transformation Over the Japan Sea in Winter," J. Meteor. Soc. Japan, Vol. 43, No. 1, 1965, pp. 1-7.

30 Leipper, D. F., "Fog Development at San Diego, California, Sear Sound," J. Marine Res., Vol. 7, 1948, pp. 337-346.

31 Murray, F. W., "On the Computation of Saturation Vapor Pressure," J. Appl. Meteor., Vol. 6, 1967, pp. 203-204.

32 Plate, E. J., Aerodynamic Characteristics of Atmospheric Boundary Layers, U.S.A.E.C. Critical Review Ser., TID-25465, 1971, p. 190.

33 Byrne, W. M., and Lee, S. C., "A Differential Method for the Prediction of the Effects of Atmospheric Boundary Layer Turbulence," Proc. Symp. on Air Pollution Turbulence and Diffusion, Sandia Lab., Albuquerque, N. Mex., 1972, pp. 231-243.
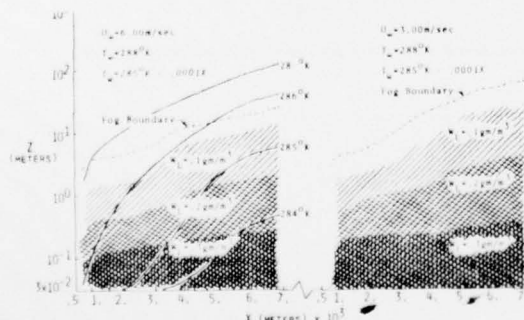

Fig. 7 Fog-layer height affected by wind velocity

APPENDIX

The source terms used in the governing equations are derived from information available in the current literature. For the reader's convenience, a brief summary is given in the following.

Momentum Equation. Pressure, gravity, buoyancy, and Coriolis forces may all be involved in the source term; however, in the studied cases, only the pressure force is significant.

$$F_m = -(\partial P/\partial X) \qquad (A-1)$$

and

$$P = P_{sl}\exp(-gZ/R_a T) \qquad (A-2)$$

in which P_{sl} is the atmospheric pressure at sea level, and R_a is the gas constant of air.

Temperature Equation. Latent heat and radiation are considered by the relation

$$F_h = \{L_h\dot{C}_s - (\partial R/\partial Z)\}/c_p \qquad (A-3)$$

in which L_h is the latent heat of evaporation at a given temperature, and $\dot{C}_s$ is the rate of formation of condensed liquid water at a given temperature and its corresponding partial pressure of vapor. In order to calculate $\dot{C}_s$, the saturation adjustment procedures of McDonald [28] and Asai [29] may be outlined as follows: Assuming air and water vapor can be treated as ideal gases, the amount of condensed liquid water can be expressed as

$$\omega_s = 0.622\frac{P_v - P_{vg}}{P_a} \sim 0.622\frac{P_v - P_{vg}}{P} \qquad (A-4)$$

for each unit of air mass, in which P_{vg} is the partial pressure of vapor at saturation, P_v is the partial pressure of vapor at each thermodynamic state of the atmosphere, and P_a is the partial pressure of air which is approximately equal to the total pressure of the atmosphere, P. By using the Clausius-Clapeyron equation for liquid-vapor phase change, the change of vapor pressure corresponding to the change of temperature can be written as

$$\frac{P_{vg} - P_g}{T_g - T} = \frac{0.622 P_g L_h}{R_a T^2} \qquad (A-5)$$

The saturation vapor pressure, P_g, which is a function of temperature only, is given by Murray [31] as

$$P_g = 6.108\exp\left\{\frac{17.269(T - 273.16)}{T - 35.86}\right\} \qquad (A-6)$$

However, the first law of thermodynamics requires that the pressure and temperature of vapor in an isobaric atmosphere satisfy the following relation

$$\frac{P_v - P_{vg}}{T_g - T} = \frac{c_p P}{0.622 L_h} \qquad (A-7)$$

in which c_p is the specific heat of air. By eliminating P_{vg} between equations (A-5) and (A-7), the change of temperature before and after condensation becomes

$$T_g - T = \frac{0.622(p_v - p_g)L_h R_a T^2}{pc_p R_a T^2 + 0.387 L_h^2 p_g}. \qquad (A-8)$$

By combining equation (A-8), (A-6), and (A-4), the amount of liquid water condensed per unit air mass becomes

$$\omega_s = \frac{c_p}{L_h}(T_g - T). \qquad (A-9)$$

The rate of formation of liquid water may then be written as

$$\dot{C}_s = \int_A \rho U\omega_s dZ \qquad (A-10)$$

The radiation term occurring in equation (A-3) may be written in the form suggested by Mack, et al. [23]

$$R(Z) = \beta\sigma T_w^4\exp\left(-1.6k_\lambda\int_{Z_b}^{Z_t}\rho\omega^m dZ\right) \qquad (A-11)$$

in which β is the emissivity of a nonblack surface ($\beta = 0.25$), σ is the Stefan-Boltzmann constant, T_w is the surface temperature, k_λ is a single spectrally-averaged mass absorption coefficient ($k_\lambda = 1.5 \times 10$ cm/gm), and Z_t and Z_b are the top and bottom of the fog layer, respectively. The gradient of the radiation effect then becomes

$$\frac{\partial R}{\partial Z} = 1.6\beta\sigma T_w^4 k_\lambda\rho\omega^m\exp\left(-1.6k_\lambda\int_{Z_b}^{Z_t}\rho\omega^m dZ\right) \qquad (A-12)$$

in which ω^m is the liquid water content per unit air mass.

Species Equation. Three species are considered in the fog model: air ($m = 1$), water vapor ($m = 2$), and liquid water ($m = 3$). No air can be formed during fog formation and dissipation processes. Consequently,

$$F_c^1 = 0 \qquad (A-13)$$

Water vapor can only be formed at the expense of liquid water, thus

$$F_c^2 = -\dot{C}_s \qquad (A-14)$$

Liquid water can be formed by condensation of water vapor and also be removed by fallout as water drops. This leads to the expression

$$F_c^3 = \dot{C}_s + \frac{\partial}{\partial Z}(V_d\rho\omega^m) \qquad (A-15)$$

where V_d is the falling velocity of water drops

$$V_d = 5.3 \times 10^3\left(\frac{\omega^m}{N}\right)^{2/3} \qquad (A-16)$$

with N representing the number of drops per unit volume. It is noted that equation (A-16) is based on the assumption that all drops are less than 20 μm in radius. Assuming a drop concentration of N = 50 cm^{-3},

$$V_d = 4 \times 10^2(\omega^m)^{2/3} \text{ (cm/s)}. \qquad (A-17)$$

Turbulence Kinetic Energy. Production, P_q, and dissipation, D_q, of the turbulence kinetic energy are discussed by Lee, et al. [22] and Plate [32]. The production term may be written as

$$P_q = K_m\left(\frac{\partial U}{\partial Z}\right)^2\left(1 - \frac{R_i}{\sigma_h}\right) \qquad (A-18)$$

which consists of turbulence energy generated by the mean shear flow and the thermal stratification. The dissipation term, as discussed by Patankar and Spalding [10] and Glushko [9], may be written as

$$D_q = a\rho Q^{3/2}/\delta \qquad (A-19)$$

in which δ is the boundary layer thickness. The coefficient for non-isotropy of the turbulence, a, is given by Byrne and Lee [33] as

$$\begin{aligned} a &= 1.8 & \text{for } Z > \frac{\delta}{4}\\ a &= 1.8\left(\frac{\delta}{4Z}\right) & \text{for } Z < \frac{\delta}{4} \end{aligned} \qquad (A-20)$$

which agrees with the model used by Bradshaw, et al. [13].

B12

APPENDIX C

Published Paper on Numerical Method for

"Fog Situations in Recirculating Flow Regions"

"Numerical Methods for Separated Flow Solutions around a Circular

Cylinder", American Institute of Aeronautics and Astronautics Journal,

14, 900-907, 1976.

Numerical Methods for Separated Flow Solutions around a Circular Cylinder

C. L. Lin,* D. W. Pepper,† and S. C. Lee‡
University of Missouri-Rolla, Rolla, Mo.

Numerical solutions of the Navier-Stokes equations were obtained for separated flows around a circular cylinder at Reynolds numbers 40, 80, and 200. The flowfields were obtained by using three finite-difference techniques. The implicit scheme solved by matrix factorizations gave the best accuracy and used the least computer time. The flow pattern in the recirculating region of a circular cylinder begins to oscillate as the Reynolds number exceeds 40. The calculated drag coefficients, separation angles, and Strouhal numbers were compared with available experimental data. Computational inaccuracy resulting from numerical approximations needs to be identified before a complicated flow phenomenon can be realistically analyzed.

Nomenclature

a = arbitrary constant for coordinate transformation
f = frequency of Kármán vortex street
$[L]$ = lower matrix after modification
$[M]$ = coefficient matrix
m = number of iterations
$[N]$ = modifier of the coefficient matrix
n = number of time-steps
$\{q\}$ = column matrix
r = radial coordinate
R = radius of the cylinder
Re = Reynolds number, $2UR/v$
S = Strouhal number, $2fR/U$
t = time
$[U]$ = upper matrix after modification
U = freestream velocity
V_θ = velocity in the θ direction
V_r = velocity in the r direction
Z = nondimensionalized radial coordinate
ω = vorticity
ψ = stream function
v = kinematic viscosity
θ = angular coordinate
Δt = time increment
$\Delta\theta$ = angular increment
ΔZ = radial increment
$\{\Phi\}$ = column matrix

I. Introduction

BECAUSE the Navier-Stokes equations are nonlinear, exact solutions are not currently available. The necessity of providing reasonable estimates for complicated flow phenomena leaves research engineers very little choice. The numerical method is one of the very few acceptable tools that is capable of making any contribution to engineering designs or environmental controls. Recent developments in high-speed digital computers make this approach both effective and popular; however, every numerical approach for a given physical problem requires both physical assumptions

and mathematical approximations. Computer solutions, especially in practical problems of questionable physical assumptions such as an unverified closure scheme for turbulent flows as discussed by Lee and Harsha[1] and Pepper and Lee,[2] may appear to give reasonable results by substituting unrealistic physical assumptions with incorrect mathematical approximations. One needs to test a numerical method for its accuracy in the developing stage by applying it to a given problem that requires no physical assumptions. Separated flow around a circular cylinder at relatively low Reynolds numbers is one of the thoroughly investigated problems that can provide the basis for such a study in numerical accuracy.

Numerical techniques for solving partial differential equations have been discussed by Conte,[3] Richtmyer,[4] Roache,[5] and many others. Solutions for separated flow problems usually require substantial computer time because of the elliptical nature of the governing equations. Multidimensional separated flows occur in many engineering and environmental problems, which require not only the solution of the Navier-Stokes equations but also the simultaneous solutions of the energy and species equations. Past experience indicates that some numerical techniques may give better accuracy, whereas others may need less computer time. To avoid an unnecessary waste of effort and resources, we conducted a preliminary investigation in which we applied several commonly used numerical methods to a thoroughly investigated problem for the purpose of comparing the numerical accuracy and the required computer time.

The problem of separated flow around a circular cylinder has been thoroughly investigated both experimentally and theoretically. Available information on drag coefficients, separation angles, and Strouhal numbers has been reported by Schlichting,[6] Thoman and Szewczyk,[7] and many others. In the present study, physical evidence will be used for investigating the effect of numerical approximations on solutions of elliptical partial differential equations.

II. Analysis

The governing equations for an incompressible, two-dimensional, unsteady laminar flow over a circular cylinder can be written as

$$\frac{\partial\omega}{\partial t} + \frac{1}{r}\frac{\partial(r\omega V_r)}{\partial r} + \frac{1}{r}\frac{\partial(\omega V_\theta)}{\partial\theta} = v\left[\frac{1}{r}\frac{\partial}{\partial r}\left(r\frac{\partial\omega}{\partial r}\right) + \frac{1}{r^2}\frac{\partial^2\omega}{\partial\theta^2}\right] \quad (1)$$

with

$$\omega = \frac{1}{r}\left[\frac{\partial(rV_\theta)}{\partial r} - \frac{\partial V_r}{\partial\theta}\right] \quad (2)$$

In these equations, ω is the vorticity, and V_r and V_θ are the velocity components in the r and θ directions, respectively. In terms of the stream function ψ the velocity components may be written as

$$V_r = [(1/r)(\partial\psi/\partial\theta)], \quad V_\theta = \partial\psi/\partial r \tag{3}$$

When radius R is used as the characteristic length and the freestream velocity U as the characteristic velocity, the nondimensionalized stream function and vorticity become

$$\psi' = \psi/UR, \quad \omega' = \omega R/U \tag{4}$$

The independent variables of t, r, and θ are

$$t' = tU/R, \quad r' = r/R, \quad \theta' = \theta/a \tag{5}$$

in which a is an arbitrary constant for controlling the increment of the transformed coordinate. Because the flowfield variations take place more rapidly in the vicinity of the cylinder than in regions at large distances from the cylinder, it is convenient to transform the radial coordinate by an exponential function,

$$e^{aZ} = r/R \tag{6}$$

The nondimensionalized governing equations with the primes eliminated for simplicity then become:

$$a^2 e^{2aZ}\frac{\partial\omega}{\partial t} - \frac{\partial\psi}{\partial\theta}\frac{\partial\omega}{\partial Z} + \frac{\partial\psi}{\partial Z}\frac{\partial\omega}{\partial\theta} = \frac{2}{Re}\left[\frac{\partial^2\omega}{\partial Z^2} + \frac{\partial^2\omega}{\partial\theta^2}\right] \tag{7}$$

and

$$\omega = \frac{1}{a^2 e^{2aZ}}\left[\frac{\partial^2\psi}{\partial Z^2} + \frac{\partial^2\psi}{\partial\theta^2}\right] \tag{8}$$

in which Re is the Reynolds number based on the diameter of the circular cylinder and the freestream velocity.

III. Finite-Difference Methods

Numerical solutions were obtained by writing the governing differential equations of vorticity, Eq. (7), and stream function, Eq. (8), into finite difference forms. By using i and j to denote the locations in the θ and Z directions, respectively, and employing m for the number of iterations and n for the number of time-steps, numerical solutions for the separated flow around a circular cylinder were obtained with the following three methods.

A. DDE-GSI

The directional difference explicit (DDE) method, as discussed by Thoman and Szewczyk,[7] was used for solving the vorticity equation. The values of $\omega_{i,j}$ at the $(n+1)$th time-step were calculated by using those of the (n)th time-step through the following relation

$$\omega_{i,j}^{n+1} = \frac{\Delta t}{a^2 e^{2aZ}}\left[1 - \frac{4}{Re}\left(\frac{1}{(\Delta Z)^2} + \frac{1}{(\Delta\theta)^2}\right)\right]\omega_{i,j}^n$$
$$+ \frac{2}{Re}\left[\frac{\omega_{i,j+1}^n + \omega_{i,j-1}^n}{(\Delta Z)^2} + \frac{\omega_{i+1,j}^n + \omega_{i-1,j}^n}{(\Delta\theta)^2}\right]$$
$$+ \left[\left(\frac{\partial\psi}{\partial\theta}\omega\right)_{i,j+1}^n - \left(\frac{\partial\psi}{\partial\theta}\omega\right)_{i,j}^n\right]\frac{1}{\Delta Z}$$
$$- \left[\left(\frac{\partial\psi}{\partial Z}\omega\right)_{i+1,j}^n - \left(\frac{\partial\psi}{\partial Z}\omega\right)_{i,j}^n\right]\frac{1}{\Delta\theta} \tag{9}$$

Equation (9) is an explicit form of the nonlinear vorticity equation. In order to maintain numerical stability, the following restrictions were suggested by Thoman and Szewczyk[7] for the nonlinear terms

$$(\partial\psi/\partial\theta)_{i,j} > 0 \qquad \omega_{i+1,j} = \omega_{i,j} \tag{10a}$$

$$(\partial\psi/\partial\theta)_{i,j+\frac{1}{2}} < 0 \qquad \omega_{i,j+\frac{1}{2}} = \omega_{i,j+1} \tag{10b}$$

$$(\partial\psi/\partial\theta)_{i,j-\frac{1}{2}} > 0 \qquad \omega_{i,j-\frac{1}{2}} = \omega_{i,j-1} \tag{10c}$$

$$(\partial\psi/\partial\theta)_{i,j-\frac{1}{2}} < 0 \qquad \omega_{i,j-\frac{1}{2}} = \omega_{i,j} \tag{10d}$$

$$(\partial\psi/\partial Z)_{i+\frac{1}{2},j} > 0 \qquad \omega_{i+\frac{1}{2},j} = \omega_{i+1,j} \tag{10e}$$

$$(\partial\psi/\partial Z)_{i+\frac{1}{2},j} < 0 \qquad \omega_{i+\frac{1}{2},j} = \omega_{i,j} \tag{10f}$$

$$(\partial\psi/\partial Z)_{i-\frac{1}{2},j} > 0 \qquad \omega_{i-\frac{1}{2},j} = \omega_{i,j} \tag{10g}$$

$$(\partial\psi/\partial Z)_{i-\frac{1}{2},j} < 0 \qquad \omega_{i-\frac{1}{2},j} = \omega_{i-1,j} \tag{10h}$$

Once the vorticity values were obtained, the stream functions could be calculated by using the Gauss-Seidel iteration (GSI) method as discussed by Conte.[3] The values of $\psi_{i,j}$ at the $(n+1)$th time-step and the $(m+1)$th iteration were calculated by using the following relation

$$\psi_{i,j}^{m+1} = \frac{1}{d_{i,j}}\left[-a^2 e^{2aZ}\omega_{i,j}^n + \frac{1}{(\Delta Z)^2}\left(\psi_{i,j+1}^m + \psi_{i,j-1}^{m+1}\right)\right.$$
$$\left. + \frac{1}{(\Delta\theta)^2}\left(\psi_{i+1,j}^m + \psi_{i-1,j}^{m+1}\right)\right] \tag{11}$$

in which $d_{i,j} = [2/(\Delta Z)^2] + [2/(\Delta\theta)^2]$. The iteration process was completed when the difference of the numerical values of ψ between the $(m+1)$th and the (m)th iterations was less than a prescribed tolerance. The same procedure was repeated for the successive time-steps until steady-state solutions were reached.

B. ADI-SOR

The alternating directional implicit (ADI) method was proposed by Peaceman and Rachford[8] for solving linear differential equations and modified by Douglas,[9] Wachspress,[10] and many others for improving computational accuracy. Son and Hanratty[11] used the method for flow around circular cylinders with the assumption that the flowfield is symmetric to the axis of the flow direction. Lin and Lee[12] used the method for calculating transient flows around a sphere. However, it was noted that for most Reynolds numbers separated flow oscillates in the wake region. By eliminating the assumption of flow symmetry in the wake region, an extension of Lin and Lee's approach was used for solving the vorticity equation. Two half-time steps were used. The first half-time step is an implicit finite difference equation in the θ direction

$$T_{i+1,j}\omega_{i+1,j}^{n+\frac{1}{2}} + T_{i,j}\omega_{i,j}^{n+\frac{1}{2}} + T_{i-1,j}\omega_{i-1,j}^{n+\frac{1}{2}} = T \tag{12}$$

in which

$$T_{i+1,j} = \frac{1}{4\Delta Z\Delta\theta}(\psi_{i,j+1}^n - \psi_{i,j-1}^n) - \frac{2}{Re(\Delta\theta)^2} \tag{13a}$$

$$T_{i,j} = \frac{2a^2 e^{2aZ}}{\Delta t} + \frac{4}{Re(\Delta\theta)^2} \tag{13b}$$

$$T_{i-1,j} = -\frac{1}{4\Delta Z\Delta\theta}(\psi_{i,j+1}^n - \psi_{i,j-1}^n) - \frac{2}{Re(\Delta\theta)^2} \tag{13c}$$

and

$$T = \left[\frac{1}{4\Delta Z\Delta\theta}(\psi_{i+1,j}^n - \psi_{i-1,j}^n) + \frac{2}{Re(\Delta Z)^2}\right]\omega_{i,j+1}^n$$
$$+ \left[\frac{2a^2 e^{2aZ}}{\Delta t} - \frac{4}{Re(\Delta Z)^2}\right]\omega_{i,j}^n + \left[\frac{2}{Re(\Delta Z)^2}\right.$$
$$\left. - \frac{1}{4\Delta Z\Delta\theta}(\psi_{i+1,j}^n - \psi_{i-1,j}^n)\right]\omega_{i,j-1}^n \tag{13d}$$

The second half-time step is an implicit finite-difference equation in the Z direction

$$S_{i,j+1}\omega_{i,j+1}^{n+1} + S_{i,j}^{n+1}\omega_{i,j} + S_{i,j-1}^{n+1}\omega_{i,j-1} = S \qquad (14)$$

in which

$$S_{i,j+1} = -\frac{1}{4\Delta Z\Delta\theta}(\psi_{i+1,j}^n - \psi_{i-1,j}^n) - \frac{2}{Re(\Delta Z)^2} \qquad (15a)$$

$$S_{i,j} = \frac{2a^2 e^{2aZ}}{\Delta t} + \frac{2}{Re(\Delta Z)^2} \qquad (15b)$$

$$S_{i,j-1} = \frac{1}{4\Delta Z\Delta\theta}(\psi_{i+1,j}^n - \psi_{i-1,j}^n) - \frac{2}{Re(\Delta Z)^2} \qquad (15c)$$

and

$$S = \left[\frac{1}{4\Delta Z\Delta\theta}(\psi_{i,j+1}^n - \psi_{i,j-1}^n) + \frac{2}{Re(\Delta\theta)^2}\right]\omega_{i+1,j}^{n+1/2}$$

$$+ \left[\frac{2a^2 e^{2aZ}}{\Delta t} - \frac{4}{Re(\Delta\theta)^2}\right]\omega_{i+1,j}^{n+1/2}$$

$$+ \left[\frac{\psi_{i,j+1}^n - \psi_{i,j-1}^n}{4\Delta Z\Delta\theta} + \frac{2}{Re(\Delta\theta)^2}\right]\omega_{i-1,j}^{n+1/2} \qquad (15d)$$

Solutions of $\omega_{i,j}$ at the $(n+1)$th time-step were used in a successive over-relaxation (SOR) method for calculating the stream functions by the following relation

$$\psi_{i,j}^{m+1} = \psi_{i,j}^m + \frac{\lambda}{S_{i,j}'}[a^2 e^{2aZ}\omega_{i,j}^{n+1} - S_{i,j-1}'\psi_{i,j-1}^{m+1} - S_{i-1,j}'\psi_{i-1,j}^{m+1}$$

$$- S_{i,j}'\psi_{i,j}^m - S_{i+1,j}'\psi_{i+1,j}^m - S_{i,j+1}'\psi_{i,j+1}^m] \qquad (16)$$

in which

$$S_{i,j-1}' = \frac{1}{(\Delta Z)^2}, \quad S_{i+1,j}' = \frac{1}{(\Delta\theta)^2}, \quad S_{i,j}' = -\frac{2}{(\Delta Z)^2} - \frac{2}{(\Delta\theta)^2},$$

$$S_{i+1,j}' = S_{i-1,j}', \quad S_{i,j+1}' = S_{i,j-1}' \qquad (17a-e)$$

The term λ indicates the optimum relaxation factor. The value of λ, which equals 1.65, was used in the analysis based on the method given by Carre.[13] The stream functions $\psi_{i,j}$ at the $(n+1)$th time step were obtained when the difference between the $(m+1)$th iteration and the (m)th iteration was within a prescribed tolerance. The same procedures were repeated for the successive time-steps until the steady state was reached.

C. SIP-SIP

The strongly implicit procedure (SIP) was proposed by Stone[14] for solving linear elliptical partial differential equations. Solutions of vorticity and stream function were obtained separately at each time-step. The vorticity values at the $(n+1)$ time-step were calculated by using the following finite difference equation

$$B_{i,j}\omega_{i,j-1}^{n+1} + D_{i,j}\omega_{i-1,j}^{n+1} + E_{i,j}\omega_{i,j}^{n+1} + F_{i,j}\omega_{i+1,j}^{n+1} + H_{i,j}\omega_{i,j+1}^{n+1} = q_{i,j} \qquad (18)$$

in which

$$B_{i,j} = \frac{\psi_{i+1,j}^n - \psi_{i-1,j}^n}{4\Delta Z\Delta\theta} - \frac{2}{Re(\Delta Z)^2} \qquad (19a)$$

$$D_{i,j} = -\frac{\psi_{i,j+1}^n - \psi_{i,j-1}^n}{4\Delta Z\Delta\theta} - \frac{2}{Re(\Delta\theta)^2} \qquad (19b)$$

$$E_{i,j} = \frac{4}{Re}\left[\frac{1}{(\Delta Z)^2} + \frac{1}{(\Delta\theta)^2}\right] + \frac{a^2 e^{2aZ}}{\Delta t} \qquad (19c)$$

$$F_{i,j} = \frac{\psi_{i,j+1}^n - \psi_{i,j-1}^n}{4\Delta Z\Delta\theta} - \frac{2}{Re(\Delta\theta)^2} \qquad (19d)$$

$$H_{i,j} = -\frac{\psi_{i+1,j}^n - \psi_{i-1,j}^n}{4\Delta Z\Delta\theta} - \frac{2}{Re(\Delta Z)^2} \qquad (19e)$$

$$q_{i,j} = \frac{a^2 e^{2aZ}\omega_{i,j}^n}{\Delta t} \qquad (19f)$$

The SIP method uses a technique of matrix factorization and elimination, as discussed by Stone[14] and Weinstein et al.[15] Detailed procedures are given in the Appendix. The values of stream function were obtained by the same SIP method through the application of the following finite-difference equation

$$B_{i,j}'\psi_{i,j-1}^{n+1} + D_{i,j}'\psi_{i-1,j}^{n+1} + E_{i,j}'\psi_{i,j}^{n+1} + F_{i,j}'\psi_{i+1,j}^{n+1} + H_{i,j}'\psi_{i,j+1}^{n+1} = q_{i,j}' \qquad (20)$$

in which

$$B_{i,j}' = \frac{1}{(\Delta Z)^2}, \quad D_{i,j}' = \frac{1}{(\Delta\theta)^2}, \quad E_{i,j}' = -\frac{2}{(\Delta Z)^2} - \frac{2}{(\Delta\theta)^2},$$

$$F_{i,j}' = D_{i,j}', \quad H_{i,j}' = B_{i,j}', \quad q_{i,j}' = a^2 e^{2aZ}\omega_{i,j}^{n+1} \qquad (21a-f)$$

Theoretically, the SIP-SIP method could be used directly for steady-state solutions if the boundary conditions were known. Our problem was that the vorticity values at the surface of the cylinder could not be prescribed. Moreover, we were interested in investigating the oscillation phenomenon in the wake region. Consequently, vorticity solutions of successive time-steps were necessary.

IV.   Boundary Conditions

Based on no-slip conditions, the velocity components are zero at the surface of the cylinder, whereas a uniform flowfield of velocity U surrounds the cylinder. The boundary conditions for the stream functions and vorticities in terms of the transformed coordinates (Z,θ) are given in Fig. 1. It is noted that the vorticity values at the cylinder surface can only be determined from the second derivatives of the local stream functions by the relation

$$\omega = \left[\frac{1}{a^2 e^{2aZ}}\frac{\partial^2\psi}{\partial Z^2}\right]_{Z=0} \text{ for all } \theta \qquad (22)$$

In finite-difference form at $Z=0$, the vorticity values for all θ become

$$\omega_{i,j} = [\psi_{i,j+1} - 2\psi_{i,j} + \psi_{i,j-1}]/a^2(\Delta Z)^2 \qquad (23)$$

On the surface of the cylinder, $Z=0$, the stream function is zero, $\psi_{i,j}=0$. The stream function inside the cylinder, $\psi_{i,j-1}$, is assumed to be the mirror image of the stream function around the cylinder, $\psi_{i,j+1}$, because of zero gradient. Consequently, the values of $\omega_{i,j}$ on the surface for all θ can be written as

$$\omega_{i,j} = 2\psi_{i,j+1}/a^2(\Delta Z)^2 \qquad (24)$$

The values of $\psi_{i,j+1}$, which are not known at steady state, can, in an iteration process, be arbitrarily assumed to determine the steady-state condition. The number of iterations, if they converge, may depend on the initial assumptions that require some criteria in order to have any consistency. Because we were interested in finding steady-state solution for both
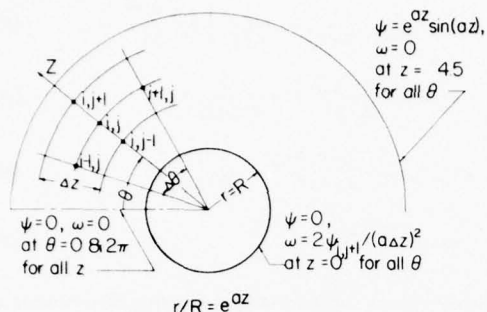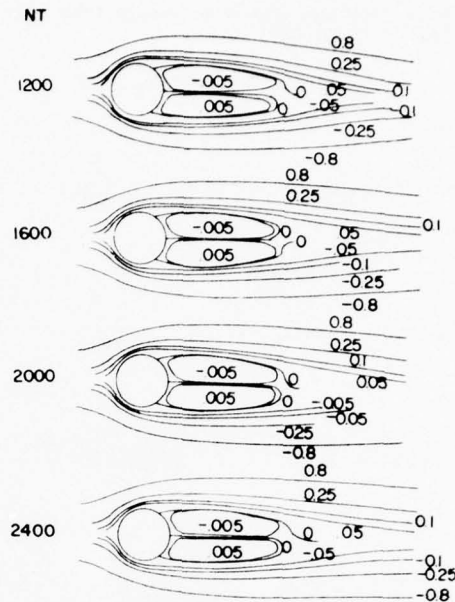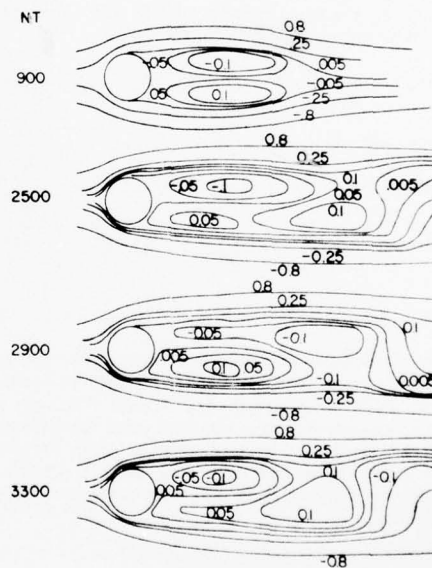
Fig. 1   Boundary conditions.

oscillating and nonoscillating flows, it was to our advantage to use the impulsively started flow as the initial condition. The number of time-steps (NT) indicates the history of flow oscillations. Because the oscillation phenomenon is a part of two-dimensional separated flows, steady state is defined by the following conditions: 1) For nonoscillating flows, the values of ψ and ω remain constant at a given Z and θ location as NT increases; 2) For oscillating flows, the variations of ψ and ω in the Z and θ plane repeat themselves with a definite pattern as NT increases. Numerical solutions for separated flow around a circular cylinder were calculated at three Reynolds numbers (40, 80, and 200) by using three different numerical methods.

V.   Results and Discussion

The effect of mesh sizes and outer boundary locations on numerical accuracy has been discussed by Lin and Lee[12] for solutions of Navier-Stokes equations. The current study was undertaken to investigate the relative accuracy and computer time of three different methods. Only one standard mesh size of $\Delta Z = 0.1$, $\Delta\theta = 6°$, and $\Delta t = 0.02$ was used for a flowfield with an outer boundary of 90 radii of the cylinder. To determine the relative accuracy of each method, calculated results of drag coefficient, separation angle, and Strouhal number were compared with available experimental data. It was found that the SIP-SIP method gave the same accuracy as the ADI-SOR method, which proved better accuracy than the DDE-GSI method. The required computer time on an IBM 370-168 computer is shown in Table 1. It is evident that the SIP-SIP method is a more efficient method for the investigated problem. In order to provide a complete picture of the investigated result, the discussion is divided into two parts.

A.   Flow Patterns

The stream function pattern calculated from the SIP-SIP method is shown in Fig. 2 for the case of Reynolds number 40. It is noted that the separated flow in the wake of a circular cylinder is symmetric and steady as long as the Reynolds number is less than 40. The wake length is two to three times as great as the cylinder diameter, and the separation angle is about 126° from the leading edge. Figure 3 shows that streamline pattern for the case of Reynolds number 80. The separation angle is about 114°. The recirculating flow in the wake region oscillates with a definite frequency. The flow pattern appears to repeat itself between 2500 NT and 3150 NT. By using the dimensionless time increment $\Delta t = 0.02$, the

Table 1   Computer time comparisons

	IBM 370-168		
Re/Time (min)	DDE-GSI	ADI-SOR	SIP-SIP
40	100	100	40
80	120	120	50
200	—	—	60

Fig. 2   Streamline patterns, $Re = 40$.

Fig. 3   Streamline patterns, $Re = 80$.

oscillating frequency can be calculated by the following equation

$$f = U/R\Delta t[(NT)_2 - (NT)_1] \tag{25}$$

The Strouhal number, given by the relation

$$S = 2Rf/U \tag{26}$$

has a value of 0.154 for the case of Reynolds number 80. Figure 4 shows the streamline pattern for the case of Reynolds number 200. The separation angle is about 102° from the stagnation point of the leading edge. The flow pattern appears to repeat itself between 2400 NT and 2950 NT. This gives a Strouhal number of 0.182 for the case of Reynolds number
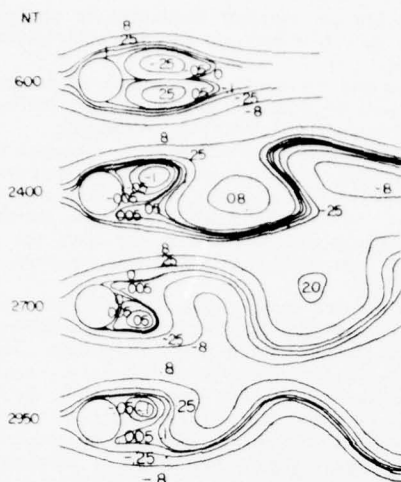
Fig. 4 Streamline patterns.

200. By using the ADI-SOR method, the flow pattern calculations were obtained for cases of Reynolds number 40 and 80 only. The appearances of streamline distributions are very much similar to those of the shown results which were obtained by the SIP-SIP method. The streamline patterns obtained by the DDE-GSI method deviated noticeably from the shown results. In order to answer the question of the relative accuracy of each method, it was necessary to compare the results with available experimental data.

B. Comparison with Experimental Data

Experimental data are available in terms of drag coefficient, separation angle, and Strouhal number. The total drag coefficient is calculated by the summation of the pressure drag coefficient,

$$(C_D)_p = \frac{2}{Re} \int_0^{2\pi} \left\{ \int_0^\infty \frac{\partial \omega}{\partial \theta} \bigg|_{\theta=0} dZ + \int_0^\theta \frac{\partial \omega}{\partial Z} \bigg|_{Z=0} d\theta' \right\} \cos\theta \; d\theta \tag{27}$$

and the skin friction drag coefficient,

$$(C_D)_f \approx \frac{2}{Re} \int_0^{2\pi} \omega \bigg|_{Z=0} \sin\theta d\theta \tag{28}$$

By using the obtained values of vorticity and vorticity gradient along the surface of the cylinder, the drag coefficient for each Reynolds number case was determined and compared with available experimental data.

Numerical solutions were also obtained by other investigators who used one of the three different methods. The DDE-GSI method was used by Thoman and Szewczyk who compared their results with the experimental data of Relf and Simmons as well as with the data of Morkovin. The ADI-SOR method was used by Son and Hanratty who also discussed the numerical results of Kawaguati and Jain. When we used the DDE-GSI method for our calculations in the drag coefficient, we obtained practically the same results as Thoman and Szewczyk; however, when we used the ADI-SOR method for our drag calculations, we got the same results as those obtained by the SIP-SIP method, which is developed in the present work. The assumption that a line of symmetry exists in the wake region appears to be the source of inaccuracy in the numerical results of Son and Hanratty at Reynolds numbers greater than 40. When compared with the experimental data of Perry[16] and Roshko[17] as shown in Fig. 5, this ob-
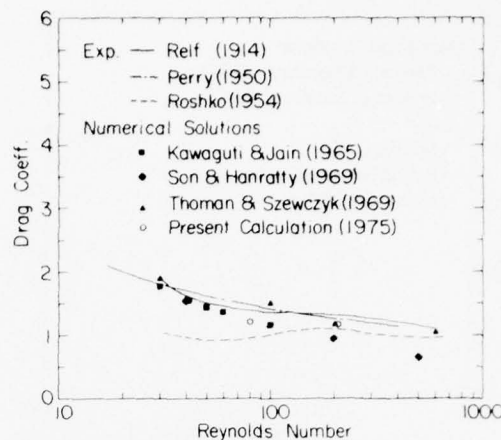

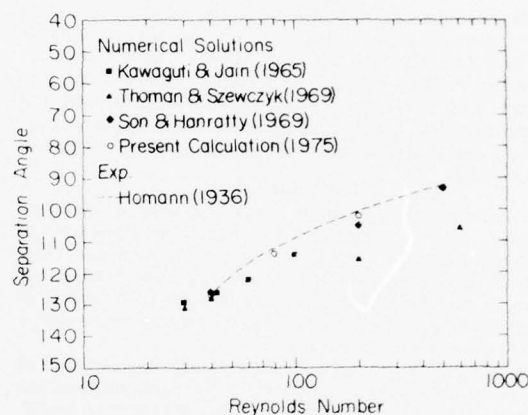Fig. 5   Drag coefficient comparisons.

Fig. 6   Separation angle comparisons.

servation was confirmed. It is interesting to note that the discrepancy between experimental data is greater than that of the numerical results at the lower Reynolds number region. The experimental results were also compared with analytical results on separation angles as shown in Fig. 6. The experimental data obtained by Homann[18] at Reynolds number 40 agree well with all analytical results. The DDE-GSI method of Thoman and Szewczyk appears to give the most inaccurate predictions at other Reynolds numbers. This is to be expected, because the criteria given in Eq. (10) for numerical stability tend to generate larger values of inaccuracy in the close vicinity of a solid boundary where the flow separation is originated. Moreover, the assumption of symmetry in the wake region that was used by Son and Hanratty apparently gives reasonable predictions for separation angles because they are located upstream of the wake region. The experimental and numerical results on Strouhal numbers can also be compared as shown in Fig. 7. Because the Strouhal number is related to the shedding of vorticities in the wake region, as given in Eqs. (25) and (26), numerical methods to predict Strouhal numbers cannot assume the line of symmetry in that region. The experimental data of Roshko[17] appear to be consistent at all tested Reynolds numbers. The experimental data of Relf and Simmons as well as the data of Morkovin were used by Thoman and Szewczyk for comparison with their numerical results, which were obtained by the DDE-GSI method. The ADI-SOR method used by Son and Hanratty cannot predict Strouhal numbers, because it assumes symmetry in the wake region. The ADI-SOR method used in the present study gives similar results as the SIP-SIP
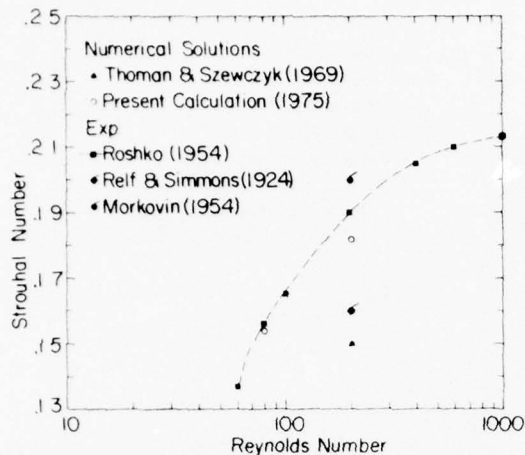
Fig. 7   Strouhal number comparisons.

method for the case of Reynolds number 80 and uses more than twice the amount of computer time than the latter method. Consequently, only the SIP-SIP method has been used for studying the case of Reynolds number 200. It is evident that discrepancies exist in both experimental and numerical results for Strouhal numbers. The present study appears to agree better with Roshko's data than with the data in other studies.

VI. Conclusions

It is necessary to examine a newly developed numerical method for the purpose of correcting questionable mathematical approximations. For solving nonlinear elliptical differential equations, the numerical method which appears to give the best accuracy and uses the least amount of computer time is the implicit finite difference scheme that is solved by matrix factorizations.

Separated flow around a circular cylinder can have a line of symmetry in the wake region only at Reynolds numbers less than 40. In the case of oscillating flows, there are two factors which cause errors in numerical solutions. One is the mathematical approximation of the nonlinear terms that is used to achieve numerical stability. The other is the physical assumption of the wake symmetry. Calculations of the drag coefficient appear to be within the limit of experimental accuracy if the physical reality of flow oscillations is allowed in the wake region. Calculations of the separation angle appear to be affected more significantly by the mathematical approximation than the physical assumption. Calculations of the Strouhal number, however, require an adequate treatment of both factors.

The question on computer simulations vs wind-tunnel simulations can only be answered according to the purpose of applications.

1) For laminar flows at relatively low Reynolds numbers, it is economically advantageous to use computer simulations because the technology available today is adequate.

2) As the Reynolds numbers increase to the region of instability, computer simulations using unsteady-state Navier-Stokes equations are questionable, because the numerical instability is not distinguishable from flow instability. However, wind-tunnel simulations may have the same problem of super-positioning mechanical vibrations upon flow instabilities.

3) In the turbulent flow region, computer simulations need to use time-steps at least one order of magnitude smaller than the smallest period of the turbulent fluctuation. This will enable us to solve the unsteady-state Navier-Stokes equations by considering the fluctuating velocities as time dependent variables of the momentary velocity components. However, today's computer technology cannot reach the required computational speed. Computer simulations of turbulent flow problems are presently being conducted by using a closure scheme to relate the turbulent fluctuations with the time-averaged components. Owing to the limited availability of reliable experimental data, there is a possibility of super-positioning questionable mathematical approximations upon unrealistic physical assumptions. This is particularly true when the solution of nonlinear elliptical partial differential equations is required for turbulent flows in the separation region. The present study is intended to minimize the numerical inaccuracy before a closure scheme is introduced into turbulent flow problems. Consequently, computer and wind-tunnel simulations are both necessary to improve our current understanding of turbulent flows.

4) Turbulent flows with heat, mass, and momentum transfer often simultaneously occur in many practical problems, such as combustion engineering, environmental pollution, and weather prediction. A realistic computer simulation technique will require the advanced technology in both computational speed and computer storage which are yet to be developed to the operational stage. In the foreseeable future, wind-tunnel simulation is considered to be the most reliable method before full-scale testing for any successful engineering design can be realized. However, the economical reality in conducting extensive experimental investigations makes it necessary for computer simulations of approximate nature to be used to supplement both wind-tunnel simulations and full-scale testing. For practical purposes, both computers and wind tunnels are necessary to supplement each other to provide the reliablity and economy that are required for all successful engineering endeavors.

Table 2   Elements of matrices $[M]$, $\{\Phi\}$, and $\{q\}$ [a]

[a] I is the maximum number of points in the i direction; J is the maximum number of points in the j direction.

Appendix

Using the SIP Method to Obtain the Matrix Solution

The governing equations, in matrix form, with five nonzero diagonal elements as the coefficient matrix may be written for either Eq. (18) or Eq. (20) as follows

$$[M] \cdot \{\Phi^{n+l}\} = \{q^n\} \tag{A1}$$

The term $[M]$ is the coefficient matrix of the column matrix $\{\Phi^{n+l}\}$, which represents either the stream function ψ or the vorticity ω at the $(n+l)$th time-step for every grid point in the flowfield. The column matrix $\{q^n\}$ results from the known values of the flowfield at the (n)th time-step. The elements of matrices $[M]$, $\{\Phi\}$, and $\{q\}$ are given in Table 2. In order to accelerate the solution procedure, matrix $[M]$ is modified as matrix $[M+N]$, which consists of seven nonzero diagonal elements. Equation (A1) then becomes

$$[M+N] \{\Phi^{n+l}\}^{m+l} = \{q^n\} + [N] \{\Phi^{n+l}\}^m \tag{A2}$$

in which m is the number of iterations for determining the column matrix $\{\Phi\}$ at the $(n+l)$th time-step. The modifier matrix $[N]$ has to fulfill the requirement that the coefficient matrix $[M+N]$ can be factored into the product of a lower matrix $[L]$ and an upper matrix $[U]$; each consists of three nonzero diagonal elements in the lower and upper portions, respectively, as follows:

$$[M+N] = [L][U] \tag{A3}$$

$$(A4)$$

in which

$$\bigcirc = b_{i,j}$$

$$\bigcirc = b_{i,j} e_{i,j-1}$$

$$\bigcirc = c_{i,j}$$

$$\bigcirc = d_{i,j} + b_{i,j} f_{i,j-1} + c_{i,j} e_{i-1,j}$$

$$\bigcirc = d_{i,j} e_{i,j}$$

$$\bigcirc = c_{i,j} f_{i-1,j}$$

$$\bigcirc = d_{i,j} f_{i,j}$$

with

$$b_{i,j} = B_{i,j} / (1 + \alpha e_{i,j-1})$$

$$c_{i,j} = D_{i,j} / (1 + \alpha f_{i-1,j})$$

$$d_{i,j} = E_{i,j} + \alpha(b_{i,j} e_{i,j-1} + c_{i,j} f_{i-1,j}) - b_{i,j} f_{i,j-1} - c_{i,j} e_{i-1,j}$$

$$e_{i,j} = (F_{i,j} - \alpha b_{i,j} e_{i,j-1}) / d_{i,j}$$

$$f_{i,j} = (H_{i,j} - \alpha c_{i,j} f_{i-1,j}) / d_{i,j}$$

The iteration parameter α is allowed to vary between zero and unity. According to Stone[14] values near unity tend to reduce the low-frequency errors more rapidly. In this analysis, ten values of α between zero and unity are evenly distributed in the range between the high and low frequencies.

The purpose of this modification is to determine the column matrix $\{\Phi^{n+l}\}$ by having the difference between the $(m+l)$th and the (m)th iterations within a prescribed tolerance. If a column matrix $\{\Delta\Phi\}$ at the $(m+l)$th iteration is defined as

$$\{\Delta\Phi^{n+l}\}^{m+l} = \{\Phi^{n+l}\}^{m+l} - \{\Phi^{n+l}\}^m \tag{A5}$$

then Eq. (A2) can be written as

$$[M+N] \{\Delta\Phi^{n+l}\}^{m+l} = \{q^n\} - [M]\{\Phi^{n+l}\}^m \tag{A6}$$

If one uses the lower and upper matrices given by Eq. (A3), Eq. (A6) can be expressed as

$$[L][U] \{\Delta\Phi^{n+l}\}^{m+l} = \{q^n\} - [M]\{\Phi^{n+l}\}^m \tag{A7}$$

The use of matrices $[L]$ and $[U]$ accelerates the solution procedures by successive eliminations. Once the column matrix $\{\Delta\Phi^{n+l}\}$ at the $(m+l)$th iteration is equal to or less than the prescribed tolerance, the values of $\{\Phi^{n+l}\}$ at the (m)th iteration become the solutions of either the vorticity or the stream function at the $(n+l)$th time-step.

References

[1]Lee, S. C. and Harsha, P. T., "Use of Turbulent Kinetic Energy in Free Turbulent Mixing Studies," *AIAA Journal*, Vol. 8, June 1970, pp. 1026-1032.

[2]Pepper, D. W. and Lee, S. C., "Transport Phenomena in Thermally Stratified Boundary Layers," *Journal of Heat Transfer*, Vol. 97, Feb. 1975, pp. 60-65.

[3]Conte, S. D., *Elementary Numerical Analysis*, McGraw-Hill, New York, 1965, p. 179.

[4]Richtmyer, R. D., *Difference Methods for Initial-Value Problems*, Interscience Pub., New York, 1957, p. 238.

[5]Roache, P. J., *Computational Fluid Dynamics*, Hermosa Publishers, Albuquerque, N.M. 972, p. 434.

[6]Schlichting, H., *Boundary Layer Theory*, 6th Edition, McGraw-Hill, New York, 1968, p. 747.

[7]Thoman, D. C. and Szewczyk, A. A., "Time-Dependent Viscous Flow Over a Circular Cylinder," *Physics of Fluid Supplement*, Vol. 12, Dec. 1969, pp. 76-86.

[8]Peaceman, D. W. and Rachford, H. H., Jr., "The Numerical Solution of Parabolic and Elliptic Differential Equations," *Journal of the Society of Industrial and Applied Mathematics*, Vol. 3, 1955, pp. 28-41.

[9]Douglas, J., "On the Numerical Integration of $\partial^2 U/\partial X^2 + \partial^2/\partial Y^2 = \partial U/\partial t$ by Implicit Methods," *Journal of the Society of Industrial and Applied Mathematics*, Vol. 3, 1955, pp. 42-65.

[10]Wachspress, E. L., "Optimum Alternating-Direction-Implicit Iteration Parameters for a Model Problem," *Journal of the Society of Industrial and Applied Mathematics*, Vol. 3, 1955, pp. 42-65.

[11]Son, J. S. and Hanratty, T. J., "Numerical Solution for the Flow around a Cylinder at Reynolds Numbers of 40, 200 and 500," *Journal of Fluid Mechanics*, Vol. 35, 1969, pp. 369-386.

[12]Lin, C. L. and Lee, S. C., "Transient State Analysis of Separated Flow around a Sphere," *International Journal of Computer and Fluids*, Vol. 1, 1973, pp. 235-250.

[13]Carre, B. A., "The Determination of the Optimum Accelerating Factor for Successive Over-Relaxation," *Computer Journal*, Vol. 4, 1961, pp. 73-78.

[14] Stone, H. L., "Iterative Solution of Implicit Approximations of Multidimensional Partial Differential Equations," *SIAM Journal of Numerical Analysis*, Vol. 5, 1968, pp. 530-558.

[15] Weinstein, H. G., Stone, H. L., and Kwan, T. V., "Simultaneous Solution of Multiphase Reservoir Flow Equations," *Society of Petroleum Engineers Journal*, 1970, pp. 99-111.

[16] Perry, T., *Chemical Engineering Handbook*, McGraw Hill, New York, 1950, pp. 1017.

[17] Roshko, A., "On the Development of Turbulent Wakes from Vortex Streets," NACA Rept., 1191, 1954.

[18] Homann, F., "Einfluss grosser Zähigkeit bei Stromung um Zylinder," *Forschung Gebiet im Ingenieur Wesens*, Vol. 7, 1936, pp. 1-10.

DISTRIBUTION LIST

Office of Naval Research [1]
Atmospheric Science Program
Code 465
Arlington, VA 22217

Cognizant ONR Branch Office [1]
Code N62880
536 South Clark Street
Chicago, IL 60605

Office of Naval Research [6]
Code 102 IP
Arlington, VA 22217

Naval Research Laboratory [6]
Code 2627
Washington, D. C. 20375

Defense Documentation Center [12]
Code S47031
Bldg. 5, Cameron Station
Alexandria, VA 22314

Naval Electronics Laboratory Center [1]
Code 2220
271 Catalina Boulevard
San Diego, CA 92152

Naval Environmental Prediction [1]
Research Facility
Monterey, CA 93940

Fleet Numerical Weather Central [1]
Monterey, CA 93921

Naval Air Systems Command [1]
Code Air 370C
Arlington, VA 22217

Dr. Dale F. Leipper [2]
Department of Oceanography
Naval Postgraduate School
Monterey, CA 93940

Eugene J. Mack [1]
Environmental Systems Department
Calspan Corporation
Buffalo, New York 14221

Graduate Center for Cloud Physics Research [1]
Univ. of Mo.-Rolla
Rolla, MO 65401

Dept. of Meteorology [1]
San Jose State Univ.
San Jose, CA 95150

Laboratory of Atmospheric Physics [1]
Univ. of Nevada
Reno, NV 89507

Cloud Physics Laboratory [1]
Univ. of Denver
Denver, CO 80210

Aeronautical Research Association [1]
of Princeton
50 Washington Road
Princeton, NJ 08540

Naval Avionics Facility [1]
Code 812
6000 E. 21 Street
Indianapolis, IN 46218

Naval Weapons Center [2]
Codes 602, 3173
China Lake, CA 93555

Air Force Geophysics Laboratory [2]
Bedford, MA 01730